

https://dspace.org/

Low temperature oxidation of volatile organic compounds using gold-based catalysts

Kwenda, Ellen

2011-09-13
http://hdl.handle.net/10539/10408

Downloaded from a DSpace repository. https://dspace.org/

LOW TEMPERATURE OXIDATION OF VOLATILE ORGANIC COMPOUNDS USING GOLD-BASED CATALYSTS

Ellen Kwenda

LOW TEMPERATURE OXIDATION OF VOLATILE ORGANIC COMPOUNDS USING GOLD-BASED CATALYSTS

Ellen Kwenda

A dissertation submitted to the Faculty of Science at The University of the Witwatersrand, Johannesburg

In fulfilment of the requirements for the degree of

Masters of Science

Johannesburg 2011

Declaration

I know the meaning of plagiarism and I declare that all the work in this dissertation is my own, unaided work. It is being submitted for the degree of Masters of Science in the University of the Witwatersrand, Johannesburg. It has not been submitted before for any degree or examination in any other body or organization or person outside the University of the Witwatersrand, Johannesburg.

_____

Ellen Kwenda

_____ Day of _____ 2011

ABSTRACT

In this work, a detailed study of the evaluation of gold-based catalysts supported on manganese oxides for the oxidation of volatile organic compounds (VOCs) has been undertaken. Model catalysts were prepared by deposition-precipitation methods to establish the effect of the support on the catalytic activity of the gold catalysts. The catalysts were characterised by X-ray diffraction, transmission electron microscopy, N_2–physisorption measurements and temperature programmed reduction techniques. The activity of the catalysts for VOC oxidation reactions were tested in a continuous flow fix bed glass reactor. The products were analysed by GC/TCD and GC/FID.

The catalysts Au/TiO_2, Au/Al_2O_3, Au/ZnO and Au/MnO_2 were used for the VOC oxidation reaction. 2-propanol, 2-butanol and toluene were used as VOCs for the study. These were chosen because they are important indoor pollutants given their wide laboratory use and high volatility. Toluene was found to be the most difficult to oxidise, followed by 2-propanol.

The effect of calcination temperature and preparation procedure was evaluated for the gold/manganese oxide catalysts. $Au/\beta\text{-}MnO_2$ catalysts prepared by deposition-precipitation showed some catalytic performance which was less than the performance shown by Au/MnO_x, prepared by co-precipitation. $\gamma\text{-}MnO_2$ proved to be more efficient in the oxidation of 2-propanol than pyrosulite phase MnO_2. The addition of gold to any metal oxide support was found to enhance the oxidation of VOCs. Gold-based catalysts were more active than the Ce/MnO_2 catalyst.

Catalytic tests showed that Au/CeO_2 was the superior catalyst for the total oxidation of toluene, 2-propanol and 2-butanol. Ceria is a highly reducible oxide and the formation of gold–ceria interactions produced an even more easily reduced material.

ACKNOWLEDGEMENTS

I would like to thank my supervisor, Prof.M.S. Scurrell. Thank you for introducing me to the interesting field of gold catalysis research. Thank you for all the advice and support you continued to provide for the duration of this project. Thank you, Prof. N. Coville, for your tireless input in helping and efforts to help me finish.

Also, thank you James Luluzi, Mpfunzeni Raphulu, Gary Pattrick and Jason McPherson for all the technical and professional advice. To Basil Chassolbous, thank you for your help with assembling and servicing my rig. You taught me a lot and it was a pleasure to work with you.

Thank you to the electron microscopy unit and gate house staff for all the assistance with sample analysis. Thank you the University of the Witwatersrand, Johannesburg and School of Chemistry for allowing me to undertake my research in an open and free environment and encouraging the best for each individual. The financial support from Mintek and Mintek Project AuTEK is acknowledged with much appreciation.

Not forgetting CATOMMAT group for your helpfulness and positive criticism that helped to mature me as a researcher and tireless assistance in the lab. I really enjoyed the times spend together- it was never a dull moment.

To my family; thank you for the encouragement and for believing in me. I love you and this one is for you. And finally thank you God for the strength you gave me to see this project through.

PRESENTATIONS AND PUBLICATION

Parts of this work was presented as follows:

POSTER PRESENTATION

"The low temperature oxidation of 2-propanol using gold-based catalysts",

CATSA conference, Rawsonville, 8-11 November 2009

ORAL PRESENTATION

"The low temperature oxidation of volatile organic compounds using gold-based catalysts", Mintek Student Day, Randburg, 13 November 2008

PAPER PUBLICATION

"The catalytic oxidation of volatile organic compounds using Au/MnO_2 catalysts",

E. Kwenda, M.S. Scurrell and G. Pattrick [to be published]

CONTENTS

ABSTRACT i

ACKNOWEDGEMENTS ii

PRESENTATION AND PUBLICATION iii

CONTENTS iv

LIST OF FIGURES vii

LIST OF TABLES x

NOMECLATURE xi

CHAPTER 1 1

1. INTRODUCTION 1

1.1 Volatile organic compounds 1

1.2 VOC removal technologies 2

1.3 Catalytic oxidation 4

1.4 Aim 5

1.5 Thesis content 6

1.6 Reference 7

CHAPTER 2 8

2. LITERATURE REVIEW 8

2.1. Gold catalysis 8

2.2. Gold catalyst preparation methods 9

2.2.1. Impregnation and co-precipitation method 9

2.2.2. Colloidal gold 10

2.2.3. Deposition-precipitation 11

2.2.4. Other preparation methods 14

2.3 Characterisation techniques for gold-based catalysts 14

2.3.1 Electron microscopy (EM) technique 15

2.3.2 Temperature programmed reduction 15

2.3.3 X-ray diffraction (XRD) technique 16

2.3.4 Other characterisation techniques 17

2.4 Gold catalysts in oxidation reaction 19

2.4.1 VOC oxidation reactions 19

2.5 MnO_x based catalysts 21

2.6 Ce and Au/CeO_2 catalyst **24**
2.7. Reference **25**
CHAPTER 3 ..... **29**
3. EXPERIMENTAL METHODS **29**
3.1 Apparatus and chemicals **29**
3.2 Catalyst preparation **30**
3.2.1 Preparation of Au-Mn based catalysts **31**
3.2.2. Preparation of CeO_2 and Au/CeO_2 ..... **33**
3.2.3. Preparation of Ce/β-MnO_2 catalysts with various amounts of Ce **33**
3.2.4. Gold supported on Al_2O_3, TiO_2 and ZnO **33**
3.3. Characterisation of the catalysts **34**
3.3.1. Temperature programmed reduction (TPR) **34**
3.3.2. Electron microscopy (EM) **34**
3.3.3. X-ray diffraction (XRD) **35**
3.3.4. N_2 physisorption **35**
3.3.5 Inductively coupled argon plasma emission spectroscopy (ICP-AES) **36**
3.3.6 Thermal gravimetric analysis (TGA) **36**
3.4. Reactor Studies **36**
3.5. Reference **39**
CHAPTER 4 ..... **40**
4. RESULTS AND DISCUSSION **40**
4.1 Catalyst synthesis **40**
4.2 Catalyst characterisation **42**
4.2.1 Surface area measurements **42**
4.2.2 Transmission electron microscopy studies **43**
4.2.3. X-ray diffraction **51**
4.2.4 H_2-Temperature programmed reduction **57**
4.2.5 Thermogravimetric analysis (TGA) **65**
4.3 Reactor studies **65**
4.3.1 2-Propanol catalytic oxidation **66**
4.3.2. 2-Butanol catalytic oxidation **83**
4.3.3. Toluene catalytic oxidation **89**

4.4. References 91

CHAPTER 5 93

5. CONCLUSIONS 93

FUTURE STUDIES 95

BIBLIOGRAPHY 97

APPENDIX A 98

APPENDIX B 100

APPENDIX C 101

APPENDIX D 102

LIST OF FIGURES

CHAPTER 3

Figure 3.1: Rig used to evaluate catalyst performance 36

CHAPTER 4

Figure 4.1: (a) A TEM image of the Au/TiO_2 catalyst showing Au particles as small dark spots (see arrows) and (b) bar graph showing gold particle size distribution 44

Figure 4.2: (a) TEM image of the Au/Al_2O_3 catalyst showing Au particles and (b) bar graph showing gold particle size distribution 45

Figure 4.3: (a) TEM image of Au/ZnO catalyst showing Au particles and (b) bar graph showing gold particle size distribution 45

Figure 4.4: TEM image of the Au/β-MnO_2 catalyst calcined at 300 ^{o}C and (b) bar graph showing Au particle size distribution with average Au particle size of 3.4 nm 46

Figure 4.5:(a) TEM image of the Au/β-MnO_2 catalyst at calcined 350 ^{o}C and and (b) bar graph showing the Au particle size distribution average Au particle size 4.8 nm 47

Figure 4.6: (a) TEM images of Au/β-MnO_2 GP catalyst prepared by colloid formation; (b) the UV-Vis spectrum of Au nanoparticle with PEG showing Au surface plasmon resonance peak at 545 nm and (c) gold particle size distribution bar graph 48

igure 4.7: The TEM image showing amorphous particles of Au/γ-MnO_2 catalyst.....49

Figure 4.8: The TEM image showing Au/MnO_x catalyst prepared by co-precipitation.....49

Figure 4.9: (a) TEM image of Au/CeO_2 catalyst and (b) bar graph showing gold particle size distribution.....50

Figure 4.10: TEM image of a) 1% Ce/β-MnO_2 b) 10% Ce/β-MnO_2 catalysts 51

Figure 4.11: XRD pattern of (a) β-MnO_2, (b) Au/β-MnO_2 300, (c) Au/β-MnO_2 350 and (d) Au/β-MnO_2 GP catalysts (⁎ peaks due to β-MnO_2 phases).....52

Figure 4.12: XRD pattern of Au/MnO_x catalyst prepared by co-precipitation of mixed oxides ; calcined at 300 ^oC (⁎ peaks due to MnO_x phases).....53

Figure 4.13: XRD pattern of a) γ-MnO_2 and b) Au/γ-MnO_2 catalysts prepared by oxidative combustion $MnCO_3$ (⁎ peaks due to γ-MnO_2 phases).....54

Figure 4.14: XRD patterns of a) CeO_2 and b) Au/CeO_2 catalysts (⁎ peaks due to CeO_2 phases).....56

Figure 4.15: XRD patterns of Ce loaded β-MnO_2 catalysts a) β-MnO_2 b) 1 % Ce/β-MnO_2 and c) 10% Ce/β-MnO_2 calcined at 400 ^oC (⁎ peaks due to β-MnO_2 phases).....57

Figure 4.16: H_2-TPR profiles of gold-manganese based catalysts (a) β-MnO_2 (b) Au/β-MnO_2 300 ^oC, (c) Au/β-MnO_2 350 ^oC and (d) Au/β-MnO_2 GP.....59

Figure 4.17: H_2-TPR profiles of a) γ-MnO_2 b) Au/γ-MnO_2 catalysts prepared by oxidative combustion of $MnCO_3$.....61

Figure 4.18: H_2-TPR profiles of a) MnO_x and b) Au/MnO_x catalysts prepared by co-precipitation.....62

Figure 4.19: H_2-TPR profiles of a) CeO_2 and b) Au/CeO_2 catalyst.....63

Figure 4.20: H_2-TPR profiles of a) β-MnO_2 b) 1% Ce/β-MnO_2 and c) 5% Ce/β-MnO_2 d) 10% Ce/β-MnO_2.....64

Figure 4.21: Conversion of 2-propanol to various products over the Au/Al_2O_3 catalyst.....67

Figure 4.22: Conversion of 2-propanol to various products over the Au/ZnO catalyst.....68

Figure 4.23: Conversion of 2-propanol to various products over Au/TiO_2.....69

Figure 4.24: Conversion of 2-propanol to various products over Au/CeO_2 catalyst.....70

Figure 4.25: Conversion of 2-propanol to various products over support β-MnO_2 71

Figure 4.26: Conversion of 2-propanol to various products over Au/β-MnO_2 catalyst calcined at 300 ^{o}C.....72

Figure 4.27: Conversion of 2-propanol to various products over Au/MnO_2 catalyst calcined at 350 ^{o}C.....73

Figure 4.28: Conversion of 2-propanol to various product distribution over Au/MnO_2 GP catalyst prepared by colloid formation 74

Figure 4.29: MnO_x prepared by co-precipitation and used for 2-propanol oxidation 77

Figure 4.30: Au/MnO_x catalyst prepared by co-precipitation for the 2-propanol oxidation into various products 78

Figure 4.31: 2-Propanol oxidation over γ-MnO_2 catalyst 79

Figure 4.32: 2-Propanol oxidation over the Au/γ-MnO_2 catalyst 80

Figure 4.33: 2-Propanol oxidation over a 1% Ce/β-MnO_2 catalyst.....82

Figure 4.34: 2-Propanol oxidation over a 10% Ce/β-MnO_2 catalyst.....82

Figure 4.35: 2-Butanol oxidation over the Au/ZnO catalyst.....85

Figure 4.36: 2-Butanol oxidation over the Au/Al_2O_3 catalyst.....86

Figure 4.37: 2-Butanol oxidation over the Au/TiO_2 catalyst.....87

Figure 4.38: 2-Butanol oxidation over the Au/MnO_2 300 catalyst.....88

Figure 4.39: 2-Butanol oxidation over Au/CeO_2 catalyst.....89

Figure 4.40: Toluene oxidation by gold catalyst.....90

Figure 4.41: CO_2 selectivity for toluene oxidation over various gold-based catalysts 91

LIST OF TABLES

CHAPTER 3

Table 3.1: Listing of all catalysts prepared for 2-propanol oxidation 30

CHAPTER 4

Table 4.1: Properties of catalysts used for VOC oxidation along with their surface areas (S_{BET}), gold loadings and average particle sizes 41

Table 4.2: H_2-TPR peak temperatures for all samples studied 58

Table 4.3: Light off temperatures for 2-propanol oxidation 65

Table 4.4: The temperatures at which 50% and 90% 2-butanol was converted over various catalysts 84

NOMENCLATURE

BET	Brunauer-Emmet-Teller method
CO_2	Carbon dioxide
CO	Carbon monoxide
CPT	Co-precipitation
DP	Deposition-precipitation
GC	Gas chromatography
GP	Gold nanoparticle
$HAuCl_4$	Chloroauric acid; hydrogen tetrachloroaurate
ICP	Inductively coupled plasma
IWP	Incipient wetness impregnation
MnO_2	Manganese dioxide
PEG	Polyethylene glycol
S_{CO_2}	Selectivity of carbon dioxide
$S_{actetone}$	Selectivity of acetone
$S_{propene}$	Selectivity of propene
TEM	Transition electron microscopy
TPR	Temperature programmed reductions
T_{50}	Temperature at which 50% VOC is converted
T_{90}	Temperature at which 90% VOC is converted

UV-Vis	Ultra-violet visible
WHSV	Weight hourly space velocity
Wt.%	Weight percentage
XRD	X-ray diffraction
VOC	Volatile organic compound

CHAPTER 1

1. INTRODUCTION

1.1 Volatile organic compounds

Volatile organic compounds (VOCs) are an important class of pollutants and there has been a substantial release of these compounds into the environment in recent years [1]. VOCs can be defined as carbon containing compounds excluding molecules containing carbon such as CO, CO_2 and CS_2. They are usually found as gases but at 1 atm and 20 ^{o}C may be liquids or solids with high enough vapour pressure to evaporate into the atmosphere. Volatile organic compounds released into the atmosphere are broken down into CO_2 or other more toxic organic compounds such as dioxins. There are a large number of compounds that are specified under this single class of pollutants and they include alkanes, alkenes and aromatic compounds amongst many others.

VOCs can be derived from many sources including those made from either anthropogenic or biogenic origins. Biogenic sources involve emissions primarily from vegetation and contribute significantly to poor air quality. Anthropogenic sources include emission from the use of paints, fuels storage and distribution, evaporation of solvents, tobacco smoke, dry cleaning solvents and vehicle emissions. Also, some industrial processes result in the emissions of VOCs into the atmosphere. Volatile organic compounds also arise from incomplete combustion of fuels.

VOCs contribute to the formation of photochemical smog, in the lowest atmospheric levels, and dioxins. Some VOCs accumulate in the atmosphere over time [2]. Detected compounds include aromatics; mostly benzene, toluene, ethyl benzene and xylene (BTEX), various alcohols and alkenes. Today the emission of VOCs has increased in industrial and city atmospheres [3]. Once released into the environment, VOCs pose a health risk to living

organisms and can damage buildings [4]. VOCs may be present at low concentrations and long term exposure may result in mutagenic and carcinogenic effects [5].

Poor air quality, both indoor and outdoor, is a major concern in most developed countries. The majority of people in the city spend their time indoors thus being exposed to various indoor pollutants. Most importantly, poor air quality has induced a prevalence of poor health in humans [6] . Indoor sources are varied and include smoking, textiles, photocopiers and outdoor air that is circulated indoors. Negative effects arising from pollution has led to the development of VOC technologies to remove the pollutants. Volatile organic compounds are irritants and pollutants in the environment. Increasing VOC levels in the atmosphere has increased VOC emission awareness worldwide. Strict legislation is required to achieve effective VOC abatement.

1.2 VOC removal technologies

There are various VOC removal technologies that have been developed. They include: i) adsorption, ii) oxidation (thermal combustion) iii) photocatalytic degradation and iv) catalytic combustion. While they are normally used as separate technologies they can be developed in combination to provide higher efficiencies in VOC removal from the atmosphere. These abatement technologies are used to either recover or destroy VOCs.

Adsorption of VOCs on a suitable porous material is one of the simplest procedures used to remove VOCs. Materials such as activated carbon and zeolites are commonly used [7, 8]. The adsorption process is adversely affected by moisture, high concentrations of VOCs and the adsorption temperature [7]. Adsorption is merely a transfer of the pollutants from one phase (gas or liquid) into another phase (solid). The process is an equilibrium process and for adsorption to be effective, desorption processes must not occur to any significant extent. Also, key to effective adsorption is a materials ability to efficiently adsorb the VOCs

as concentration increases. Some materials also have the ability to absorb compounds discriminately.

Oxidation (thermal combustion) technologies involve the combustion of VOCs into carbon dioxide and water (1.1).

$$C_xH_y \ + \ O_2 \xrightarrow{\Delta} CO_2 \ + \ H_2O \qquad (1.1)$$

Traditionally the abatement of VOCs has primarily been by thermal combustion procedures. Thermal oxidation is the incineration of organic compounds in a gaseous feed containing oxygen to generate less harmful compounds. The difference between thermal oxidation and catalytic oxidation is that the latter entails the use of a catalyst. A thermal oxidation process is most inefficient in an air deficient environment and then requires high temperatures (> 500 ^{o}C) to effectively decompose VOCs. Low VOC concentrations also limit the extent of thermal incineration. This is problematic when there is a shortage of oxygen in the combustion reaction. The challenge that exists in air purification systems is to remove VOCs under ambient conditions from buildings in domestic and commercial settings.

Factors contributing to the photocatalytic degradation of VOCs include the wavelength of the UV radiation, the concentration of reactants in a homogenised mixture, operating temperatures and the radiant flux [9].

Catalysts permit oxidation to occur at lower temperatures (as low as 100 ^{o}C) than used in thermal oxidation. The advantage of using a catalyst is that it requires less energy and can eliminate VOCs present in a low concentration. It can be effective for both liquid and gas streams. Since it can be applied in an air medium, possible applications of catalysts for VOCs abatement are in cars, gas masks and in buildings.

1.3 Catalytic oxidation

Catalysts have been employed in various processes to generate safer and cleaner environments. Catalysts offer many advantages over other routes such as thermal oxidation for VOCs removal. Catalytic oxidation provides a high efficiency methodology to eradicate VOCs. In order for a successful catalytic oxidiser to be employed, the catalyst has to completely oxidize organic compounds into solely carbon dioxide and water. Partial oxidation can lead to the generation of dioxins and aldehydes.

Numerous catalyst systems have been produced to eliminate VOCs. These catalysts include first row transition metal oxides [10-12], lanthanide oxides such as such cerium and precious metals, such as typically platinum, palladium and gold [13, 14]. Precious metals are usually deposited on various support materials. An example of an industrially used catalyst for the CO oxidation reaction is Hopcalite [15, 16]. Hopcalite is a mixture Mn and Cu oxide in different ratios.

Major disadvantages of using a catalyst is that the catalyst can deactivate over time, due to chemical poisoning from elements such as sulphur and chlorine. Fouling can also occur. The cost of replacing a catalyst is often expensive when metals such as platinum are used. Some of these challenges can be overcome by re-activating the catalyst or simply avoiding the presence of contaminants in the inlet stream. Platinum based catalysts exhibit excellent activities for the decomposition of VOCs. The main challenge remains the cost of platinum.

One metal that has recently been used to remove VOCs is gold. Gold catalysts have been demonstrated to offer promising alternatives in combating pollution. Recently their effectiveness has been shown by studies of CO, NO_x and hydrocarbon oxidation. For many years gold was considered as chemically inactive. Since the 1980s gold is now seen as a

useful catalyst [17]. Gold has the potential to be used in alcohol, alkene and aromatic emission control systems and in hydrocarbon fuel combustion systems.

1.4 Aim

The aims of this study are indicated below:

- There exists a need for improved VOC abatement under ambient air conditions to enhance the quality of air. Catalytic combustion is a sought-after method for the removal of VOCs. In this thesis, the objective is to find a promising gold catalyst for use in low temperature VOC oxidation studies. The objective is thus to develop a catalytic combustion catalyst based on gold catalyst for VOC abatement.

- Another objective was to identify suitable compounds as VOC reactants, which could represent a range of volatile organic compounds, for catalytic combustion studies using gold-based catalysts.

- It was expected that gold catalysts could be synthesised by suitable wet chemical methods such as deposition-precipitation and co-precipitation. The new catalysts were to be characterised and activity studies performed on these gold catalysts.

- Manganese oxide would be studied as a support for the gold catalysts. The new Au/MnO_x complexes were to be compared with Au supported on TiO_2, CeO_2, Al_2O_3 and ZnO. The influence of the support on the gold catalysts and its activity towards VOC oxidation reactions was to be studied. Catalytic combustion reactions were to be carried out in a simple laboratory rig. Catalytic activity measurements were to be measured.

- In order to have a better understanding of the catalytic activity measurements; characterisation of the various supports and catalysts was to be carried out. This necessitated the use of diverse characterisation techniques such as, powder X-ray diffraction (XRD), H_2-temperature programmed reduction (TPR), N_2 physisorption and electron microscopy (EM). Inductively coupled plasma (ICP) measurements were used to evaluate the elemental composition of the new materials.

1.5 Thesis content

- Chapter 2 comprises a literature review featuring the use of gold catalysts, with regards to CO and hydrocarbon oxidation reactions. The main focus was on literature that relates to VOC oxidation reactions by solid gold catalysts. An outline of various catalyst preparation methods and characterisations techniques is also given.

- In Chapter 3, the experimental work is described. This includes a discussion of the synthesis of the various catalyst samples and the characterisation methods used to elucidate the properties of the catalyst and support. Reactor studies are also described.

- Chapter 4 covers the results obtained from the activity studies and correlates the data with the properties of the catalyst and its support. The catalyst chosen were Au supported on range of manganese oxide materials. This would be more detailed later.

- Conclusions of this study, along with a brief summary of the findings are given in Chapter 5. The goals, set in chapter 1, are reviewed and matched up to the conclusions to answer the research questions.

1.6 Reference

[1] A.B. Hansen and F. Palmgren, Sci. Total Environ. 189-190 (1996) 451-457.

[2] W. Jiang, D.L. Singleton, M. Hedley and R. McLaren, Atmos. Environ. 31 (1997) 627-638.

[3] S.O. Baek, Y.S. Kim and R. Perry, Atmos. Environ. 31 (1997) 529-544.

[4] E. Gallego, X. Roca, J.F. Perales and X. Guardino, J. Environ. Sci. 21 (2009) 333-339.

[5] M.R. Ashmore and C. Dimitroulopoulou, Atmos. Environ. 43 (2009) 128-141.

[6] J.M. Samet, M.C. Marbury and J.D. Spengler, J. Allergy Clin. Immunol. 79 (1987) 685-700.

[7] B. Garrot, M.H. Simonot-Grange and B. Clausse, Stud. Surf. Sci. Catal. 125 (1999) 683-690.

[8] X. Canet, J. Nokerman and M. Frère, Adsorption 11 (2005) 213--216.

[9] D. Vildozo, C. Ferronato, M. Sleiman and J.-. Chovelon, Appl. Catal. B: Environ. 94 (2010) 303-310.

[10] L.A. Palacio, J. Velásquez, A. Echavarría, A. Faro, F.R. Ribeiro and M.F. Ribeiro, J. Hazard. Mater. 177 (2010) 407-413.

[11] D.P. Debecker, R. Delaigle, P. Eloy and E.M. Gaigneaux, J. Mol. Catal. A: Chem. 289 (2008) 38-43.

[12] J.I. Gutiérrez-Ortiz, B. de Rivas, R. López-Fonseca and J.R. González-Velasco, Appl. Catal. B: Environ. 65 (2006) 191-200.

[13] J.J. Spivey and J.B. Butt, Catal. Today 11 (1992) 465-500.

[14] E.M. Cordi and J.L. Falconer, J. Catal 162 (1996) 104-117.

[15] A.B. Lamb, W.C. Bray and J.C.W. Frazer, J. Ind. Eng. Chem. 12 (1920) 213-221.

[16] E.C. Njagi, C.H. Chen, H. Genuino, H. Galindo, H. Huang and S.L. Suib, Appl. Catal. B: Environ. 99 (2010) 103-110.

[17] M. Haruta, N. Yamada, T. Kobayashi and S. Iijima, J. Catal 115 (1989) 301-309.

CHAPTER 2

2. LITERATURE REVIEW

2.1. Gold catalysis

Having discussed in the previous chapter the need for catalysts in the removal of volatile organic compounds (VOCs), this chapter presents a discussion about the use of gold based catalysts; in particular the development and improvement of gold catalysts for oxidation reactions. This information will provide the basis of studying gold catalysts in the oxidation of VOCs. A survey of the literature shows that gold catalysts can be used for the oxidation of a wide range of compounds [1-4]. Oxidation reactions are an important class of reactions; these include both partial and complete oxidation, in both industrial and environmental applications. CO oxidation (2.1) is one of the most studied oxidation reactions over gold catalysts.

$$2CO + O_2 \xrightarrow{\Delta} 2CO_2 \qquad 2.1$$

There are many catalysts involving transition metals that have been used in the CO oxidation reaction, V_2O_5 being one of them. CO oxidation is an important reaction required for industrial and environmental air purification. Our understanding of gold catalysts is to a large extent built on the study of the CO oxidation reactions. Prior to the 1986 report by Haruta and co-workers, there were reports on the use of gold catalysts in hydrogenation and isomerisation reactions. In 1973, Bond and Sermon reported on the use of gold catalysts, Au/SiO_2 and Au/Al_2O_3, prepared by an impregnation method. Although the activity was not correlated with particle size (50 nm) adding gold to the support created active sites on the supports that were able to facilitate the hydrogenation reaction of pent-1-ene, buta-1,3-diene and but-2-yne at 100 ^{o}C [5, 6]. Gold was however disregarded as a partial oxidation and complete oxidation reaction catalyst. This was justified by electron orbital arguments. Gold contains very diffuse s and p valence orbitals and an absence of partially

filled d-orbitals and consequently chemisorption of small molecules such as hydrogen and oxygen below 200 ^{o}C was not expected [7].

From the literature it is evident that one of the most important experimental parameters, for obtaining good catalytic activity is the preparation method of the catalyst. The preparation method determines the structure of the catalyst which has an implication on the reaction. It has been shown that different catalyst preparation methods lead to different catalytic activities and surface characteristics [8-10]. There are many synthesis procedures used for the making of gold catalysts. These include impregnation, co-precipitation, co-sputtering, gas or liquid phase grafting, direct anion exchange, cation deposition, UV photoactivation, colloid formation and deposition-precipitation [8-14]. A list of general preparation methods for the synthesis of gold catalysts is outlined below. These methods have relevance with regards to the synthesis of Au/MnO_x catalysts described in this dissertation.

2.2. Gold catalyst preparation methods

2.2.1. Impregnation and co-precipitation method

The impregnation method is a simple preparation method. A gold solution is added to the powdered support, and allowed to dry before the solid catalyst is heat treated. Gold prepared by the impregnation method leads to the formation of poorly dispersed large gold particles with high chlorine content [5, 6, 15]. Gold catalysts prepared using this method are uncommon. Gold particle size is an important characteristic of a gold catalyst. Small hemispherical gold particles were formed on Fe_2O_3 support particles prepared by a co-precipitation method. These were found to be active for the CO and H_2 oxidation reactions [16]. In co-precipitation, the gold and support are precipitated from solution by adding a base to the precursors. This process results in the formation of solid metal hydroxide

species. The formation of the metal oxide is obtained by heat treatment. Ivanova and co-workers have claimed a new preparation method involving direct anionic exchange. In this method, a gold solution is added to a metal oxide, and the gold reacts through anionic exchange with the metal support hydroxyl surface groups. This method proved to be successful for adding gold to alumina and silica. It appears as a variation of the impregnation method [14].

2.2.2. Colloidal gold

Colloidal gold is a suspension of nanometer-sized gold particles in a solvent. Gold nanoparticles can be easily produced by adding a reducing agent such as sodium citrate, sodium borohydride or sodium alginate to chloroauric gold solution with vigorous stirring [11, 17]. Prefabricated gold particles formed as colloids can be deposited on different support materials. The deposition process does not change the gold particle sizes. TiO_2, Al_2O_3 and ZnO are typically used as support materials. This allows for the evaluation of the support effects on the catalytic activity.

Reducing and stabilising agents are of importance in the synthesis of gold colloids. These need to be freshly prepared prior to use. Both sodium citrate and borohydride can act as reducing agents. They cause Au^{3+} ions to be reduced to neutral gold atoms; eventually gold starts to precipitate in the form of nano particles. To encourage colloid stability, stabilizing agents are added. The stabilizing agents adsorbed onto the gold nanoparticles introduce a surface charge onto the gold nanoparticle surface. The charged gold nanoparticles repel each other and this prevents aggregation. Stabilizing agents can be functionalized with various organic ligands to create materials with advanced properties. Poly(n-vinylalcohol) (PVA) and polyethylene glycol (PEG) are commonly used as stabilising agents. Pal and co-workers showed that when sodium alginate was used, the reagent concentration altered the different particle sizes [12]. The sodium alginate acted as a reducing agent and stabilising agent. The stabilising agent contains terminal carboxyl groups which have a high

affinity towards oxygen groups found on the metal support. The presence of terminal groups on the nanoparticles is chosen with this application in mind.

The properties of gold nanoparticles depend on the shape of particles in addition to their sizes. UV-vis spectra of Au nanoparticles solution show a peak at 545 nm that relates to the energy state of the conduction band of the metal commonly known as its surface plasmon resonance. This is an important property of gold nanoparticles and is associated with new materials and their properties. The most notable characteristic of a gold colloid solution is its colour which also gives an indication of its particle size. An intense red-wine to purple colour indicates particles that are < 100 nm and a yellow colour is associated with particles > 100 nm. The Au particles have unique optical and electronic properties and thus have found many uses. These include their use as colouring agents in biological applications, standards in sizing applications such as UV-Vis, EM and AFM, solar cell efficiency enhancement studies, nanotechnology, medicinal environments and the synthesis of new materials with specific properties.

2.2.3. Deposition-precipitation

The deposition-precipitation (DP) method is widely used to make gold catalysts. DP involves the slow precipitation of gold onto the support while monitoring the pH and temperature of the solution. A major drawback with the DP process is that it is difficult to control and this can lead to a catalyst with varying properties. It can also be difficult to reproduce the exact product composition using this method. A change in the pH, base, time, reaction temperature and gold solution concentration results in catalysts with dissimilar catalytic properties and activity. Thus, Au/Fe_2O_3 samples produced by Khoudiakov and co-workers [18] gave catalysts with varying properties as the conditions were varied.

The DP method is pH sensitive. Different gold species are formed at different pH values. $Au(OH)_4^+$ is formed at pH 6-10 and is deposited on an added support where it appears as $Au(OH)_3$ species [19, 20]. The formed species adds to the support surface hydroxyl groups as shown below

$$M - OH + [Au(OH)_x]^- + Cl^- \rightarrow M - [O - Au(OH)_{x-1}]^- + H_2O + Cl^-$$

An isoelectric point (IEP) or point of zero charge (PZC) for the support that is ≥ 5 is essential for the effective adsorption of gold particles onto a support. This necessitates using a gold solution with a concentration of 10^{-3} M [21]. Gold is not easily added to supports like carbon and SiO_2 by the DP method because they have a low IEP. Particle size formation is sensitive to pH changes [22]. Haruta and co-workers found a positive relationship between pH and particle size. At pH 6-10 particle have sizes with daimeters 5 nm and below [20].

The gold precursor solution concentration also plays a role in the particle size formation. A high $HAuCl_4$ solution concentration was found to give larger particles. Hence, low gold solution concentrations are used to prepare the supported gold catalysts. CO conversion increase with Au loadings but higher loading than 10 wt.% has been shown to be detrimental to activity [20]. Various bases have been used to precipitate Au in the DP synthesis. These include urea, ammonia, NaOH and Na_2CO_3 [22, 23]. The type of base used in a DP process has an effect on the physio-chemical properties of the catalyst. This has been examined by Lamallem and co-workers. In their comparison, $Au/Ce_{0.3}Ti_{0.7}O_2$ prepared from urea was more active for propene oxidation than the same catalyst prepared with NaOH in the same reaction [15]. The use of ammonia as base is avoided because it could lead to fulminating gold [24]. DP using NaOH or urea is the most used method for depositing gold because the methods allow for high OH concentrations leading to higher Au loadings. The solution is heated to 70 - 80 °C to allow for urea decomposition. Also deposition time has an impact on the Au particle size and loadings [8].

Washing of the catalyst prior to study is a significant step in making supported catalysts. This is to remove impurity ions. The washing process allows for the removal of Cl ions from

highly dispersed gold nanoparticles. This occurs when the $HAuCl_4$ precursor is used as the source of gold. Chlorine promotes gold mobility on a support thus leading to Au agglomeration [25]. Catalysts can be washed with ammonia to remove Cl ions [26]. Washing with ammonia assists in controlling the particle size, yeilding a narrow Au particle size and size ranges as opposed to the conventional DP process [9, 14]. An alternative to $HAuCl_4$ as the gold precursor is to use $[Au(en)_2]Cl$ [9, 27]. $HAuCl_4$ is commercially available and much easier to handle.

Calcination temperature effects have revealed that at temperatures above 300 °C larger Au particles form. Also the calcination atmosphere has an impact on the Au particle size. Calcining under N_2 at 250 °C gives Au with a particle size of 2.7 nm while under air the average particle size was 3.3 nm [20]. Beyond 450 ^{o}C gold particles start to sinter [28]. Haruta et al and Buffet et al have indicated that Au particles > 5 nm are easily reduced and agglomerate when Au particles are heated above 400 ^{o}C. The thermal treatment of the gold catalysts above 400 ^{o}C resulted in a decreased activity for the Au catalysed CO oxidation reaction.

Calcination temperatures can also influence the surface area of both support and the gold catalyst [26]. Optimum temperatures are required. A low temperature has no effect while too high a temperature results in a coalesced structure. Improvement of support crystallinity can be attained by a high calcination temperature. Calcination leads to the formation of spherical gold particles being deposited on a metal support. Calcination temperature provides differential characteristics for a catalyst. Catalyst treatment is also essential for establishing Au-support interactions which are strong or make the catalyst more resistant to deactivation. Also, the reduction of a gold catalyst has been undertaken by Boyd et al. Partial reduction by reducing agents such as $NaBH_4$ promoted formation of ionic Au (Au^{+}). Although gold particles with a size of 10 nm were made by treatment with sodium borohydride, markedly improved CO oxidation catalytic activity was observed. But ionic gold species can be observed on a catalyst without partial reduction [27]. Haruta and

Hugon et al have opposing views with regards to the effect of Au catalysts treatment by H_2 reduction.

Haruta reported that DP has an advantage over co-precipitation methods in making Au particles [29]. This is because the DP method favours a high gold surface coverage and thus more active metal atoms are exposed during reaction [18].

2.2.4. Other preparation methods

As already mentioned, there are many methods of preparation that are used to make Au particles. Other techniques worth mentioning are the laser ablation of gold metal discs to produce gold nanoparticle reported by Singh and co-workers [30]. Also, a photo-irradiation method which involves deposition of Au particles onto the support while irradiating a Au solution with UV light [12].

2.3 Characterisation techniques for gold based catalysts

We now turn to the structure of the catalyst; the structure impacts on the inherent properties of the catalyst. This includes the oxidation state of the Au catalyst, the Au particles size or distribution, metal-support interactions and the nature of the support. The activity of catalyst depends on the properties of the catalyst. Different analysis techniques were used for the investigation to determine the different properties of the gold catalysts. The techniques used in this study include: powder X-ray diffraction (XRD), H_2-temperature programmed reduction (TPR), N_2 physisorption and electron microscopy (EM).

2.3.1 Electron microscopy (EM) technique

This is a very useful technique to characterise gold catalysts. Gold particle size, morphology and particle size distribution is determined by electron microscopy. As with any technique there are thresholds; poor image contrast between gold and support particles can lead to misleading results. The electron Dispersion X-ray (Scanning) (EDX-S) method coupled with EM allows for the possibility of measuring the Au concentration and even detects the presence of species present and their location. The EM images give an insight into the nature of active sites and the chemical composition of the material.

High resolution-electron microscopy (HR-TEM) images proved useful in elucidating the Au particle phases when particles are embedded on a support. The phase of individual particles can be investigated. Fine tuning the particle size alters the band gap and thus the reactivity of the metal. The gold nanoparticles observed under TEM are usually seen as hemispheres or as full ellipsoids.

2.3.2 Temperature programmed reduction

Amongst the very diverse properties used to elucidate the chemical properties of a catalyst is its reduction state. Temperature programmed reduction (TPR) studies attempt to elucidate the thermal stability of a catalyst and can be used for composition determination. Reduction characteristics of supported metal samples are often different from a catalyst, due to metal-support contributions. Supports, such as SiO_2 and Al_2O_3, are considered “inert” as they have a poor ability to supply oxygen species under reaction conditions. Other supports involve a flow of electrons from the lattice to surface sites through creation of vacant sites.

The change in reducibility of the metal can be affected by a spillover of hydrogen from the metal to a support. Hydrogen spillover is a process whereby hydrogen atoms are transferred onto the metal oxide or support by a heterogeneous metal catalyst. This spillover results from hydrogen that was initially adsorbed on the metal. Thus a strong gold support interaction allows hydrogen to react with the support. Yamashita and co-workers reported Au-Mn catalyst prepared by the co-precipitation method. A redox cycle involving Mn^{2+}/Mn^{4+} and Au^{3+}/Au^{0} favoured the formation of Mn-O-Au bonds [31].

Gold is easily reduced; thus drying and calcining of a Au catalyst can result in a reduction of Au ions to the metal state. When TPR studies are performed on a Au-supported material no gold reduction peaks are observed. Wang et al postulated that the low surface gold species could be a result of gold encapsulation into the internal structure of a support [32] as a result of strong metal-support interactions. Gold particle sizes have been shown to have an influence on the activity of Au/ZrO_2 towards CO oxidation [33]. Gold particles are well dispersed on the support and conceivably interact strongly with the support as seen by a shift of TPR peaks. But the nature of support also seems to play a role owing to the reducibility of oxides.

2.3.3 X-ray diffraction (XRD) technique

Solids samples can be characterised by powder X-ray diffraction (XRD) spectroscopy at room temperature to give information on the catalyst phase composition. Diffraction patterns are recorded over 2 theta ranges which will enable relevant peaks to be identified for evaluation of the crystalline phase of the catalyst. The Scherrer equation is used to measure the crystallite size (equation 2.1):

$$d = \frac{0.9\,\lambda}{\beta\ Cos\ \theta} \tag{2.1}$$

where d is the mean crystallite size, λ is the wavelength of the X-ray source, β the width of the diffraction peak taken at half maximum intensity and θ is the diffraction peak angle.

XRD reveals the overall bulk proportion of a sample. It can be used to determine gold particle sizes on various supports such as Al_2O_3 [23]. The support crystallinity and integrity can be validated by comparison with XRD patterns of known materials. For example strong intense peaks for bulk gold are observed at 2θ = 38 and 44°. A 1 wt.% gold loading of Au only gives very weak diffraction signals, but the Au particle size can be measured by line broadening of the 2θ bands at 38 and 44 °. XRD can measure particle sizes of ~ 5 nm.

2.3.4 Other characterisation techniques

X-ray photoelectron spectroscopy (XPS) is a surface analysis technique that measures the surface composition of a local structure. The spectrum from an XPS profile shows the binding energy of inner core electrons which appear at particular energies. A set of characteristic peaks of precise energy indicates the presence of a specific element. The intensity of the peaks relates to the amount of the specified element. X-ray photoelectron spectroscopy (XPS) determines the surface composition of a catalyst and the nature of active sites. XPS can be used to follow changes in the catalyst surface. The presence of ionic or metallic Au can be established on a catalyst by XPS. There is contention in the literature about which Au oxidation state is most influential in oxidation reactions. A study of the catalyst by XPS can reveal the gold surface coverage.

Catalysis is mostly a surface phenomenon. Thus activity is proportional to surface area assuming all other factors are constant. Many catalysts are prepared with a relativity high surface area and include Au/Fe_2O_3. High surface areas can stabilise Au particles and decrease sintering [26]. It is generally accepted that high surface area catalysts have more active species exposed and ultimately this leads to higher activity. Gold catalysts are no exception.

2.4 Gold catalysts in oxidation reactions

The use of gold catalysts in homogeneous and heterogeneous catalytic reactions is now firmly established. Gold clusters and complexes involving Au^{+1} and Au^{+3}, have been prepared and can perform various homogeneous organic transformations. Some of the reactions include: coupling, metathesis, hydrogenation and chlorination of hydrocarbons [1-3]. Gold catalysts have been used in many heterogeneous reactions. These include: the water-gas shift, epoxidation of propene and oxidation of hydrocarbons.

Advancement in fuel cell technology has led to growing interest in the low temperature water gas shift (WGS) reaction. The WGS reaction is a potential method for producing high purity H_2 gas for fuel cells. Also, in the WGS reaction removal of CO from automobile exhausts by reaction of CO with H_2O to give CO_2 and H_2 is possible:

$$CO + H_2O \rightarrow CO_2 + H_2.$$

Studies on Au nanoparticles deposited on CeO_2, TiO_2, Al_2O_3 and Fe_2O_3 have shown that Au is active for the WGS reaction [34, 35]. The WGS reaction over gold as a catalyst strongly depends on the interaction of Au nanoparticles with the support which creates suitable sites for the CO adsorption. A strong CO adsorption is a pre-requisite for reaction to occur. The Au cationic species have a high affinity for CO which is reduced on dissociation of H_2 and water molecules which take place on the defects created on the support. Costello showed how Au/Al_2O_3 in the presence of water or H_2 in the CO oxidation reaction improved the activity of the catalyst towards CO oxidation [4].

Also, propylene or propene epoxidation is a widely studied reaction on gold catalysts. Propene epoxidation by gold catalysts was only reported recently. Propene epoxidation produces propylene oxide (1,2-propylene oxide), an important precursor in the production of polyurethane. A supported gold catalyst showed very high selectivity for the propene epoxidation. Much of this work has recently been reviewed by Sinha et al [36]. Sinha et al demonstrated that formation of propylene oxide on Au-titanosilicates occurred on the

hydroxyl groups on the support surface. This was critical in order to avoid production of propanol, acetone and CO_2.

2.4.1 VOC oxidation reactions

We now turn to gold based catalysts used in the oxidation reaction of volatile organic compounds using air as a source of oxygen. The ideal total oxidation catalyst would be one that adsorbs and activates the reactants and is able to completely oxidise the organic compound and even the partial oxidation products. The study of VOC oxidation is largely performed using one component in the gas stream. Multiple VOCs in the gas stream are a better reflection of real working conditions but introduce complexity via competing reactions [37]. Lahousse showed that hexane conversion decreased by 30% when ethylacetate was also present in the gas stream. Volatile organic compound oxidation catalysts typically involve metal oxides and precious metals supported on metal oxides.

Base metals have been tested for the oxidation of VOCs and show poor activity. However, when used as novel materials such mesoporous and ternary oxides have been shown to give improved reactivity. Scire et al showed mesoporous chromium oxide was a good material for the potential adsorption and combustion of toluene and acetaldehyde compared to commercial chromium oxides [38]. Titanosilicate, with the titania well dispersed onto the silica, was found to be effective for the propene oxidation reaction. $Ce_xTi_{1-x}O_2$ samples were investigated by Lamellem and co-workers and by varying x, the mole fraction in the ceria (x= 0 - 0.3) varying catalytic activities were observed [15]. Increasing Ce content greatly improved the catalyst for propene oxidation.

The catalytic oxidation of VOCs is generally performed on industrial samples that contain methanol, ethanol, 2-propanol, toluene, benzene, propene, hexane, ethyl acetate, formaldehyde and acetyl aldehyde. Scire et al studied the oxidation of three VOCs including

methanol, 2-propanol and toluene over Au/Fe_2O_3. Methanol and toluene were decomposed to CO_2 and water only and 2-propanol oxidation products included partial oxidation to acetone [39]. Au/Fe_2O_3 maintained a low temperature light off reaching T_{90} at 130 °C while the Ag/Fe_2O_3 and Cu/Fe_2O_3 occurred at temperatures above 200 °C. Haruta et al reported activity studies on Au/Fe_2O_3 and found that 50% methanol could be oxidized to CO_2 at temperature about 100 °C. The reaction was accompanied by formation of formaldehyde, formic acid and water [20]. They reported that H_2CO and HCO_2H were partial oxidation products. When H_2CO and HCO_2H were oxidised by the same catalyst, they were oxidised at lower temperatures than found for methanol.

The oxidation of VOCs is proposed to go via a Mars van Krevelen mechanism. This requires the presence of active lattice oxygen (nucleophillic) and surface oxygen (electrophobic) sites. The most important step in a combustion reaction is the rate at which oxygen is activated. There is a positive correlation between a higher degree of reducibility and the catalytic oxidation of VOC. It was suggested that the effects of the reducibility of the catalyst can override the effects of particle size distribution [40]. Also the reactant orientation and absorption rate determine whether partial or complete oxidation products are formed.

The active oxygen on gold is consumed in the oxidation of hydrocarbons or CO. In the case of CO oxidation the reducible oxide acts as the oxygen carrier [26]. A possibility of oxygen spillover is proposed to occur. Gluhoi et al prepared Au/Al_2O_3 and showed that it was able to activate CO, O_2 and H_2 at low temperature [23]. Much attention has been given to elucidating the active site rather than the gold particle sizes. This does not diminish the importance of Au nanoparticles in creating active catalysts. The active site varied with the preparation method and support used. DP produced mixed surface Au species (Au°, Au^{1+} and Au^{+3}). Also the cation present depended on the support used. Metallic gold was not the active site but the Au^{+1} which is stabilised as AuO^- by the mobile surface oxygen from the reducible oxide support was found to be the active site. A catalyst produced by a solvated metal atom dispersion (SMAD) method showed no ionic Au species and these catalysts were active for CO oxidation [41]. Pireaux and co workers studied the interactions of an Au surface with oxygen and showed that Au either adsorbs atomic or molecular oxygen on its

(110) and (111) surface. These were the more influential sites for the oxidation reaction than other Au crystal planes because of the higher surface area and higher concentration of OH groups [42].

The lower dissociative energy of C-H bonds would result in a higher rate of C-H bond cleavage as was determined by Finocchio et al [43]. Poorly polar were compounds such as methane required high temperatures for C-H activation. Polar reactants catalysed at low temperature and proceeded through intermediate carbonyl compounds which further oxidised to CO and CO_2.

2.5 MnO_x based catalysts

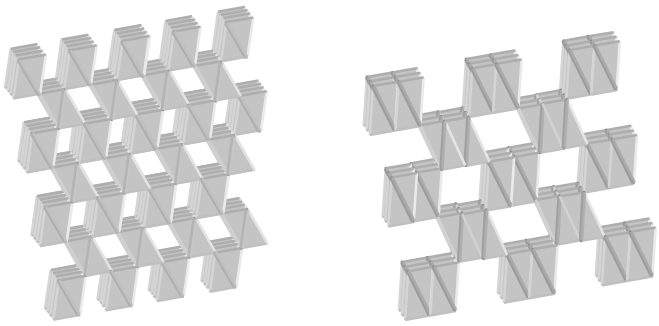
Manganese oxides, in varied oxidation states, have been shown to be active for CO and VOC oxidation reactions [40, 44-47]. The activity of Mn oxide catalysts is attributed to the availability of labile oxygen atoms [48] which facilitate the reducibility of the metal oxide. However, Mn based catalysts in conjunction with noble metals offer a superior catalyst [45, 49].

MnO_2

In a recent paper, Sinha and co-workers investigated γ-MnO_2 for the catalytic oxidation of toluene and acetyldehyde at 100 ^{o}C [49]. Lahousse also showed γ-MnO_2 was a better catalyst than a Pt/TiO_2 catalyst for the oxidation of ethylacetate and hexane. A 100 % conversion of hexane to CO_2 and water over γ-MnO_2 at 180 ^{o}C was observed. At the same temperature, 180 ^{o}C, only 30% ethylacetate conversion was observed when Pt/TiO_2 was used. Cellier et al [10] studied the oxidation of n-hexane over Au supported catalysts and found that T_{90} was reached at 177 $^{\circ}$C for Au/γ-MnO_2 while using the same conditions, oxidation over Au/TiO_2 T_{90} was reached at 319 $^{\circ}$ C.

Mn_3O_4 [46] oxidation of various allyl compounds (acetone, propane, propene, propanol, propenal) was achieved at a light off temperature of 350 °C. The bulk of studies on manganese oxides has been based on mixed valent complexes. Other manganese oxides include cryptomelane and Mn_2O_3 have been tested in oxidation reactions [44, 50]. The oxidation state of Mn is most influential when using amanganese oxidise based catalyst [44].

MnO_2 has many polymorphic states and the most common ones are α, β, γ and λ [51]. β-MnO_2 (pyrolusite) is the most naturally abundant MnO_2 polymorph. MnO_2 phases are constructed from chains of MnO_6 octahedra units, which are linked in different ways. β-MnO_2 has a rutile structure with the oxygen atoms forming a slightly distorted hexagonal closely packed array. The basic motif of this tetragonal structure is an infinite chain of octahedral sharing opposite edges, with each corner linked by four similar chains forming (1x1) tunnels.



Pyrosulite ramsedillite

The ramsdellite structure consists of double chains with each octahedron sharing an edge, with its neighbour chain forming (2x2) tunnels.

The γ-MnO_2 structure is known to incorporate defects: γ-MnO_2 has been described as built up from pryrosulite elements interspersed in a ramsedellite matrix combination of (1X2) and (2X2). The variation in γ-MnO_2 is possible through the combination of various De Wolf defects and microtwining [52]. De Wolff defects correspond to the percentage of rutile type structural units and microtwinning are the packing faults within the ramsedellite structure.

An increase in De Wolf defects or percentage of pyrosulite, is detected by the shift in (110) XRD peaks to higher 2θ angles [53].

The structure of β-MnO_2 is denser than that of γ-MnO_2, because of the packing of the MnO_6 units. Both have Mn vacancies replaced by Mn^{3+} or protons. The presence of Mn^{3+} in the structure causes a weakening of Mn-O bonds and strengthening of corresponding surface O-H bond (the amphoteric active sites) [54]. Also in this regard, γ-MnO_2 and β-MnO_2 can have different catalytic activities corresponding to their different surface structures. γ-MnO_2 is believed to be catalytically more active than β-MnO_2 (pyrolusite) because of its high surface area, created by internal porosity. γ-MnO_2 can be prepared by different synthetic routes to produce MnO_2 with varying morphologies, surface areas and catalytic activity [49, 55, 56]. A survey of the literature shows that not many studies have compared γ-MnO_2 and β-MnO_2 as catalysts.

The commonly used method to synthesise γ-MnO_2 is the oxidative electrodeposition method but there are simpler methods which have been used such as those outlined by Lamaita. As to be expected, different methods of preparation produced varying γ-MnO_2 characteristics [55]. The crystallinity and electrochemical properties of MnO_2 were affected.

Increasing the amount of gold loaded on a catalyst results in an increase in the activity of the Au based catalyst. However larger Au loadinds (> 15%) leads to decreased overall activity of an Au/MnO_x catalyst [45]. Probably large Au particles show poor dispersion.

Stobbe showed that manganese oxides were capable of oxidising methane in the absence of gas phase oxygen at very high temperatures [57]. The Mn oxides showed good properties suitable for oxidation reactions even under oxygen deficient conditions due to their superior lattice oxygen motion. The oxidation of ethanol with no supply of oxygen was successfully achieved at 240 ^{o}C to give only carbon dioxide and water [44]. After storing oxygen, MnO_2

can provide oxygen to the active site to oxidise CO and hydrocarbons. Buciuman et al have shown that the ability of Mn to donate oxygen helps create active sites used for the adsorption of VOC [58]. Once the oxygen is used it is replenished from the gas stream. Mn stores the oxygen and it is then mobilized as an active oxygen species to facilitate the oxidation reaction. Thus, the weaker the Mn-O bond, the higher activity expected.

It has been reported that the presence of CO_2 in a gas stream was detrimental to the activity of Pt/SnO_x but not Au/MnO_x for the CO oxidation reaction. However, the catalyst can be re-activated by heating the catalyst under air. Au/TiO_2 and Au/Fe_2O_3 were used for the alcohol oxidation in the presence of supercritical CO_2 [59]. CO oxidation using Au/β-MnO_2 and Au/CeO_2 based catalysts activity depends on the crystallinity of the support [40].

2.6 Ce and Au/CeO_2 catalyst

The ability of CeO_2 to catalyse oxidation reactions has prompted studies on its use in gold based catalysis. Au/CeO_2 was found to have high activity and stability for selective CO oxidation. Also, many studies on the use of CeO_2 in preferential CO oxidation in the presence of H_2 (PROX) and in the water gas shift (WGS) reaction have been reported. Au/CeO_2 is a very influential support in gold catalysis due to its ability to provide its lattice oxygen for reactions.

Ceria promotes oxidation reactions when added to Au/TiO_2 and Au/Al_2O_3 catalysts [60, 61]. Gold supported on ceria was found to be quite active for the oxidation of VOCs. Au/CeO_2 prepared by deposition-precipitation was more active than Au/TiO_2, Au/Al_2O_3 and Au/Fe_2O_3 for the 2-propanol oxidation reaction. These results demonstrated that ceria-supported gold can be a useful catalyst for the oxidation of volatile organic compounds. The activity of a ceria-based catalyst is known to depend greatly on its structure. Nanosized ceria shows higher activity than bulk phase ceria because of the easier reduction of the surface oxygen species on ceria nanoparticles.

$Au/Ce_{0.3}Ti_{0.7}O_2$ catalysts were more active than the support itself for the propene oxidation reaction and produced a stable catalyst able to withstand 3 cycles of reaction. Also, it was shown that high surface area and high gold loaded catalysts were more active. High surface area ceria is easily prepared by co-precipitation of a ceria nitrate solution by a base. Akita et al used high resolution TEM images of Au/CeO_2 to claim that Au particles on high surface area ceria tended to be small [62]. Although the surface area decreased when Au was loaded on the $Ce_{0.3}Ti_{0.7}O_2$ support the light off temperature for oxidation of propene decreased. Lamallem et al showed propene oxidation at T_{90} for $Au/Ce_{0.3}Ti_{0.7}O_2$ at 270°C [15].

2.7. Reference

[1] S.K. Beaumont, G. Kyriakou and R.M. Lambert, J. Am. Chem. Soc. 132 (2010) 12246-12248.

[2] B. Campo, M. Volpe, S. Ivanova and R. Touroude, J. Catal 242 (2006) 162-171.

[3] C. Nieto-Oberhuber, M.P. Muñoz, E. Buñuel, C. Nevada, D.J. Cárdenas and A.M. Echavarren, Angew. Chem. Int. Ed. 43 (2004) 2402-2406.

[4] C.K. Costello, M.C. Kung, H.S. Oh, Y. Wang and H.H. Kung, Appl . Catal. A-Gen. 232 (2002) 159-168.

[5] G.C. Bond, P.A. Sermon, G. Webb, D.A. Buchanan and P.B. Wells, J. Chem. Soc. Chem. Comm. (1973) 444-445.

[6] G.C. Bond and P.A. Sermon, Gold Bull. 6 (1973) 102-105.

[7] G.C. Bond, Gold Bull. 5 (1972) 11-13.

[8] R. Zanella, L. Delannoy and C. Louis, Appl . Catal. A-Gen. 291 (2005) 62-72.

[9] R. Zanella, S. Giorgio, C.R. Henry and C. Louis, J Phys Chem B 106 (2002) 7634-7642.

[10] C. Cellier, S. Lambert, E.M. Gaigneaux, C. Poleunis, V. Ruaux, P. Eloy, C. Lahousse, P. Bertrand, J.P. Pirard and P. Grange, Appl. Catal. B: Environ. 70 (2007) 406-416.

[11] D. Philip, Spectrochim. Acta A 71 (2008) 80–85.

[12] A. Pal, K. Esumi and T. Pal, J. Colloid Interface Sci. 288 (2005) 396-401.

[13] S. Arrii, F. Morfin, A.J. Renouprez and J.L. Rousset, J. Am. Chem. Soc. 126 (2004) 1199-1205.

[14] S. Ivanova, V. Pitchon and C. Petit, J. Mol. Catal. A: Chem. 256 (2006) 278-283.

[15] M. Lamallem and H. El Ayadi, C. Gennequin, R. Cousin, S. Siffert, F. Aïssi, A. Aboukaïs, Catal. Today 137 (2008) 367-372.

[16] M. Haruta, N. Yamada, T. Kobayashi and S. Iijima, J. Catal 115 (1989) 301-309.

[17] M. Comotti, W.C. Li, B. Spliethoff and F. Schuth, J. Am. Chem. Soc. 128 (2006) 917-924.

[18] M. Khoudiakov, M.C. Gupta and S. Deevi, Appl . Catal. A-Gen. 291 (2005) 151-161.

[19] M. Haruta, Gold Bull. 37 (2004) 27-36.

[20] M. Haruta, A. Ueda, S. Tsubota and R.M. Torres Sanchez, Catal. Today 29 (1996) 443-447.

[21] J. Hu, L. Chen, K. Zhu, A. Suchopar and R. Richards, Catal. Today 122 (2007) 277-283.

[22] A. Hugon, N.E. Kolli and C. Louis, J. Catal 274 (2010) 239-250.

[23] A.C. Gluhoi, N. Bogdanchikova and B.E. Nieuwenhuys, J. Catal 229 (2005) 154-162.

[24] J.M. Fisher, Gold Bull. 36 (2003) 155.

[25] H.S. Oh, J.H. Yang, C.K. Costello, Y.M. Wang, S.R. Bare, H.H. Kung and M.C. Kung, J. Catal 210 (2002) 375-386.

[26] S.Y. Lai, Y. Qiu and S. Wang, J. Catal 237 (2006) 303-313.

[27] D. Boyd, S. Golunski, G.R. Hearne, T. Magadzu, K. Mallick, M.C. Raphulu, A. Venugopal and M.S. Scurrell, Appl . Catal. A-Gen. 292 (2005) 76-81.

[28] P. Buffat and J.P. Borel, Phys. Rev. A 13 (1976) 2287-2298.

[29] M. Haruta, Cattech 6 (2002) 102-115.

[30] A. Singh, A. Rai and D. Bicanic, Instrumentation Science and Technology 37 (2009) 50-60.

[31] M. Yamashita, H. Ohashi, Y. Kobayashi, Y. Okaue, T. Kurisaki, H. Wakita and T. Yokoyama, J. Colloid Interface Sci. 319 (2008) 25-29.

[32] L.C. Wang, L. He, Y.M. Liu, Y.H. Cao H.Y., K.N. Fan and J.H. Zhuang, J. Catal 264 (2009) 145-153.

[33] P. Konova, A. Naydenov, T. Tabakova and D. Mehandjiev, Catal. Commun. 5 (2004) 537-542.

[34] T. Tabakova, F. Boccuzzi, M. Manzoli and D. Andreeva, Appl . Catal. A-Gen. 252 (2003) 385-397.

[35] F. Boccuzzi, A. Chiorino, M. Manzoli, D. Andreeva and T. Tabakova, J. Catal 188 (1999) 176-185.

[36] A.K. Sinha, S. Seelan, S. Tsubota and M. Haruta, Top. Catal. 29 (2004) 95-102.

[37] C. Lahousse, A. Bernier, P. Grange, B. Delmon, P. Papaefthimiou, T. Ioannides and X. Verykios, J. Catal 178 (1998) 214-225.

[38] A.K. Sinha and K. Suzuki, Appl. Catal. B: Environ. 70 (2007) 417-422.

[39] S. Scirè, S. Minicò, C. Crisafulli and S. Galvagno, Catal. Commun. 2 (2001) 229-232.

[40] L.H. Chang, N. Sasirekha, B. Rajesh and Y.W. Chen, Sep. Purif. Technol. 58 (2007) 211-218.

[41] M.P. Casaletto, A. Longo, A.M. Venezia, A. Martorana and A. Prestianni, Appl . Catal. A-Gen. 302 (2006) 309-316.

[42] J.J. Pireaux, M. Chtaïb, J.P. Delrue, P.A. Thiry, M. Liehr and R. Caudano, Surf. Sci. 141 (1984) 211-220.

[43] E. Finocchio, G. Busca, V. Lorenzelli and R.J. Willey, J. Catal 151 (1995) 204-215.

[44] S.S.T. Bastos, J.J.M. Órfão, M.M.A. Freitas, M.F.R. Pereira and J.L. Figueiredo, Appl. Catal. B: Environ. 93 (2009) 30-37.

[45] G.B. Hoflund, S.D. Gardner, D.R. Schryer, B.T. Upchurch and E.J. Kielin, Langmuir 11 (1995) 3431-3434.

[46] M. Baldi, E. Finocchio, F. Milella and G. Busca, Appl. Catal. B: Environ. 16 (1998) 43-51.

[47] M.A. Peluso, L.A. Gambaro, E. Pronsato, D. Gazzoli, H.J. Thomas and J.E. Sambeth, Catal. Today 133-135 (2008) 487-492.

[48] I. Spassova, M. Khristova, D. Panayotov and D. Mehandjiev, J. Catal 185 (1999) 43-57.

[49] A.S. Sinha, K. Suzuki, M. Takahara, H. Azuma, T. Nonaka and K. Fukumoto, Angew. Chem. Int. Ed. 46 (2007) 2891.

[50] Y.G. Yin, W.Q. Xu, Y.F. Shen, S.L. Suib and C.L. O'Young, Chem. Mater. 6 (1994) 1803-1808.

[51] H.F. McMurdie and E. Golovato, J.Res.Natl.Bur.Stand. 41 (1948) 589-600.

[52] Y. Chabre and J. Pannetier, Prog. Solid State Ch. 23 (1995) 1-130.

[53] S. Sarciaux, A. Le Gal La Salle, A. Verbaere, Y. Piffard and D. Guyomard, J. Power Sources 81-82 (1999) 656-660.

[54] A.P. Malloy and S.W. Donne, J. Colloid Interface Sci. 320 (2008) 210-218.

[55] L. Lamaita, M.A. Peluso, J.E. Sambeth and H.J. Thomas, Appl. Catal. B: Environ. 61 (2005) 114-119.

[56] X.G. Zhang, C.M. Shen and H.L. Li, Mater. Res. Bull. 36 (2001) 541-546.

[57] E.R. Stobbe, B.A. de Boer and J.W. Geus, Catal. Today 47 (1999) 161-167.

[58] F.C. Buciuman, F. Patcas and T. Hahn, Chem. Eng. Process 38 (1999) 563-569.

[59] B. Kimmerle, J.D. Grunwaldt and A. Baiker, Top. Catal. 44 (2007) 285-292.

[60] P. Lakshmanan, L. Delannoy, V. Richard, C. Méthivier, C. Potvin and C. Louis, Appl. Catal. B: Environ. 96 (2010) 117-125.

[61] P. Sangeetha and Y. Chen, Int J Hydrogen Energy 34 (2009) 7342-7347.

[62] T. Akita, M. Okumura, K. Tanaka, M. Kohyama and M. Haruta, J. Mater. Sci. 40 (2004) 3101.

CHAPTER 3

3. EXPERIMENTAL METHODS

In this section, we detail the experimental methods employed in order to achieve the dissertation aims and objectives as outlined in chapter 1. Firstly, the materials and apparatus used are given. Secondly, details on the synthesis of the supports and procedures used to add the active metal to the support are reported. Finally, the experimental 02procedures that were used to test the prepared catalysts in model VOC oxidation reaction are given. Various experiments were undertaken to investigate the effectiveness of the various gold supported catalysts. Gold supported samples were prepared by a deposition-precipitation method using chloroauric acid. Samples prepared from gold and supported on pyrosulite manganese dioxide (Au/β-MnO_2) were synthesised by deposition-precipitation. In addition, for comparison purposes, gold loaded on γ-MnO_2 was also synthesised by the same procedure. Another gold-manganese oxide catalyst was prepared by co-precipitation of chloroauric acid and manganese nitrate solutions. The solid catalysts obtained were all characterised by elemental analysis, thermal analyse, powder X-ray diffraction (XRD), H_2 temperature programmed reduction (TPR), N_2 physiosorption and transmission electron microscopy (TEM).

3.1 Apparatus and chemicals

The gases used were supplied by AFROX (African Oxygen) LTD. The metal salts and pyrosulite (β-MnO_2) used to prepare the catalysts were purchased from the Sigma-Aldrich chemical company. Also purchased were NaOH, 2-propanol, 2-butanol and toluene, polyethylene glycol (PEG), sodium citrate and sodium borohydride ($NaBH_4$). $HAuCl_4$ was purchased from SA Precious Metals (PTY) LTD. A supercul poropack column (1.8 mm x 1 m) and a carboxin packed column (1.8 mm x 1 m) were used to separate the reactants and products. A 5830A HP Gas Chromatograph (GC) coupled with a FID Varian detector was used

in conjunction with a Varian 5840A HP Gas Chromatograph (GC). Gas cylinders of air, argon, nitrogen, helium and hydrogen were purchased from AFROX (Africa Oxygen) Ltd. A series of gold catalyst (Au/Al_2O_3, Au/TiO_2 and Au/ZnO) were obtained as a gift from Mintek.

3.2 Catalyst preparation

Deposition-precipitation and co-precipitation were used for the preparation of gold based catalysts. Some catalysts were also prepared by incipient wet impregnation. The catalysts synthesized are listed in table 3.1.

Table 3.1: Listing of all catalysts prepared for 2-propanol oxidation

Catalyst	Preparation Method
1% Au/Al_2O_3[a]	Deposition-precipitation (DP)
1% Au/TiO_2 [a]	Deposition-precipitation (DP)
1% Au/TiO_2 [a]	Deposition-precipitation (DP)
1% $AuCeO_2$	Deposition-precipitation (DP)
1% Au/β-MnO_2 300[b]	Deposition-precipitation (DP)
1% Au/β-MnO_2 350[c]	Deposition-precipitation (DP)
1% Au/β-MnO_2 GP [d]	Deposition-precipitation (DP)
1% Au/MnO_x	Co-precipitation (CPT)
1% Au/γ-MnO_2	Deposition-precipitation (DP)
1% Ce/MnO_2	Incipient wet impregnation (IWP)
10% Ce/MnO_2	Incipient wet impregnation (IWP)

[a] Mintek, AuTEK Auroilite® catalyst; calcined [b] at 300 °C, [c] 350 °C and [d] colloidal Au deposited on β-MnO_2

3.2.1 Preparation of Au-Mn based catalysts

3.2.1.1. Au/β-MnO_2 prepared by deposition precipitation

A deposition-precipitation method was used to synthesize Au/β-MnO_2, similar to the method reported in the literature [1]. A 2.5 x 10^{-3} M $HAuCl_4$ solution was added dropwise to a suspension of 2 g β-MnO_2 in water. The amount of support material, β-MnO_2, was chosen to give a desired metal loading of 1 wt.% of Au. The pH of the support-gold suspension was then adjusted to 8 with 0.1 M NaOH. After 2 hours, the solution was heated at 70 ^{o}C overnight.

The suspension was filtered off and washed with hot deionised water to remove the excess chloride and sodium ions. The solid sample was washed until no AgCl precipitated when adding a drop of the precipitate to a 0.1 M $AgNO_3$ solution. The dried solid was further dried in an oven at 100 ^{o}C for 20 hours before calcination in air at 300 and 350 ^{o}C (10 ^{o}C/min) for 3 hours. The catalysts synthesised were labelled as Au/β-MnO_2 300 and Au/β-MnO_2 350; where the 300 and 350 refers to the calcination temperature.

3.2.1.2 Au/β-MnO_2 prepared by colloid gold nano particles loaded onto a β-MnO_2 support

Stabilised gold particles where first synthesised as follows. A 10^{-4} M $NaBH_4$ solution was added dropwise to a mixture containing 5 % v/v PEG and 10^{-3} M $HAuCl_4$. β-MnO_2 (2 g) was weighed and added to the solution. The solution turned clear, indicating removal of the purple gold nanoparticles. This was also confirmed by UV-vis spectra which showed the appearance of gold plasmon peak at 545 nm. The experiments were adapted from literature reports [2]. The samples were calcined at 200 ^{o}C (10 ^{o}C/min) for 3 hours. For comparison sake, gold nanoparticles were prepared without adding PEG. A small volume (2 ml) of 10^{-3} M

of $HAuCl_4$ was added to 500 ml of boiling deionised water. Slowly, 0.05 M sodium citrate was added to the boiling mixture. The solution was vigorously stirred and during the stirring time the solution changed colour from clear to purple. The nanoparticles were deposited onto the support

3.2.1.3. Au/MnO_x catalyst prepared by co-precipitation

A 2.5 x 10^{-3} M $HAuCl_4$ solution was added dropwise to a 0.2 M $Mn(NO_3)_2.6H_2O$ solution. The solution turned black as the manganese oxide precipitated out of solution. While vigorously stirring, the pH of the solution was adjusted to 8 with 0.1 M NaOH. The solution was filtered, after being heated at 70 ^oC for 16 hours. The precipitate was dried and finally calcined at 300 ^oC (10 ^oC/min). The calculated metal loading concentration was 1 wt.% for the prepared catalysts.

3.2.1.4 Oxidative decomposition of manganese carbonate γ-MnO_2

$MnCO_3$ (1 g) was placed in a fixed bed reactor and oxidized at 350 ^oC under flowing oxygen (50 ml/min). The oxygen gas was passed through a saturator filled with water [3].

3.2.1.5 Au/γ-MnO_2 catalyst prepared by deposition precipitation

A 2.5 x 10^{-3} M $HAuCl_4$ solution was added dropwise to the prepared γ-MnO_2. The pH was adjusted to 8 with 0.1 M NaOH for the deposition of gold particles onto the support. The mixture was stirred and heated overnight at 70 ^oC, while maintaining a pH of 8. The solution was filtered, washed with hot deionised water and dried for 12 hours at 100 ^oC. The dried powder was calcined at 300 ^oC (10 ^oC/min) for 3 hours.

3.2.2. Preparation of CeO_2 and Au/CeO_2

The CeO_2 support was prepared by aqueous precipitation of 0.1 M $Ce(NO_3)_3.H_2O$ in the presence of 0.1 M NaOH. The dry precipitate was oven dried at 100 ^oC for 16 hours. The yellow precipitate was calcined at 400 ^oC for 4 hours.

A 1 wt.% gold loaded catalyst was prepared by deposition-precipitation. A suitable amount of chloroauric acid ($HAuCl_4$) was dissolved in deionised water to give a concentration of 10^{-3} M. This solution was added dropwise to a weighed amount of the prepared CeO_2. NaOH (0.1 M solution) was added to adjust the pH to 8 followed by heating the solution to 70 ^oC with vigorous stirring for 16 hours. A solid product was collected after washing with hot deionised water. This was air dried prior to calcining at 300 ^oC to yield a 1 wt.% gold loaded Au/CeO_2 catalyst.

3.2.3. Preparation of Ce/β-MnO_2 catalysts with various amounts of Ce

Ce/β-MnO_2 catalysts with varying amounts of ceria (1 and 10 wt.%) were synthesised by the simple technique of incipient wet impregnation. A ceria nitrate ($Ce(NO_3)_3.H_2O$) solution was added dropwise to MnO_2, with vigorous stirring. The catalysts were calcined at 400 ^oC for 3 hours subsequent to drying at 100 ^oC for 16 hours.

3.2.4. Gold supported on Al_2O_3, TiO_2 and ZnO

Au/TiO_2, Au/Al_2O_3 and Au/ZnO were the Mintek AuTek™ Aurolite® catalysts synthesised at Mintek, South Africa (1 wt.% Au loadings).

3.3. Characterisation of the catalysts

To obtain information on the supports and the catalysts, they were characterised by a number of techniques as outlined below.

3.3.1. Temperature programmed reduction (TPR)

Temperature programmed reduction (TPR) measurements were carried out using a Micromeritics 2920 flow system. The TPR profiles were carried out in a flow reactor. A 100 mg sample was placed in a quartz tube reactor into which H_2:Ar (5%:95%) mixed gas was introduced. Prior to the run, the sample was first heated to 150 ^{o}C for 30 min in a flow of helium. The sample was cooled to 50 ^{o}C, and the gas switched to a 5% H_2 in Ar mixture with a 50 ml/min flow rate. The temperature of the sample was programmed to rise to 800 ^{o}C at 10 ^{o}C min^{-1}.

3.3.2. Electron microscopy (EM)

The calcined catalysts were investigated by using a Phillips Tecnai G2 Spirit electron microscope. Samples were prepared by adding a few granules of solid catalyst to ethanol, and then the sample was subjected to ultrasonication. The sample was mounted on SPI carbon lacey grids. The air dried samples were placed on a single tilt holder. The instrument was operated at a voltage of 120 Kv and the holder was tilted at 20 degrees. Various magnification ranges were used to obtain good resolution and morphology information on the sample. In addition to the images collected, Energy-dispersive X-ray spectroscopy (EDX) images were also collected.

3.3.3. X-ray diffraction (XRD)

The catalyst samples were analysed by room temperature X-ray powder diffraction (XRD) using a Bruker D8 Diffractometer with Cu Kα radiation (λ = 1.5418 Å) set at a voltage of 40 kV. The data was collected in the 2θ range 10-70 ° in 0.021 steps. The metals mean crystallite size (particle size) was calculated by the Scherrer equation [4] in equation 3.1:

$$d = \frac{0.9\,\lambda}{\beta\ Cos\ \theta} \tag{3.1}$$

where d is the mean crystallite size, λ is the wavelength of the X-ray source, β the width of the diffraction peak taken at half maximum intensity and θ is the diffraction peak angle.

3.3.4. N_2 physisorption

Surface measurements were carried out using the Brunauer, Emmet and Teller (BET) equation and Barrett-Joyner-Halenda (BJH) equation [5, 6]. The nitrogen physisorbtion experiments were used to measure the BET surface area (at -196 ^{o}C). The experiment was performed with a Micromeritics ASAP 1990 instrument. Before the tests, all samples (0.2 g) were degassed at 150 ^{o}C under 3 μm Hg for 4 hours in order to remove moisture and volatile compounds from the surface of the catalysts. The support and catalysts were continuously fed N_2 at various pressures to physisorb N_2. N_2 adsorption-desorption isotherms were obtained, to elucidate the pore volume and the pore size distribution along with the BET specific surface area.

3.3.5 Inductively coupled argon plasma emission spectroscopy (ICP-AES)

The gold content in the catalyst was determined by inductively coupled argon plasma emission spectroscopy (ICP-AES) on a Genesis ICP-AES Spectro instrument. The solid samples were digested in HNO_3 solution.

3.3.6 Thermal gravimetric analysis (TGA)

Thermal gravimetric analysis (TGA) profiles were measured on a Perkin Elmer Pyris 1 analyser. Thermal gravimetric analysis (TGA) was conducted on the catalysts and weight loss percentage was assessed as a function of temperature.

3.4. Reactor Studies

Catalytic activity tests were performed in a continuous-flow fixed-bed microreactor, using 300 mg of catalyst. The reactant mixture was fed to the reactor by flowing air through a saturator at 100 ml/min. The saturator contained the VOC (Figure 3.1).

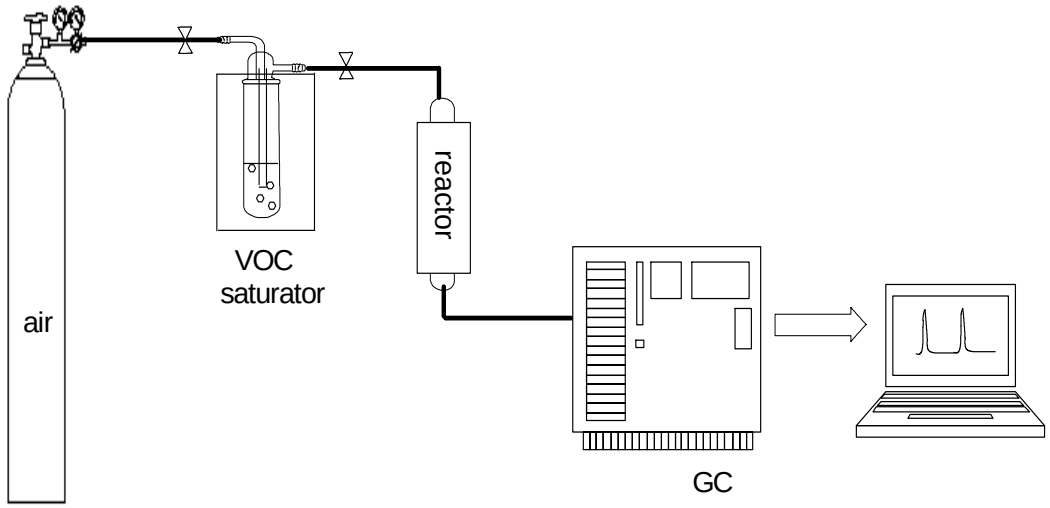


Figure 3.1: Rig used to evaluate catalyst performance

The concentration of the VOC in the air stream was calculated as:

$$C_{\%} = \frac{\mathrm{P_i}}{\mathrm{P_{total}}} \times 100 \quad (3.2)$$

where $C_{\%}$ is the concentration of VOC; $\mathrm{P_i}$ is the vapour pressure of the VOC at a specified temperature and $\mathrm{P_{total}}$ is the total pressure of the feed gas. A,B and C are Henry's constants different for each organic compound. In our experiments we set the total pressure at 760 mm Hg. The vapour pressure of each VOC was calculated to give a 1% concentration. The vapour pressure was calculated as

$$\log P_i = \mathrm{A} - \frac{\mathrm{B}}{\mathrm{T+C}} \quad (3.3)$$

A weight hourly space velocity (WHSV) of 26 h^{-1} was used. The reactant, as well as CO_2 and other possible products from incomplete combustion reactions were analysed by using an on-line gas chromatograph (GC), equipped with a carboxin packed column and a Varian TCD detector. Gases were also analysed with a Poropack column and a Varian FID detector.

The reactor was assembled as shown in the Figure 3.1. It comprises of a saturator, a reactor and a GC to monitor the reaction. The saturator (150 ml) was filled with 60 ml of an organic compound (the VOC). The saturator was cooled to maintain a 1% VOC concentration in air. The flow rate of the gas mixture was set to 100 ml/min. 2-Propanol was chosen as a suitable reactant for a model VOC oxidation reaction. Other VOCs were also chosen to study: 2-butanol and toluene. The reactor was made of quartz glass and housed the catalyst. A thermocouple was inserted into the reactor chamber to measure temperature. The thermocouple was placed above and in contact with the catalyst bed to assure correct temperature measurements. The reactor was surrounded by an electrical furnace. The reactor temperature was varied between 100 to 350 ^{o}C. The reaction was typically performed for 12 hours at each set temperature and was repeated twice. The reported values for conversion/selectivity at each set temperature are an average value from 2 experiments. The reported conversion/selectivity values at each set temperature varied within the range of ± 4.8 – 10.5.

Calculation of conversion and selectivity

The VOC conversion and the relative selectivity of the products formed were calculated using collected data from the GC traces. The amount of VOC converted into its products was calculated from

$$\%\ \text{VOC conversion} = \frac{\text{VOC}_{\text{in}} - \text{VOC}_{\text{out}}}{\text{VOC}_{\text{in}}} \times 100 \quad (3.4)$$

were

$\%\ VOC\ conversion$: is the amount of VOC converted;

VOC_{in}: is the inlet concentration of VOC

VOC_{out}: is the outlet concentration of VOC at steady state

The equation (3.4) does not account for the contraction or expansion of the reaction product number of moles for % VOC conversion (3.4) is simplified with the assumption that contraction or expansion effects will be minimal because the concentration used was low (that is 1%). The conversion and corresponding selectivity of each product was reported at the system steady state. Selectivity was calculated as the amount of each product over the amount of reactants consumed. The selectivity of each product, S_{i}, was expressed as a percentage for each of the products (CO_2 or organic product) formed in the reaction.

The selectivity of the products was calculated as shown by equations [7, 8] below:

$$S_{CO_2} = \frac{\text{CO}_{2\ \text{out}}}{\text{VOC}_{\text{in}}\ \text{x Cn}} \times 100 \quad (3.5.1)$$

$$S_{acetone} = \frac{\text{acetone}_{\ \text{out}}}{\text{VOC}_{\text{in}}} \times 100 \quad (3.5.2)$$

Where VOC_{in} is VOC (2-propanol, 2-butanol or toluene) amount fed into the reactor and $\text{CO}_{2\ \text{out}}$ is the amount of CO_2 produced for the VOC oxidation. Cn for 2-propanol, 2-butanol

and toluene oxidation is 3, 4 and 5, respectively. The equation 3.5.2, is given with respect to 2-propanol oxidation, and shows the selectivity of acetone, $S_{acetone}$, where $\text{acetone}_{\text{out}}$ represents the amount of acetone produced.

3.5. Reference

[1] M.C. Raphulu, PhD thesis University of the Witwatersrand, Johannesburg (2004) 92.

[2] D. Philip, Spectrochim. Acta A 71 (2008) 80–85.

[3] L. Lamaita, M.A. Peluso, J.E. Sambeth and H.J. Thomas, Appl. Catal. B: Environ. 61 (2005) 114-119.

[4] A.L. Patterson, Phys. Rev. 56 (1939) 978-982.

[5] S. Brunauer, P.H. Emmett and E. Teller, J. Am. Chem. Soc. 60 (1938) 309-319.

[6] E.P. Barrett, L.G. Joyner and P.P. Halenda, J. Am. Chem. Soc. 73 (1951) 373-380.

[7] D. Delimaris and T. Ioannides, Appl. Catal. B: Environ. 84 (2008) 303-312.

[8] Y. Wu, Y. Zhang, M. Liu and Z. Ma, Catalysis Today 153 (2010) 170-175.

CHAPTER 4

4. RESULTS AND DISCUSSION

In this study a range of Au supported catalysts have been synthesised and characterised and then tested for use in the oxidation of three volatile organic compounds (VOCs).

4.1 Catalyst synthesis

A range of Au catalysts supported on Al_2O_3, TiO_2, ZnO, CeO_2, β-MnO_2, MnO_x, and γ-MnO_2 were synthesised. The focus was on the use of Mn supports which were β-MnO_2, MnO_x, and γ-MnO_2. Manganese oxides (MnO_2) have many crystallographic structures but in this study we limited the study to β-MnO_2 and γ-MnO_2. The β-MnO_2 support was purchased from Aldrich. It is the pyrosulite phase MnO_2; the most abundant MnO_2 phase. In this dissertation MnO_2 will often be used as a shorthand notation for β-MnO_2. The γ-MnO_2 is the nsutite phase of MnO_2, which is commonly called EMD and is used in batteries. γ-MnO_2 was prepared by the oxidative decomposition of $MnCO_3$. We also prepared a manganese oxide by a co-precipitation method; this is labelled MnO_x because it contains mixed Mn oxidation states.

The Au/Al_2O_3, Au/TiO_2, Au/ZnO, and Au/CeO_2 samples were prepared by a deposition-precipitation (DP) method. The Ce/β-MnO_2 samples were prepared by an incipient impregnation method. Au/β-MnO_2 300 and Au/β-MnO_2 350 were prepared by a deposition-precipitation method and calcined at 300 and 350 ^oC respectively. An Au/β-MnO_2 GP catalyst was prepared by deposition of pre-formed gold nanoparticles on β-MnO_2. In addition to Au/β-MnO_2 catalysts, Au/γ-MnO_2 and Au/MnO_x catalysts were also prepared.

Gold was added to γ-MnO_2 by a deposition precipitation method to make Au/γ-MnO_2. Au/MnO_x was prepared by a co-precipitation method.

It was observed that after adding gold to various supports that the samples generally changed colour from white to blue or purple. The exception was the Mn based catalysts; no colour changes took place with this support. The visual colour change was an indication that gold nanoparticles had been added to the support.

Table 4.1: Properties of catalysts used for VOC oxidation along with their surface areas (S_{BET}), gold loadings and average particle sizes

Catalyst Code	Preparation Method	S_{BET} $m^2 g^{-1}$	Au loading wt. % (actual)	Au loading wt. % (theoretical)	d_{Au} [f] (nm)
Al_2O_3	-	243	-		
Au/Al_2O_3	DP [a]	230	0.89	1	2.6
TiO_2	-	49	-		
Au/TiO_2	DP [a]	43	0.9	1	2.0
ZnO	-	59	-		
Au/ZnO	DP [a]	55	0.9	1	2.2
CeO_2	CPT [b]	70	-		
Au/CeO_2	DP [a]	51	1.2	1	3.9
β-MnO_2	-	17.0	-		
Au/β-MnO_2 300	DP [a]	5.2	1.2	1	3.4
Au/β-MnO_2 350	DP [a]	4.1	1.3	1	4.9
Au/MnO_2 GP	Colloid [d]	5.0	1.5	1	4.5
MnO_x	CPT [b]	69	-		-
Au/MnO_x	CPT [b]	86	1.3	1	-
γ-MnO_2	OD [c]	131	-		-
Au/γ-MnO_2	DP [a]	124	1.4	1	-
1% Ce/MnO_2	IWP [e]	16	-	-	-
10% Ce/MnO_2	IWP [e]	11	-	-	-

[a] deposition-precipitation [b] co-precipitation [c] oxidative decomposition [d] Au colloid [e] incipient wetness impregnation [f] determined by TEM

The samples used in this study are listed in Table 4.1. Table 4.1 indicates the catalyst name that will be used in this dissertation. The names give an indication of the support used. The metal loading of the sample, measured by ICP-AES, along with the preparation method used are also given in Table 4.1. The actual gold loadings for Au-manganese and Au/CeO_2 catalyst were unexpectedly higher than the theoretical Au loadings. We will need to verify the data by repeating the experiments to determine the analysis standard error which would be compounded by the preparation standard error; it was not measured.

4.2 Catalyst characterisation

In order to understand the influence of the gold-based catalyst towards VOC oxidation several characterisation techniques were used to evaluate some of the catalyst properties.

4.2.1 Surface area measurements

The specific surface area, S_{BET}, was determined by the measurement of the amount of N_2 physically adsorbed as a function of pressure. The adsorption data was used to calculate the surface area using the Brunauer-Emmet-Teller (BET) equation of the samples shown in Table 4.1. The pore size distribution and volume were estimated using the Barrett-Joyner-Halenda (BJH) method.

The surface area, S_{BET}, of MnO_2 was 17 m^2g^{-1}. Addition of Au gave S_{BET} 4.1 m^2g^{-1} for Au/β-MnO_2 300 and 5.2 m^2g^{-1} for Au/β-MnO_2 350. Addition of Ce to β-MnO_2 gave S_{BET} 11 and 16 m^2g^{-1} for the 1% and 10% Ce loadings respectively. Thus, adding Au and Ce to β-MnO_2 resulted in reduced surface areas (see Table 4.1) suggesting blocking of the pore structure. The addition of Ce to β-MnO_2 had less effect on the surface area of the β-MnO_2 than the Au/β-MnO_2.

The other Mn oxides samples, prepared by co-precipitation (MnO_x) and oxidative decomposition (γ-MnO_2), had higher surface areas than the β-MnO_2 support. This was associated with smaller particles in these samples. The surface area decreased when Au was added to γ-MnO_2; from 131 m^2g^{-1} to 124 m^2g^{-1}. For the co-precipitation samples Au/MnO_x catalyst (86 m^2g^{-1}) resulted in higher surface area than the MnO_x sample (69 m^2g^{-1}).

An expected decrease (28%) in the surface area on addition of gold to CeO_2 was noted. This is possibly due to gold particles that blocked some of the pores in CeO_2. Au/Al_2O_3 has the highest S_{BET} measured (243 m^2g^{-1}). Au/ZnO and Au/TiO_2 samples have comparable surface areas.

Pore volume data was also obtained on the samples. The data observed was consistent with the discussion above. The information is given in the appendix (see appendix A1 – A3)

4.2.2 Transmission electron microscopy studies

Transmission electron microscopy (TEM) was used to study a range of Au supported samples. These included Au/Al_2O_3, Au/TiO_2, Au/ZnO, Au/CeO_2, Au/β-MnO_2 300, Au/β-MnO_2 350, Au/β-MnO_2 GP, Au/MnO_x and Au/γ-MnO_2. The TEM images are shown in Figures 4.1 - 4.9. Bar graphs showing the Au particle size distributions of the Au particles supported on the different metal oxides are also given. Gold particles appear as dark spots spread over the support. Some of the particles have been indicated by arrows in the different figures. The average gold particle sizes are reported in Table 4.1 and it can be seen that the particles vary in size from 2 - 5 nm. The low gold loadings that give rise to the small gold particle sizes are expected. The small sizes and low loadings meant that the X-ray diffraction (XRD) technique could not be used to characterise the gold particles; indeed this was shown by an absence of gold crystallite peaks in the XRD profiles.

The Au/TiO_2, Au/Al_2O_3 and Au/ZnO samples all showed an average gold particle size between 2.0 - 2.7 nm for the finely dispersed gold particles (Table 4.1). The gold particle size ranges illustrated a nominal distribution from 0.5 to 5 nm (Figures 4.1-4.3). A fairly good spread of gold particles is seen in the images.

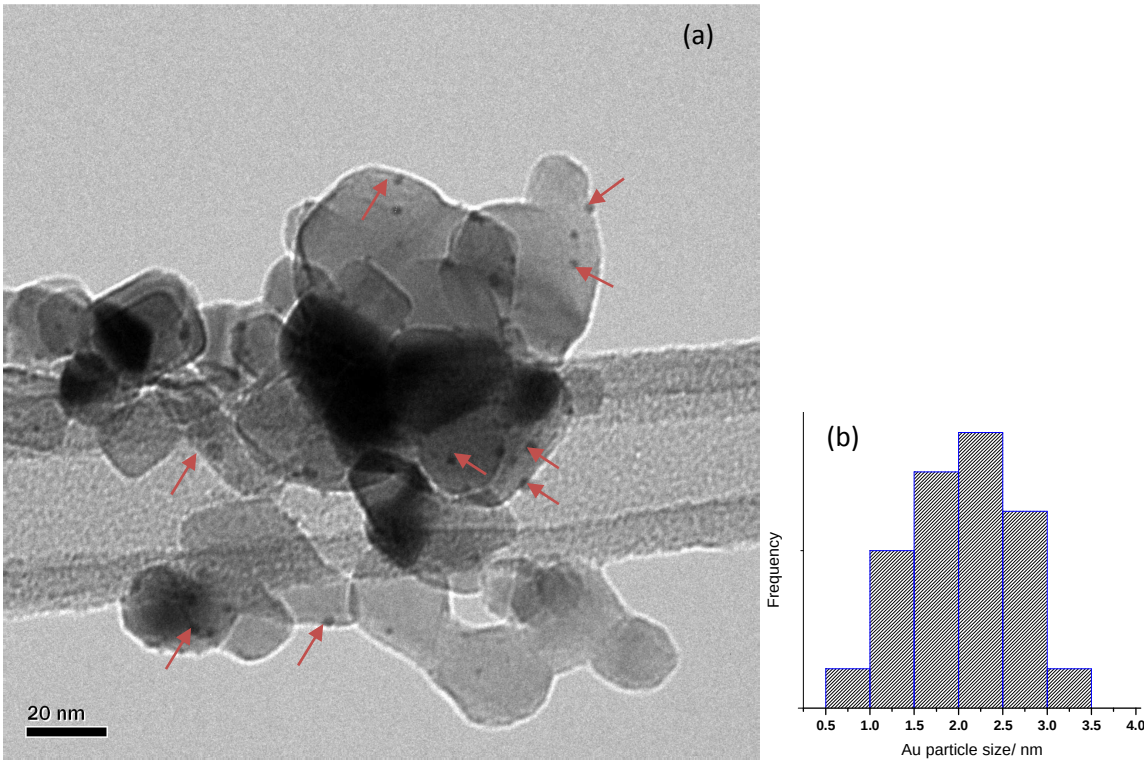


Figure 4.1: (a) A TEM image of the Au/TiO_2 catalyst showing Au particles as small dark spots (see arrows) and (b) bar graph showing gold particle size distribution

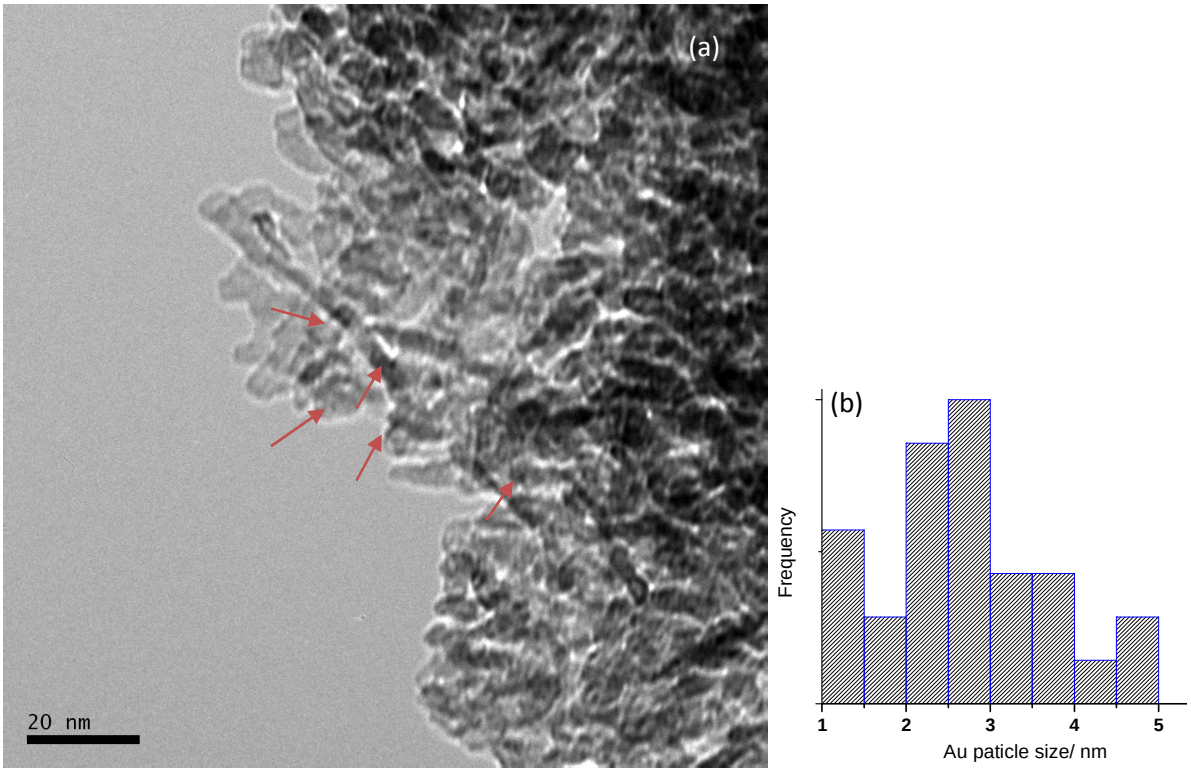


Figure 4.2: (a) TEM image of the Au/Al_2O_3 catalyst showing Au particles and (b) bar graph showing gold particle size distribution

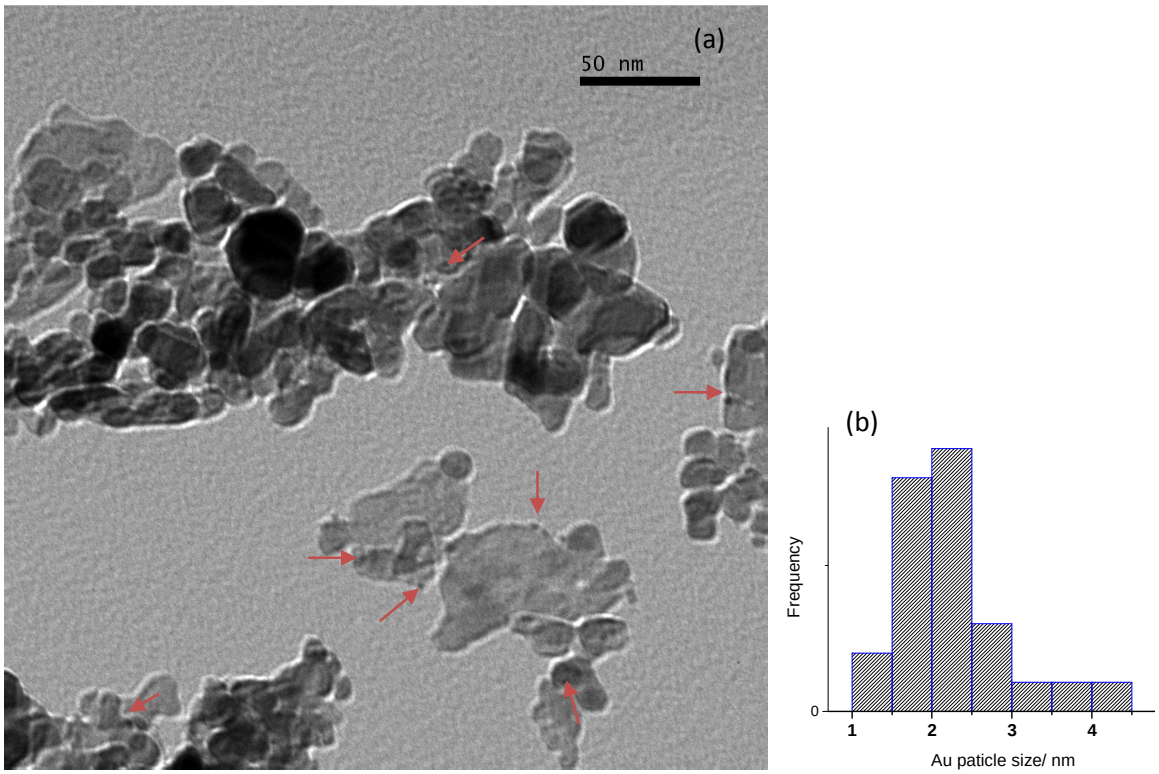


Figure 4.3: (a) TEM image of Au/ZnO catalyst showing Au particles and (b) bar graph showing gold particle size distribution

TEM images were recorded for the Au/β-MnO_2 samples after two different calcination temperatures. The TEM images were recorded after calcination at 300 ^{o}C (Figure 4.4 (a)) and 350 ^{o}C (Figure 4.5 (a)), respectively. The β-MnO_2 support consists of large rod-like particles (width, 50 nm -600 nm). The average gold particle size on Au/β-MnO_2 300 was 3.4 nm. This was smaller with a narrower particle size distribution than Au particles measured on Au/β-MnO_2 350 (4.5 nm) as shown in Figure 4.5. There were no major physical changes detected for the support as the calcination temperature was varied; merely a change in the dispersion of the small gold particles was noted. The increase in gold particle size, at the higher calcination temperature, indicated sintering of gold particles. The gold nanoparticles were smaller than the measured average pore diameter of the β-MnO_2 supported.

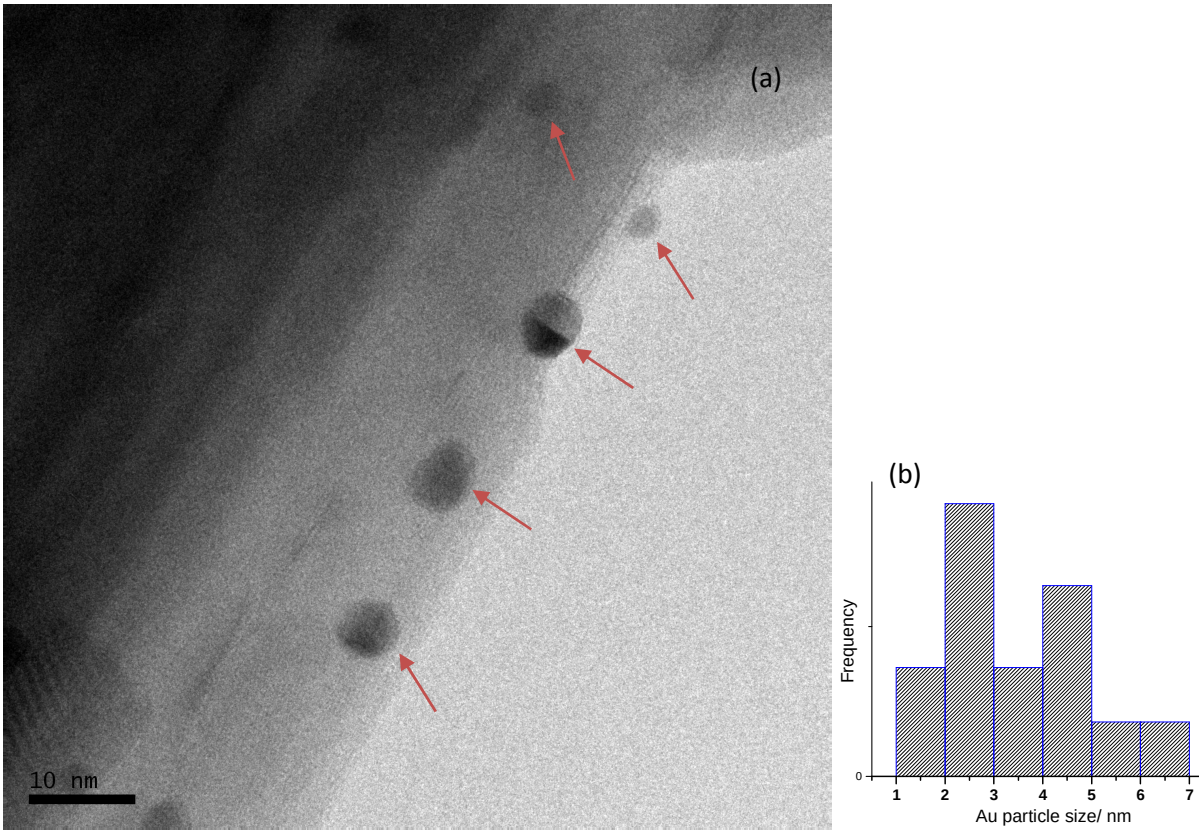


Figure 4.4: TEM image of the Au/β-MnO_2 catalyst calcined at 300 ^{o}C and (b) bar graph showing Au particle size distribution with average Au particle size of 3.4 nm

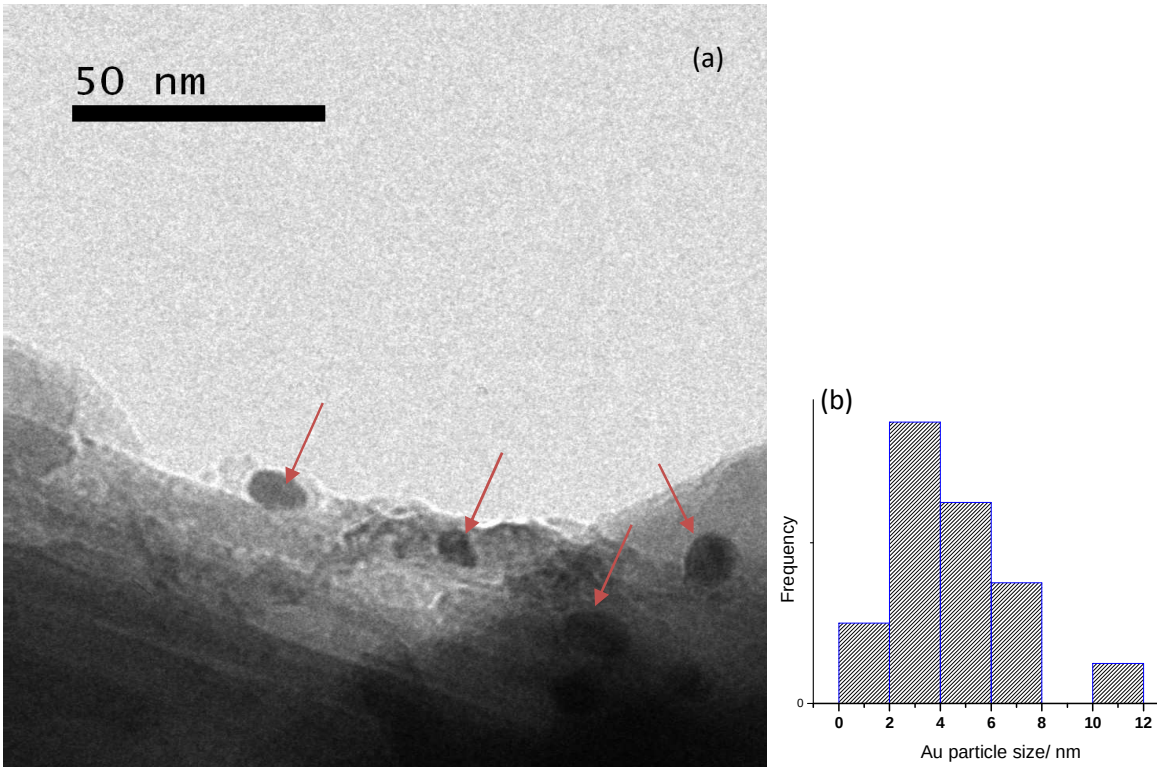


Figure 4.5:(a) TEM image of the Au/β-MnO_2 catalyst at calcined 350 ^{o}C and and (b) bar graph showing the Au particle size distribution average Au particle size 4.8 nm

A TEM image of a Au/β-MnO_2 GP sample is shown in Figure 4.6 (a). The image clearly shows the rod-like structures of the support. EDX was used to confirm that these particles were indeed Au particles. The size distribution of the Au particles was measured and is shown in Figure 4.6 (c). The particle size ranged from 2 nm to 8 nm. When polyethylene glycol (PEG) was omitted from the colloid synthesis, the particle size increased to an average of 22 nm (see appendix A1). In this regard, the results show that PEG has a stabilizing effect on the nucleation of gold seeds used in the formation of gold nanoparticles [1].

The UV-vis spectrum of the Au/β-MnO_2 GP sample was recorded and displayed in Figure 4.6(b). A single peak at 545 nm was observed. This peak is the surface plasmon resonance peak for gold and indicates the formation of gold nanoparticles which are below 60 nm [2, 3].

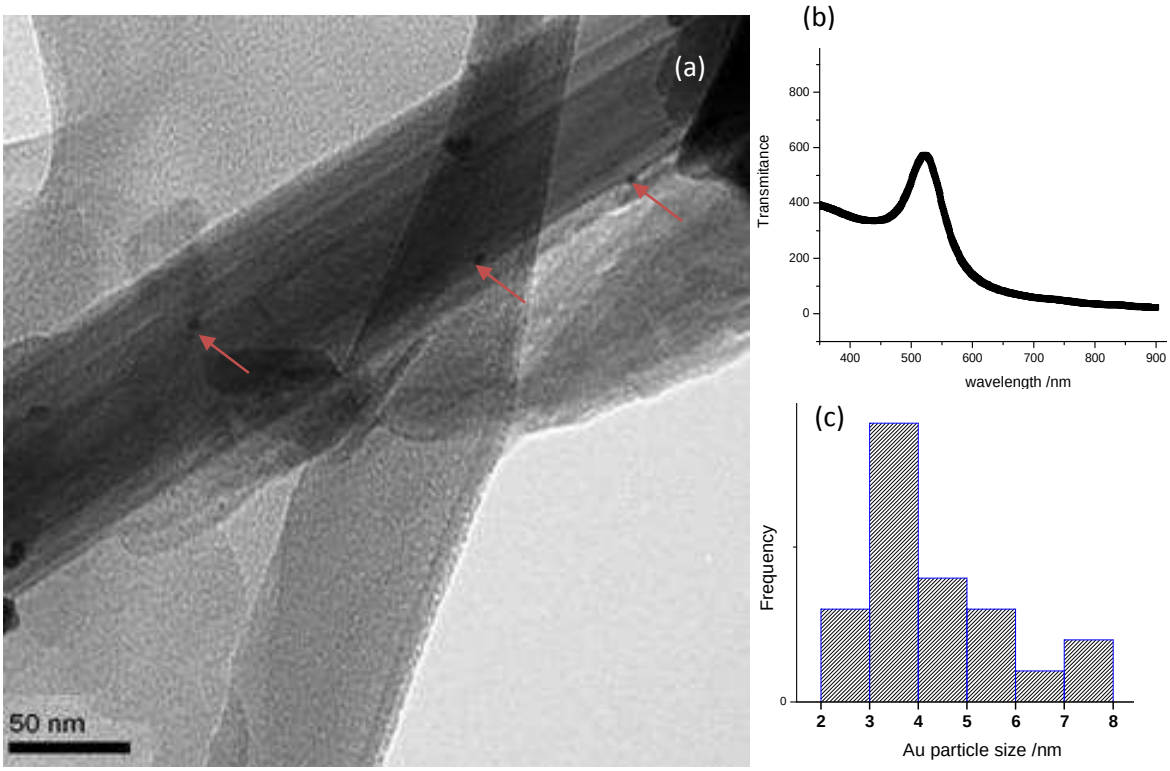


Figure 4.6: (a) TEM images of Au/β-MnO_2 GP catalyst prepared by colloid formation; (b) the UV-Vis spectrum of Au nanoparticle with PEG showing Au surface plasmon resonance peak at 545 nm and (c) gold particle size distribution bar graph

A transmission electron microscopy (TEM) image of a Au/γ-MnO_2 sample is shown in Figure 4.7. It shows γ-MnO_2 particles with a non well-defined morphology. There was no clear contrast between the gold and support particles due to the very dense nature of the γ-MnO_2 support. The Au/MnO_x sample showed a combination of rods and amorphous material (see Figure 4.8). It was also not possible to determine the gold particle sizes from the TEM images.

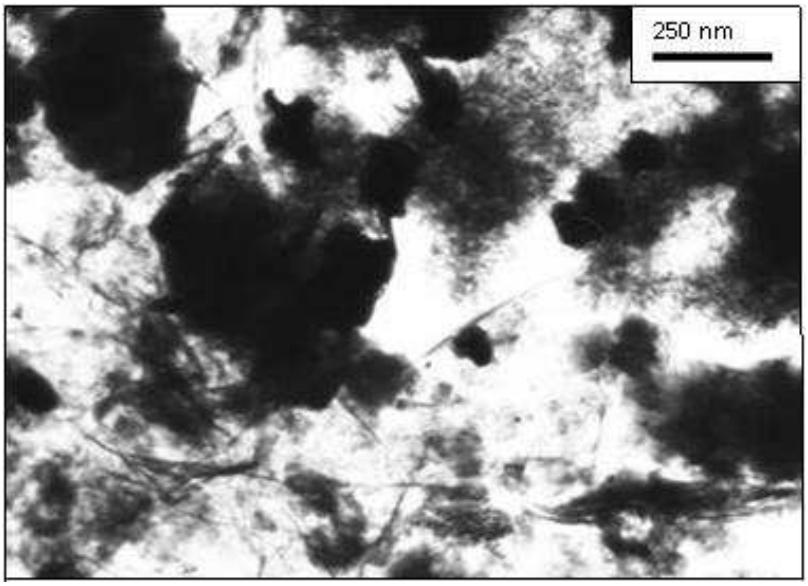


Figure 4.7: The TEM image showing amorphous particles of Au/γ-MnO_2 catalyst

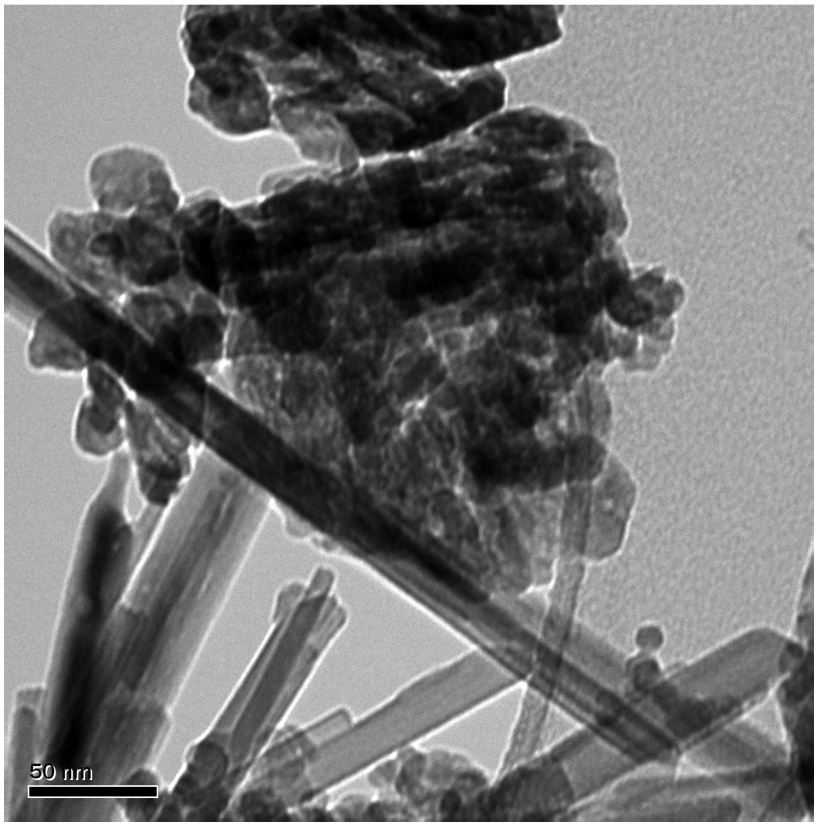


Figure 4.8: The TEM image showing Au/MnO_x catalyst prepared by co-precipitation

TEM analysis was also performed on the Au supported on CeO_2. The CeO_2 support is made up of very fine particles; the same size as the small gold particles. The average gold particle size for the Au/CeO_2 system was 3.8 nm (Figure 4.9). The gold particle size distribution was found to range between 1 and 6 nm.

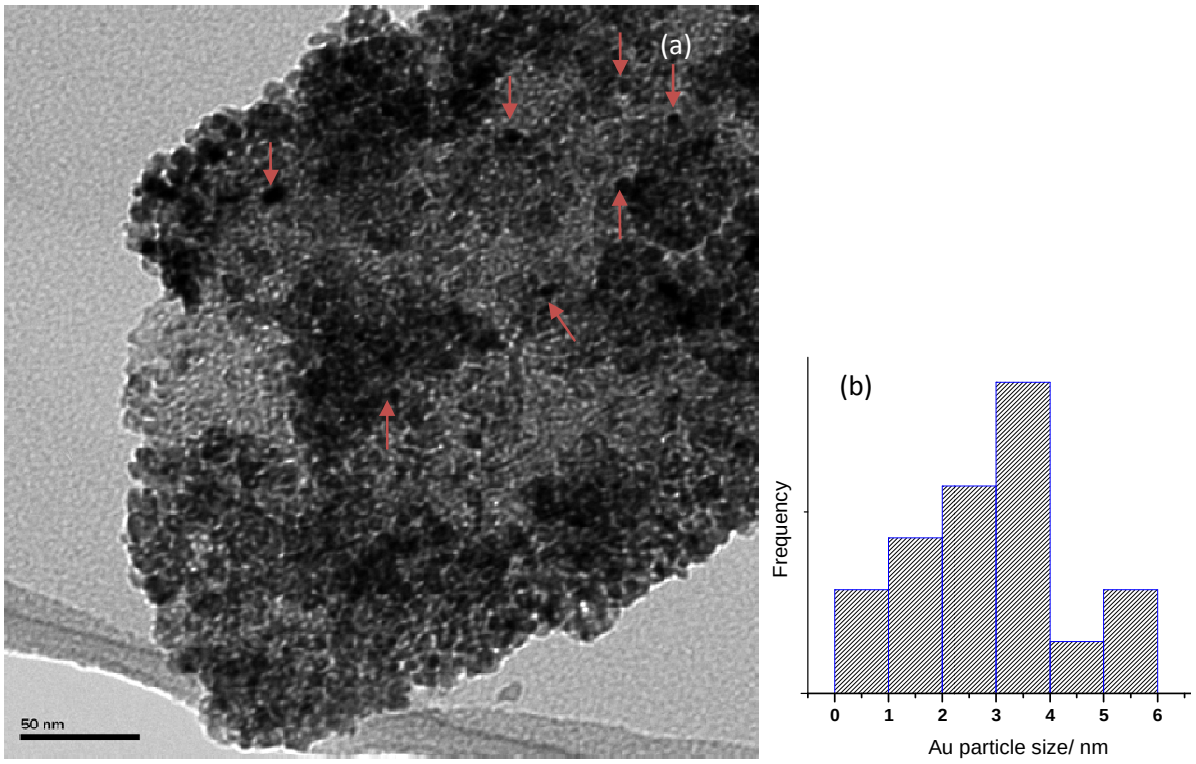


Figure 4.9: (a) TEM image of Au/CeO_2 catalyst and (b) bar graph showing gold particle size distribution

TEM images of Ce/β-MnO_2 samples

TEM images were recorded on the 1% and 10% CeO_2 loaded on β-MnO_2 (1% Ce/β-MnO_2 and 10% Ce/β-MnO_2) samples. In Figure 4.10, TEM images show small CeO_2 particles that are well dispersed on the β-MnO_2 surface. In Figure 4.10(b) it can be seen that increasing the Ce content gives larger aggregates of CeO_2 on the support surface.

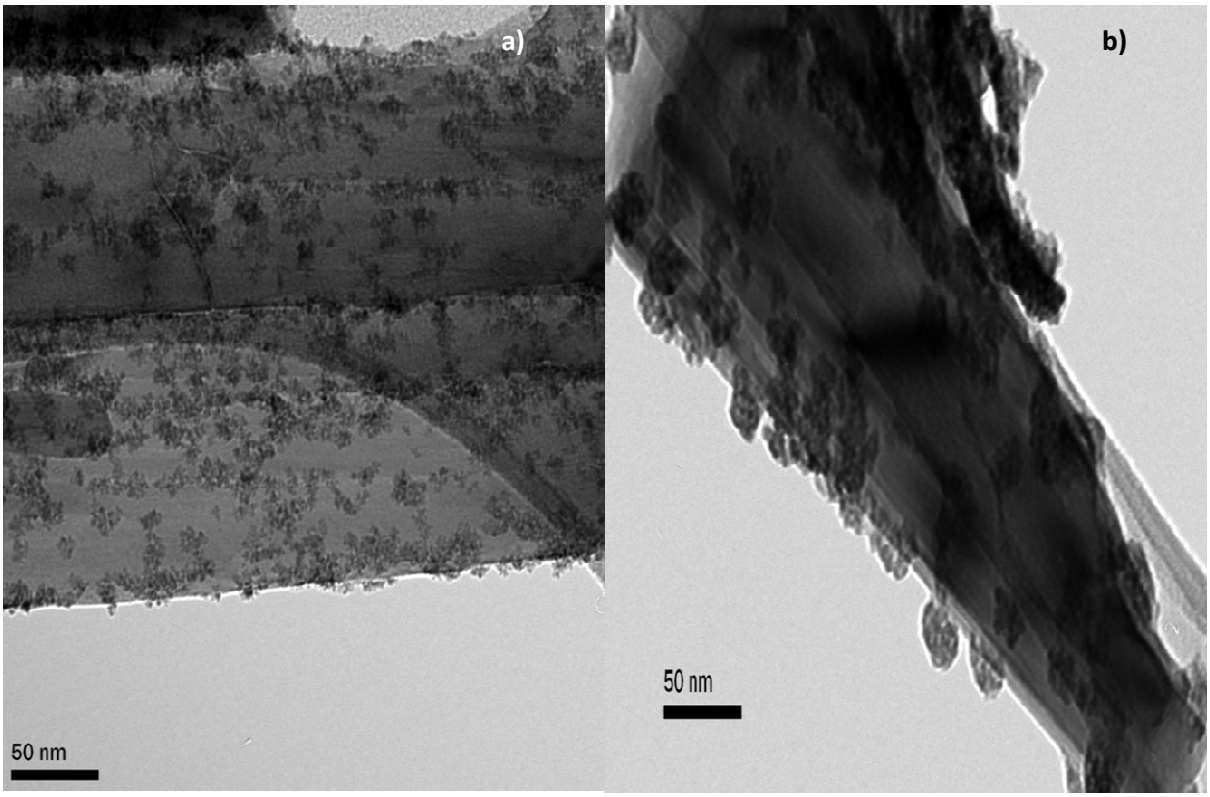


Figure 4.10: TEM image of a) 1% Ce/β-MnO_2 b) 10% Ce/β-MnO_2 catalysts

4.2.3. X-ray diffraction

4.2.3.1 X-ray diffraction (XRD) patterns of the manganese oxides and Au/manganese oxides catalysts

The XRD pattern for a β-MnO_2 sample displays sharp, high intensity peaks suggesting a well formed crystalline material (Figure 4.11(a)). The manganese dioxide sample was constituted by the pyrosulite phase identifiable by peaks at 2θ = 28, 37, 41, 56 ^{o}. The crystalline phase was identified as β-MnO_2 from literature XRD comparisons [4-6].

Manganese dioxide pyrosulite is the most common and stable phase of MnO_2. β-MnO_2 has a rutile structure, with oxygen atoms forming a slightly distorted hexagonal closely packed

array. The basic motif of this tetragonal structure is an infinite chain of MnO_6 octahedral units connected either by corner or edge sharing. All octahedral units are equivalent, and available cations such as protons act as balancing negative charge on the MnO_6 units [7]. The Mn^{4+} vacant sites are filled either with four protons to balance the charge or as in some cases, Mn^{3+} ions. Mn_2O_3 may be incorporated into the MnO_2 structure and may not be detected in XRD patterns [8]. This indicates that only Mn^{4+} was present after calcination of a catalyst, in agreement with TPR data (see later).

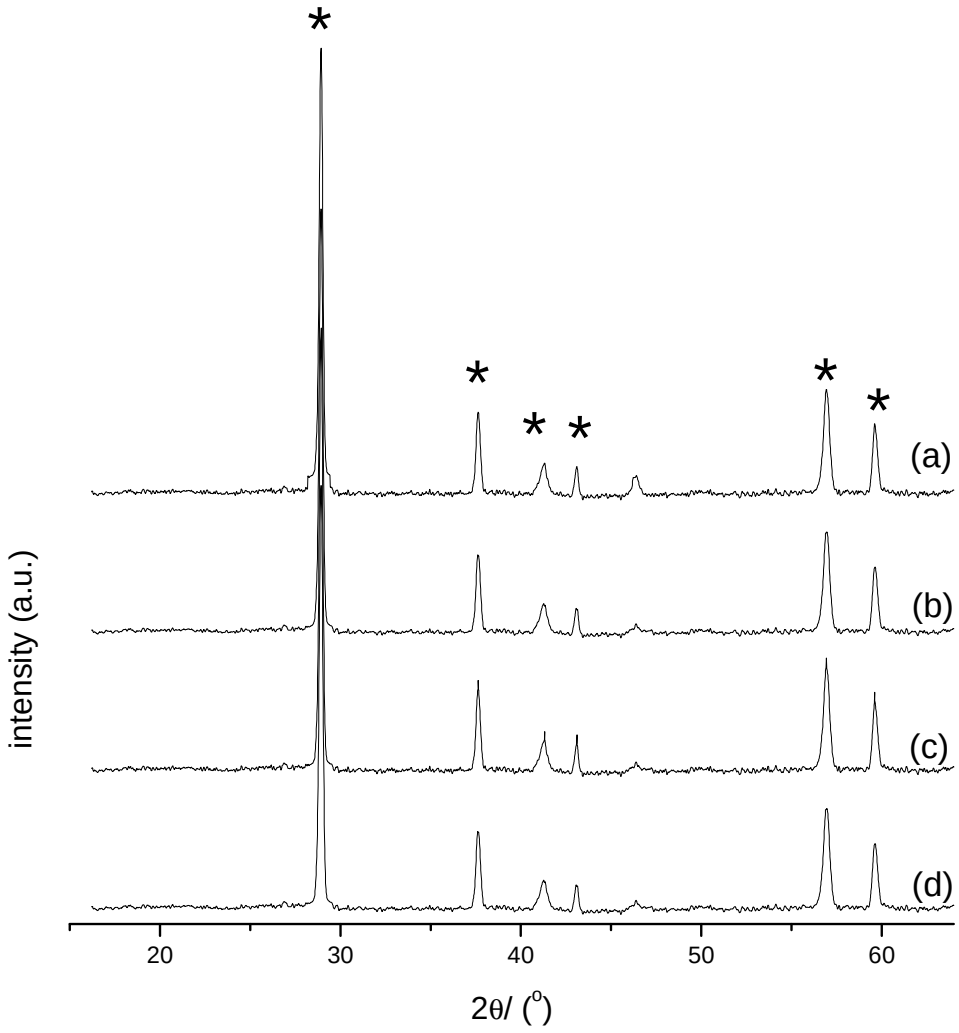


Figure 4.11: XRD pattern of (a) β-MnO_2, (b) Au/β-MnO_2 300, (c) Au/β-MnO_2 350 and (d) Au/β-MnO_2 GP catalysts (⋆ peaks due to β-MnO_2 phases)

The pyrosulite phase was also observed for Au/β-MnO_2 samples; no other phases were detected. Figure 4.11 (b)-(d) shows the diffraction patterns of Au/β-MnO_2 300, Au/β-MnO_2

350 and Au/β-MnO_2 GP samples respectively. The patterns for Au/β-MnO_2 sample were well indexed to pure pyrosulite. The intense and sharp diffraction peaks at 2θ = 28, 37, 42, 49, 56 ^{o}, were indexed to (110), (101), (200), (111), (211) and (220) respectively and belongs to the tetragonal β-MnO_2 phase. The XRD patterns of Au/β-MnO_2 samples calcined at 300 and 350 ^{o}C were no different from each other, or the β-MnO_2 with no Au.

The addition of gold has very little effect on the bulk properties of the support material. The strongest reflection peak of gold is from Au (111). This overlaps with that of β-MnO_2 at 2θ = 38 ^{o}. The average Au crystallite size could not be determined due to the very low intensity of the relevant gold peaks. The concentration of gold in the sample was too low and the well dispersed gold particles were below 5 nm as determined from TEM studies.

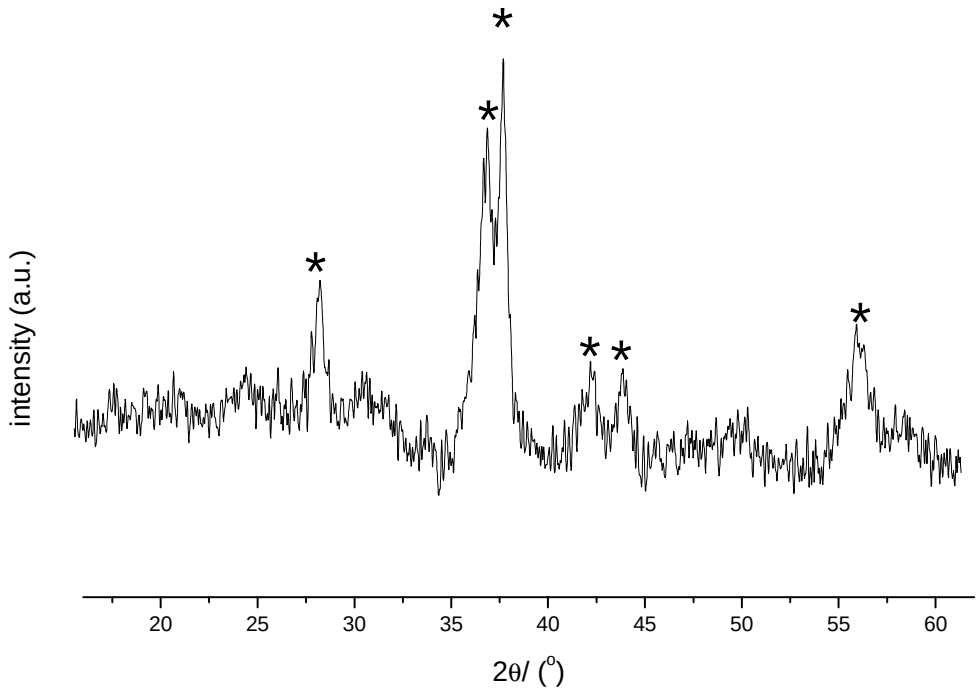


Figure 4.12: XRD pattern of Au/MnO_x catalyst prepared by co-precipitation of mixed oxides ; calcined at 300 ^{o}C (⁎ peaks due to MnO_x phases)

Gold was also loaded onto MnO_x, prepared by the co-precipitation method. The X-ray diffraction (XRD) pattern of MnO_x revealed no peaks implying that the MnO_x sample was highly amorphous (not shown). The Au/MnO_x sample showed a resolved diffraction peak at

2θ =36.9 °, characteristic of a Mn_3O_4 phase (Figure 4.12). Moreover, the XRD pattern showed the presence of some crystalline MnO_2 phase in the sample as seen by peaks at 28, 42, 44°. The co-existence of additional amorphous manganese oxide phases cannot be disregarded. The manganese oxide containing sample prepared by co-precipitation has a higher surface area and poorer crystallinity than the β-MnO_2 sample. The MnO_x consists of small crystallite aggregates forming a porous structure giving a high surface area material.

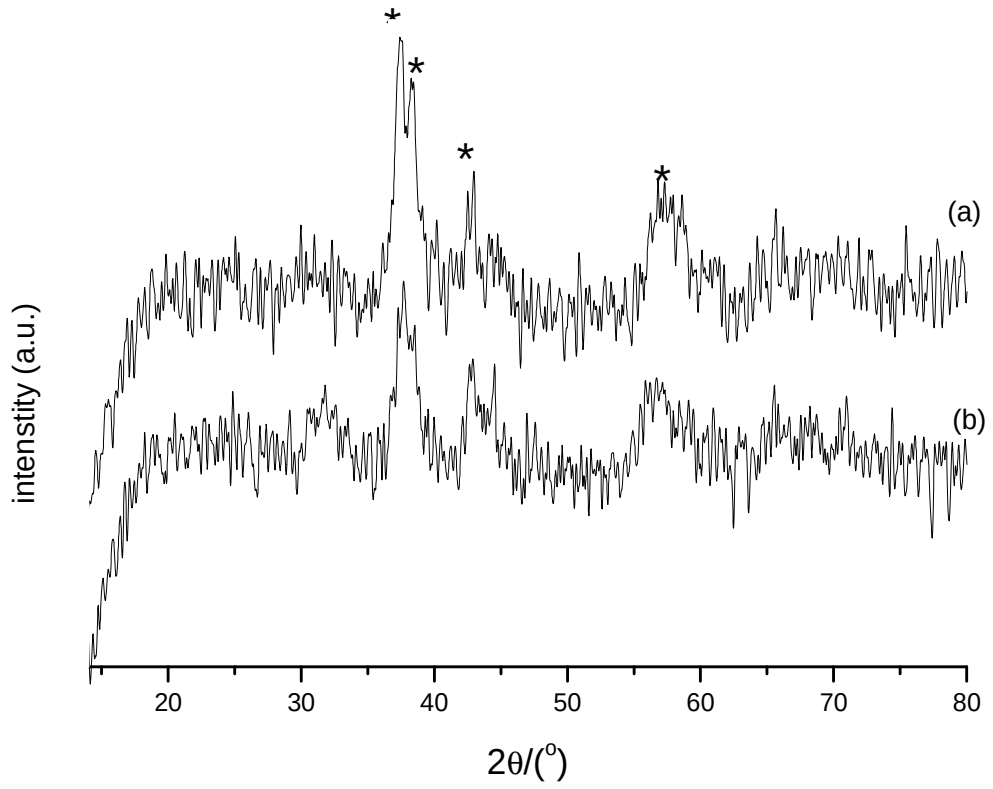


Figure 4.13: XRD pattern of a) γ-MnO_2 and b) Au/γ-MnO_2 catalysts prepared by oxidative combustion $MnCO_3$ (⋆ peaks due to γ-MnO_2 phases)

The manganese dioxide obtained from the oxidative decomposition of $MnCO_3$ showed diffraction peaks at 2θ = 37, 38, 42, 56 ° (Figure 4.13) which was attributed to the γ-MnO_2 phase which has a cubic structure. γ-MnO_2 (nsutite) is a structural inter twine of pyrosulite and ramsdellite. Defects in the structure arise due to an interplay between micro twining and pyrosulite intergrowth, in the crystal structure and this causes an absence of some peaks [9]. Figure 4.13(b) shows the XRD pattern of the Au/γ-MnO_2 sample which appears to have the same peaks at 2θ = 37, 38, 42, 49, 56 ° as /γ-MnO_2. No trace of $MnCO_3$ was

detected in Au/γ-MnO_2 or γ-MnO_2 samples. This suggests that the $MnCO_3$ was fully converted to MnO_2.

Comparing the XRD patterns for the three Mn oxide samples, it can be seen that from the XRD peak intensities and width, it is seen that the β-MnO_2 sample is the most crystalline material; more so than the γ-MnO_2 and MnO_x samples. Typically γ-MnO_2 is a poorly crystalline material due to the existence of point defects in its structure such as manganese (Mn^{4+}) vacancies [9].

4.2.3.2 X-ray diffraction patterns of the Au/CeO_2 catalyst.

Figure 4.14 (a) and (b) shows the X-ray diffraction pattern of the CeO_2 and Au/CeO_2 sample. It shows well-defined broad diffraction peaks at 2θ = 28, 33, 47, 56 and 59 ^{o} indicative of a crystalline material with a fluorite-like structure. There were no peaks observed due to the presence of gold. The crystal structure of CeO_2 remained unchanged after adding gold.

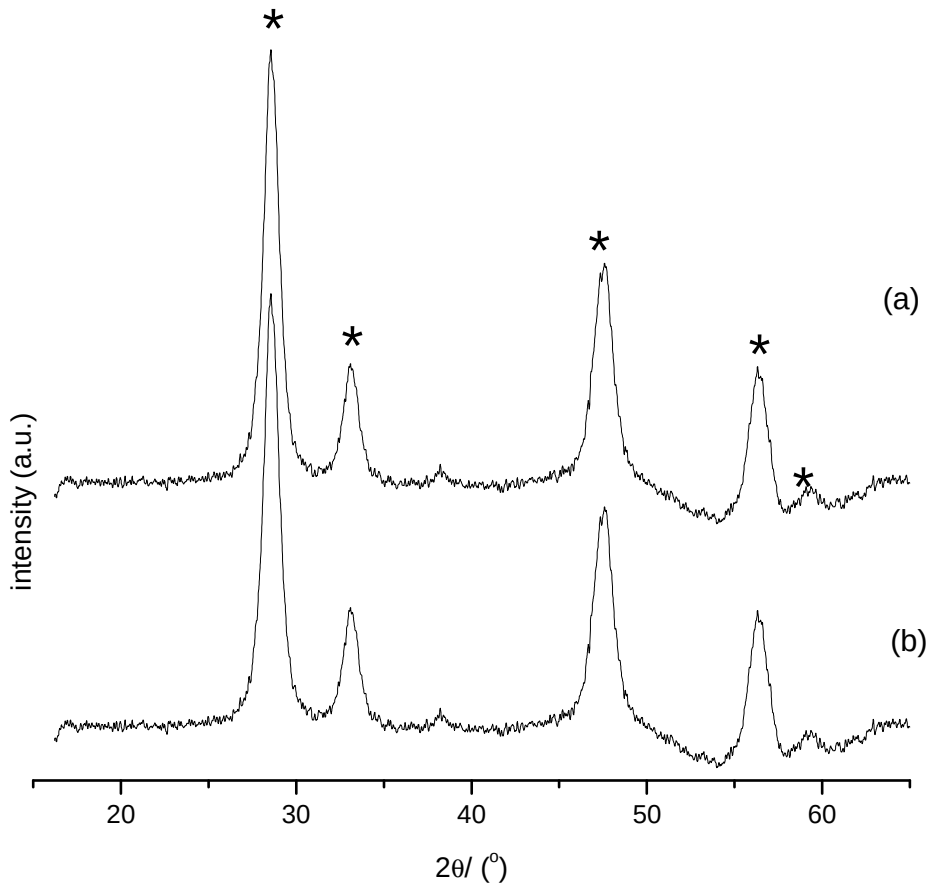


Figure 4.14: XRD patterns of a) CeO_2 and b) Au/CeO_2 catalysts (* peaks due to CeO_2 phases)

4.2.3.3 X-ray diffraction patterns of the Ce/β-MnO_2 catalyst.

Figure 4.15(a)-(c) illustrates the XRD patterns of Ce loaded on β-MnO_2. The XRD patterns of β-MnO_2, 1% Ce/β-MnO_2 and 10% Ce/β-MnO_2 samples were essentially the same. The catalyst prepared by incipient wetness impregnation showed peaks due to the crystalline structure of β-MnO_2 only. There was no change in the crystallinity of β-MnO_2 after Ce loading. No diffraction peaks due to the CeO_2 phase were observed, even at 10% loading. The CeO_2 particles must be very small and highly amorphous. The TEM images are consistent with this finding. No line broadening and no shifts in the peaks of β-MnO_2 phase were observed. It can thus be assumed that Ce is not incorporated into the MnO_2 pryosulite matrix. The Ce^{4+} ionic radius (0.094 nm) is much larger than the Mn^{4+} (0.052 nm) and Mn^{3+} (0.06nm) radii [10, 11].

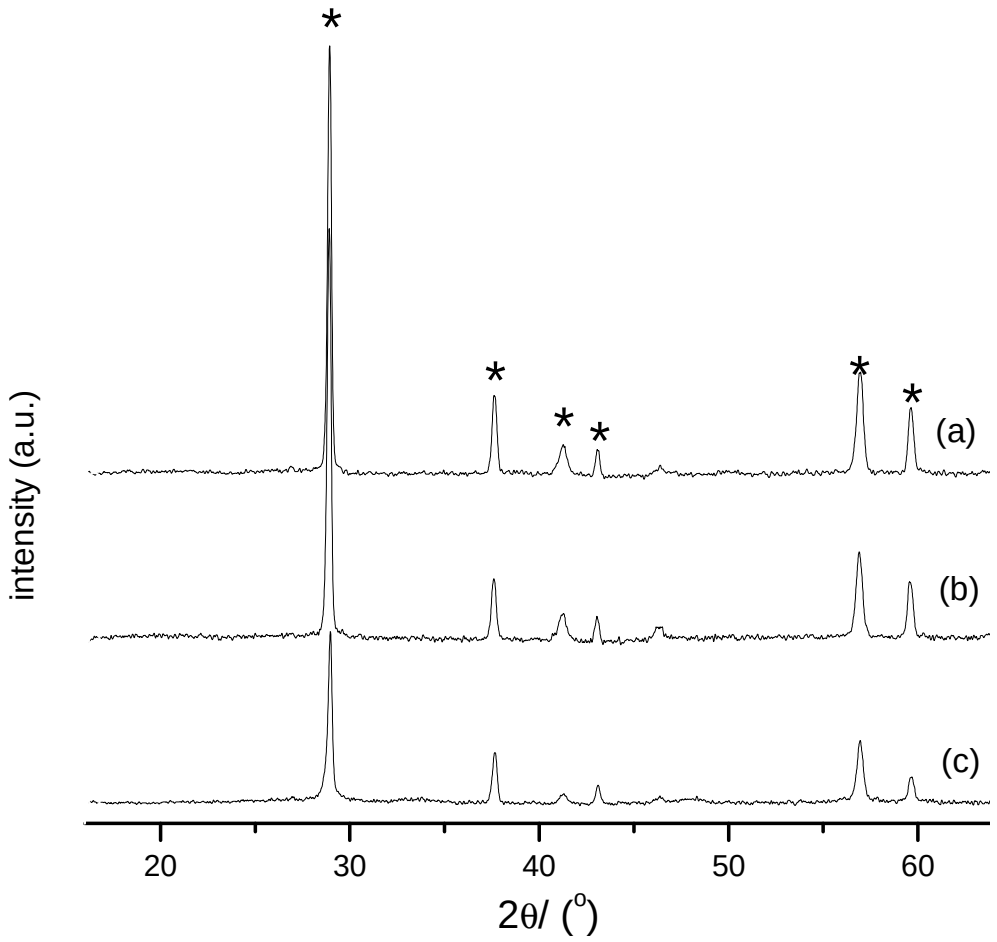


Figure 4.15: XRD patterns of Ce loaded β-MnO_2 catalysts a) β-MnO_2 b) 1% Ce/β-MnO_2 and c) 10% Ce/β-MnO_2 calcined at 400 °C (⁎ peaks due to β-MnO_2 phases)

4.2.4 H_2-Temperature programmed reduction

H_2-Temperature programmed reduction (H_2-TPR) measurements were carried out to evaluate and compare the reducibility of the supports and the catalyst samples (Figures 4.16 - 4.20). TPR profiles show the oxidation state of the original samples by evaluating the amount of hydrogen consumed with temperature. The TPR profiles show the species present in the catalyst sample and the interactions of different elements with the support material. TPR data is shown in Table 4.2.

Table 4.2: H_2-TPR peak temperatures for all samples studied

Catalysts	1st Red [a] /°C	2nd Red [a] /°C
β-MnO_2	437	494
Au/β-MnO_2 350	405	469
Au/β-MnO_2 300	394	453
Au/β-MnO_2 GP	398	479
Au/γ-MnO_2	318	460
γ-MnO_2	364	544
Au/MnO_x	297	428
MnO_x	331	456
CeO_2	541	
Au/CeO_2	162	
10% Ce/β-MnO_2	377	469
1% Ce/β-MnO_2	406	462

[a] the peak maxima from TPR profile

4.2.4.1. TPR profiles of β-MnO_2 and Au/β-MnO_2 catalysts

Figure 4.16 (a)-(d) depicts the temperature reduction program (TPR) profiles for the support (β-MnO_2) and gold loaded β-MnO_2 samples. The reduction profiles were recorded over the temperature range from 100 to 700 °C.

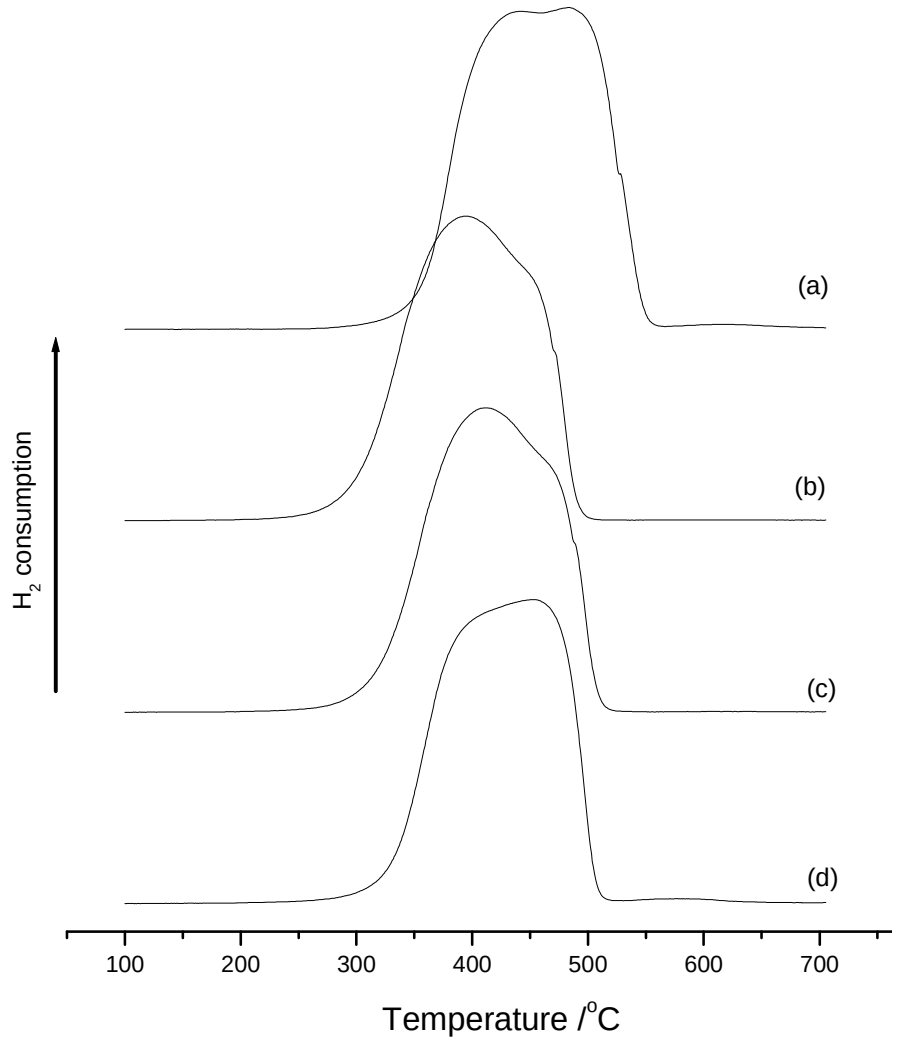


Figure 4.16: H_2-TPR profiles of gold-manganese based catalysts (a) β-MnO_2 (b) Au/β-MnO_2 300 °C, (c) Au/β-MnO_2 350 °C and (d) Au/β-MnO_2 GP

The pure manganese dioxide reduction profile showed two broad asymmetrical overlapping peaks. β-MnO_2 reduces in a two step reduction sequence $MnO_2 \longrightarrow Mn_3O_4 \longrightarrow MnO$. MnO is difficult to reduce to metallic Mn (>800 °C). The reduction profile of the β-MnO_2 sample was similar to that reported in the literature [6, 12, 13]. H_2 consumption by β-MnO_2 was observed at 437 °C and 494 °C. The lower temperature peak is assumed to be the reduction of MnO_2 to Mn_3O_4 whereas the higher temperature peak represents the reduction of Mn_3O_4 to MnO [6, 13]. The β-MnO_2 sample was reduced to MnO, and the formation of the intermediate Mn_3O_4 appears to be difficult to stabilise under the reduction conditions.

The addition of gold to the β-MnO_2 resulted in a shift of the reduction peaks to lower temperature (Figure 4.16). The Au enhanced the reduction of β-MnO_2.

Furthermore, TPR profile for the Au/β-MnO_2 300 and Au/β-MnO_2 350 samples showed that the lower calcination temperature used in the study induced a positive effect on the reducibility of the catalyst. Calcining the Au/β-MnO_2 sample at 300 ^oC decreased the reduction temperature more than when compared with the sample calcined at 350 ^oC. The reduction temperature peaks of Au/β-MnO_2 350 were at 405 ^oC and 469 ^oC, compared with Au/β-MnO_2 300 catalyst peaks at 394 ^oC and 453 ^oC. The overall effect is that both the calcination temperature and the Au enhanced the reduction of β-MnO_2. Analogous effects of adding gold were observed to an Au/ZrO_2 catalyst [14]. This observation indicates that new found metal-support interactions in the synthesized Au/β-MnO_2 resulted in a more easily reduced β-MnO_2. The change in MnO_2 reducibility is presumably influenced by the hydrogen spillover effect as seen for Pt/MnO_x catalysts [12]. A strong interaction between Au and β-MnO_2 allowed hydrogen to react with β-MnO_2 to give the metal-support interactions observed. Figure 4.16(d) shows the TPR profile of Au/β-MnO_2 GP; the colloid was prepared with PEG. In this instance Au/β-MnO_2 GP proved to be more difficult to reduce. This could be that calcining at 200 $^\circ C$ does not suffice strong Au-support interactions.

4.2.4.2. TPR profiles of γ-MnO_2 and Au/γ-MnO_2 samples

The reduction profiles of the γ-MnO_2 and Au/γ-MnO_2 samples were shown Figure 4.17 (a) and (b), respectively. The γ-MnO_2 prepared by an oxidative combustion method shows two peaks in the TPR profile similar to that seen for Au/γ-MnO_2. Upon addition of gold the TPR peaks shifted to lower temperatures but exhibited similar intensities. The first reduction temperature was lowered from 364 ^oC for the γ-MnO_2 to 318 ^oC for Au/γ-MnO_2 sample, while the second peak was also lowered from 544 ^oC to 460 ^oC. Compared with those of γ-MnO_2, the TPR peaks of Au/γ-MnO_2 sample showed low reduction temperature peaks. It can

be inferred that the Mn in Au/γ-MnO_2 is more reducible than the Mn in the γ-MnO_2 sample. Stobbe and others have also established that the reducibility of MnO_2 depends on its crystallographic structure and morphology [6, 13, 15].

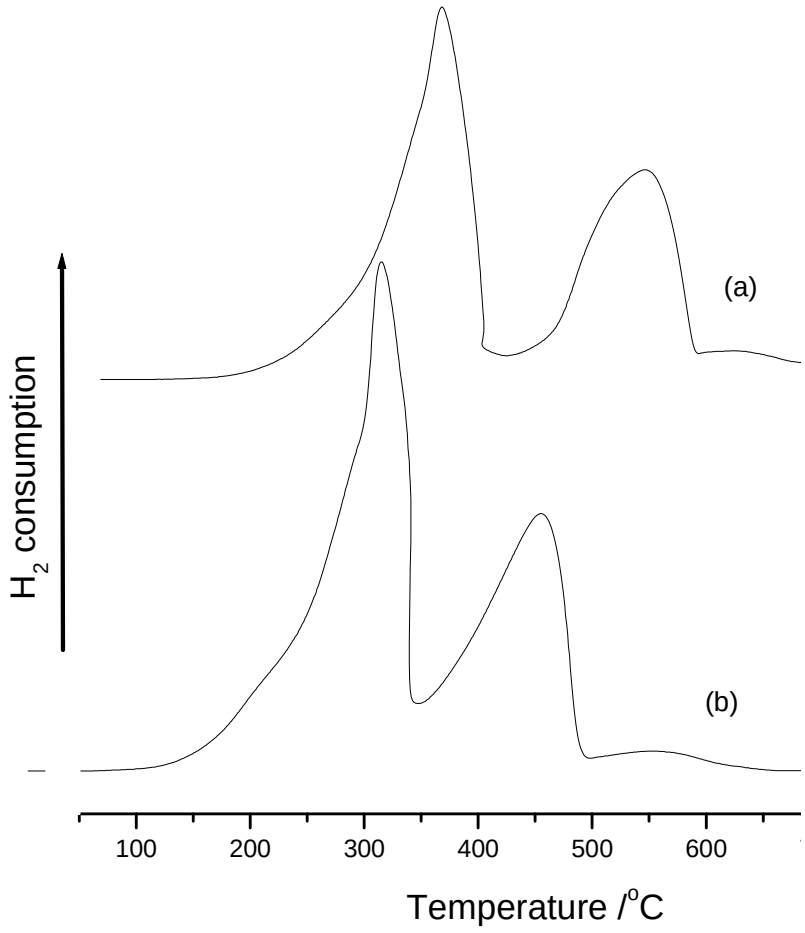


Figure 4.17: H_2-TPR profiles of a) γ-MnO_2 b) Au/γ-MnO_2 catalysts prepared by oxidative combustion of $MnCO_3$

4.2.4.3 TPR profiles of MnO_x and Au/MnO_x samples

The TPR profiles of MnO_x and Au/MnO_x were also recorded. The Au/MnO_x sample reduced at a lower temperature than the MnO_x catalyst (Table 4.2). Peaks shifted towards lower temperature suggesting that the gold assisted the Mn oxide reduction process.

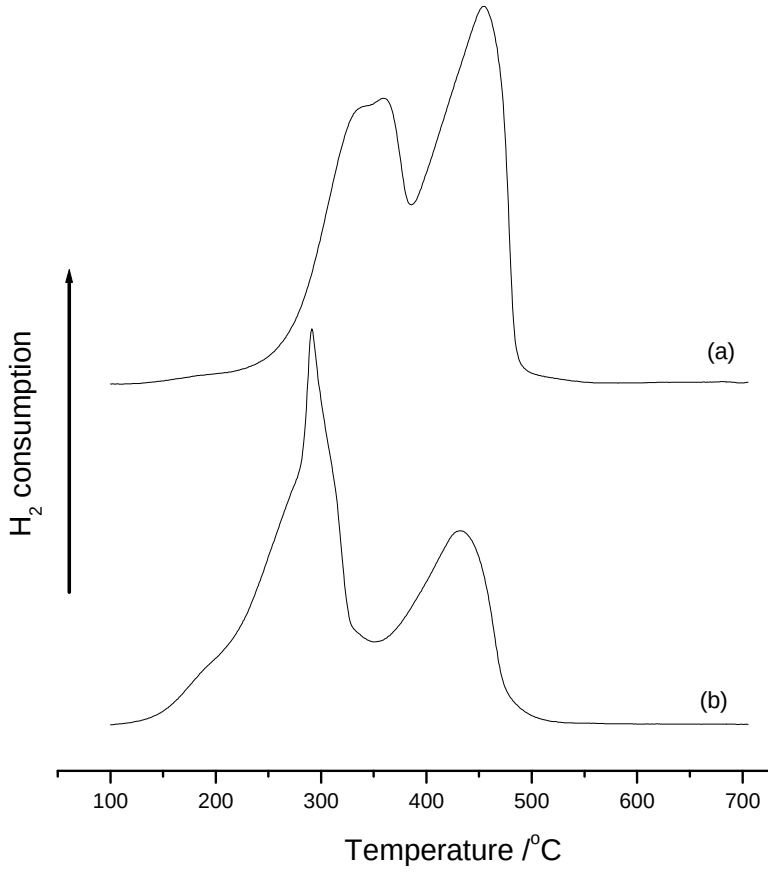


Figure 4.18: H_2-TPR profiles of a) MnO_x and b) Au/MnO_x catalysts prepared by co-precipitation

The XRD profiles confirmed that MnO_2 and Mn_3O_4 phases were generated from the Au/MnO_x sample. Two overlapping peaks, one at 331 ^oC and the other at 347 ^oC, could be due to the reduction of MnO_2 and the peak at 456 ^oC due to the reduction of Mn_3O_4. The most apparent difference with the samples is the low temperature peak in Figure 4.18. The Au/MnO_x sample shows that the first reduction peak has shifted to 279 ^oC on addition of gold. MnO would be the final reduction state from the different Mn species present.

4.2.4.4 TPR profiles of CeO_2 and Au/CeO_2 samples

TPR profiles for CeO_2 and Au/CeO_2 samples are shown in Figure 4.19 (a) and (b), respectively. Diffraction patterns showed the cubic fluorite structure of CeO_2 was present in the Au/CeO_2 sample. A large reduction peak was observed at 541 ^oC for CeO_2 (Figure 4.19(a)) but diminished when gold was added. The broad peak at 162 ^oC in Figure 4.19 (b) is said to be due to the reduction of surface-capping oxygen atoms on ceria [16, 17]. A shift in reduction temperature was caused by gold which decreased the strength of the Ce-O bond for the Ce bonded to gold through a hydrogen spillover effect and/or activation. Therefore addition of gold has markedly decreased the reduction temperature of CeO_2.

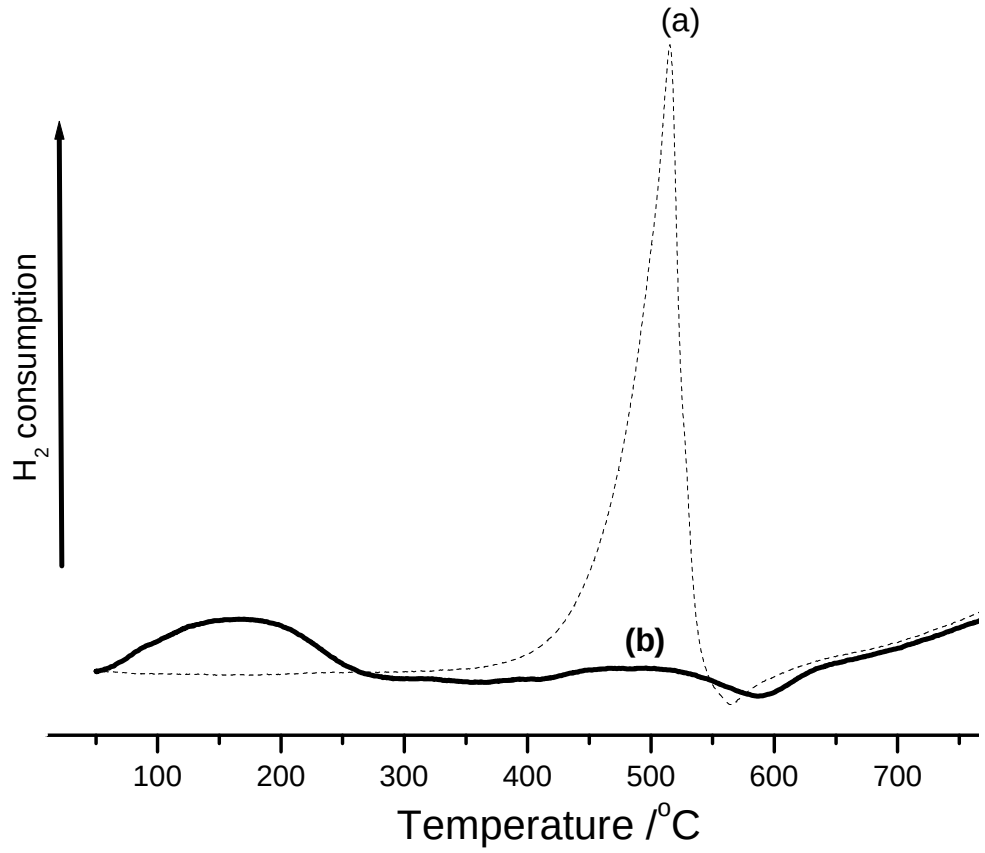


Figure 4.19: H_2-TPR profiles of a) CeO_2 and b) Au/CeO_2 catalyst

The TPR profiles of gold deposited on TiO_2, Al_2O_3 and ZnO were also measured. The H_2 consumption peaks associated with Au were found to be very weak or non-existent (TPR profiles not shown).

4.2.4.5 TPR profiles of CeO_2-MnO_2 samples

Figure 4.20 shows the reduction profile of a Ce/β-MnO_2 catalyst with varying Ce loadings (1% and 10%). There is very little difference in the 1% Ce/β-MnO_2 TPR profile (Figure 4.20 (c)) compared with β-MnO_2. The 10% Ce/β-MnO_2 sample reduction profile shows a low temperature peak at 377 ^{o}C followed by high temperature peak at 469 ^{o}C (Figure 4.21 (a)). The high temperature peak could be due to both ceria and MnO_2 reduction. Ceria reduces at 541 ^{o}C (Figure 4.20 (a)), which was in the same region as the β-MnO_2 reduction. Overall, an increase in the ceria content shifts the TPR peaks to lower temperature.

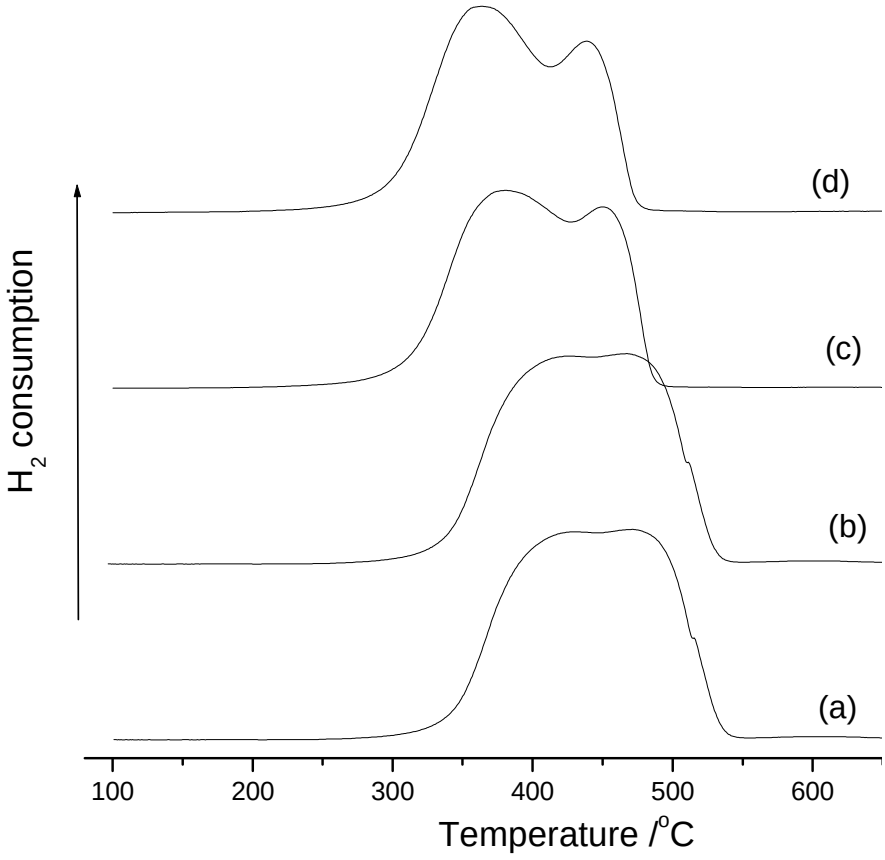


Figure 4.20: H_2-TPR profiles of a) β-MnO_2 b) 1% Ce/β-MnO_2 and c) 5% Ce/β-MnO_2 d) 10% Ce/β-MnO_2

4.2.5 Thermogravimetric analysis (TGA)

Thermogravimetric analysis (TGA) profiles were recorded on the Au/β-MnO_2 catalysts systems synthesised. Little was gleaned from the studies. The Au/β-MnO_2 GP did not show loss of carbon at 600 °C. The profile was similar as β-MnO_2 TGA profile and only showed water loss (see appendix C).

4.3 Reactor studies

The activity of the catalysts for the catalytic combustion of volatile organic compounds (VOCs) was tested in a conventional fixed bed glass reactor at atmospheric pressure. Blank tests using the reactor without the catalysts placed in the reactor (at 300 ^{o}C) showed no oxidation took place under these conditions. The VOC studied was 2-propanol. The gas mixture made up of the 1% VOC in air was then passed through 300 mg catalyst at a flow rate 26 h^{-1}. The catalysts studied are listed in Table 4.3 along with the temperature required to oxidise 50% and 90% of VOCs. These temperatures at which 50% and 90% conversion occurred are labelled T_{50} and T_{90}, respectively. The CO_2 and other products produced were detected using GC coupled to TCD and FID detectors by online analysis. The total gas flow was set at 100 ml/min.

Table 4.3: Light off temperatures for 2-propanol oxidation

Catalyst code	T_{50} /^{o}C	T_{90}/^{o}C
Au/Al_2O_3	94	245
Au/ZnO	96	228
Au/TiO_2	168	243
Au/CeO_2	171	196
Au/β-MnO_2 350	225	268
Au/β-MnO_2 300	207	275
Au/β-MnO_2 GP	162	243
Au/MnO_x	169	228

Au/γ-MnO_x	144	192
β-MnO_2	263	300
MnO_x	218	284
γ-MnO_x	164	227
10% Ce/β-MnO_2	231	297
1% Ce/β-MnO_2	253	293

T_{50} and T_{90} are the temperatures at which 50 % and 90% respectively of 2-propanol was reacted

4.3.1 2-Propanol catalytic oxidation

Propanol was taken as a model volatile organic compound (VOC) in this study. Complete combustion (100 % conversion) was obtained at or below 350^{o}C for all the catalysts. Incomplete oxidation products were detected in some cases; propene and/or acetone were produced. No CO was detected in any of the experiments.

The conversion of 2-propanol as a function of temperature is presented in Figure 4.22 -4.35. The various supports, with 1 wt.% gold loading, were used for the oxidation of 2-propanol. The conversion was measured over the temperature range of 25-350 ^{o}C. The general observation is that 2-propanol conversion steadily increased with temperature. In certain instances, incomplete oxidation of 2-propanol led to the formation of acetone and/or propene. The occurrence of partial oxidation is most prevalent at temperatures below 300 ^{o}C.

Firstly, we shall compare the effects of the support material loaded with gold particles followed by discussion of manganese supports synthesized in comparison with the commercial MnO_2 support. The various supports used exhibit different catalytic activity towards 2-propanol oxidation. A detailed analysis of the catalytic behaviour of the different materials is given below. A typical data set is shown in Figure 4.22 with T_{50} and T_{90} marked by dotted lines.

4.3.1.1 2-propanol oxidation Au on various supports: Al_2O_3, ZnO, TiO_2, and CeO_2

The Au/Al_2O_3 and Au/ZnO were active with a 2-propanol conversion > 55 % conversion at temperatures ≤100 ^oC (Figure 4.21 and 4.22). T_{50} for Au/Al_2O_3 and Au/ZnO catalysts respectively occurred at 93 ^oC and 96 ^oC. At higher temperature the selectivity towards acetone increased and eventually decreased at temperatures above 150 ^oC. This occurred together with an increase in propene production. At higher conversion, higher propene selectivity was measured as acetone production decreased. The CO_2 production increased with temperature. At T_{90}, 30 % selectivity towards CO_2 production was noted. This sample was most active towards partial oxidation of 2-propanol. The experiments were not carried out above 350 ^oC, to avoid agglomeration of Au particles and subsequent deactivation of the catalyst.

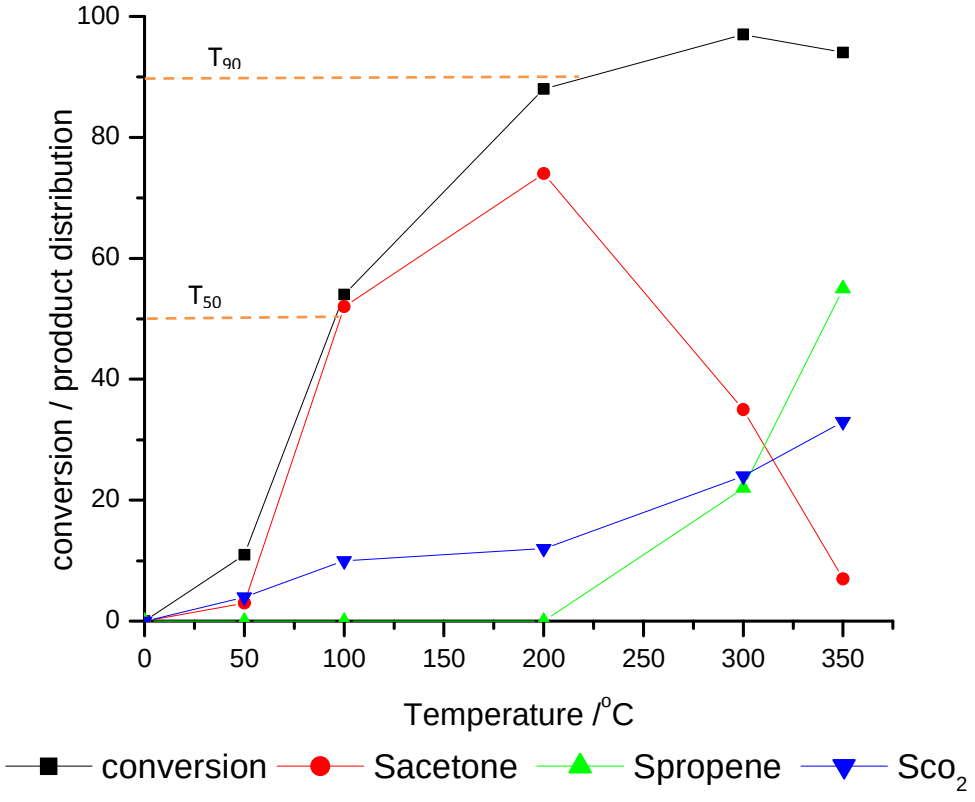


Figure 4.21: Conversion of 2-propanol to various products over the Au/Al_2O_3 catalyst

Alumina support contains a high concentration of acidic and basic sites which impacts on the adsorption and hence oxidation of 2-propanol to CO_2. There have been previous attempts to use alumina for propanol oxidation. Domiguez and co-workers found that for propanol oxidation by Au/Al_2O_3, selectivity was biased towards propene rather than acetone [18]. The results obtained correlate with earlier studies on Au/Al_2O_3 [19].

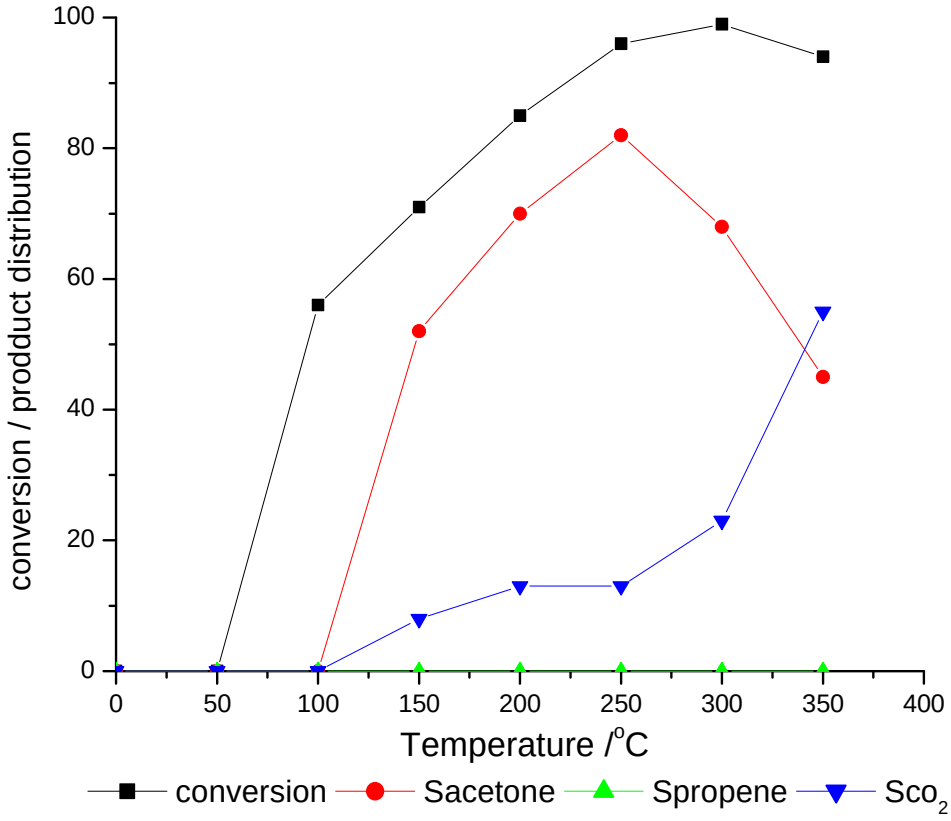


Figure 4.22: Conversion of 2-propanol to various products over the Au/ZnO catalyst

Results from the oxidation of 2-propanol over Au/ZnO are shown in Figure 4.22. The Au/ZnO sample is a very promising catalyst for acetone production. At T_{90} = 228 °C the selectivity towards acetone, $S_{acetone}$, was 75 % and selectivity towards CO_2, Sco_2 , was 13 %. At temperatures above 300 °C more CO_2 is produced. Throughout the temperature range studied no or very little propene was detected.

The oxidation of 2-propanol over Au/TiO_2 was investigated and data are shown in Figure 4.23. Au/TiO_2 behaves similarly to Au/Al_2O_3 and Au/ZnO. The Au/TiO_2 shows a steady

increase in conversion with temperature but produces less acetone than the Au/ZnO and Au/Al_2O_3 catalysts. At T_{50}, $S_{acetone}$ and Sco_2 were 33 and 8 %, respectively. T_{90} was reached at higher temperatures than found for the Au/ZnO and Au/Al_2O_3 catalysts. Selectivity towards CO_2 was improved. Complete oxidation of 2-propanol to CO_2 were attained at 350 ^oC. Trace amounts of propene was observed at 250 ^oC.

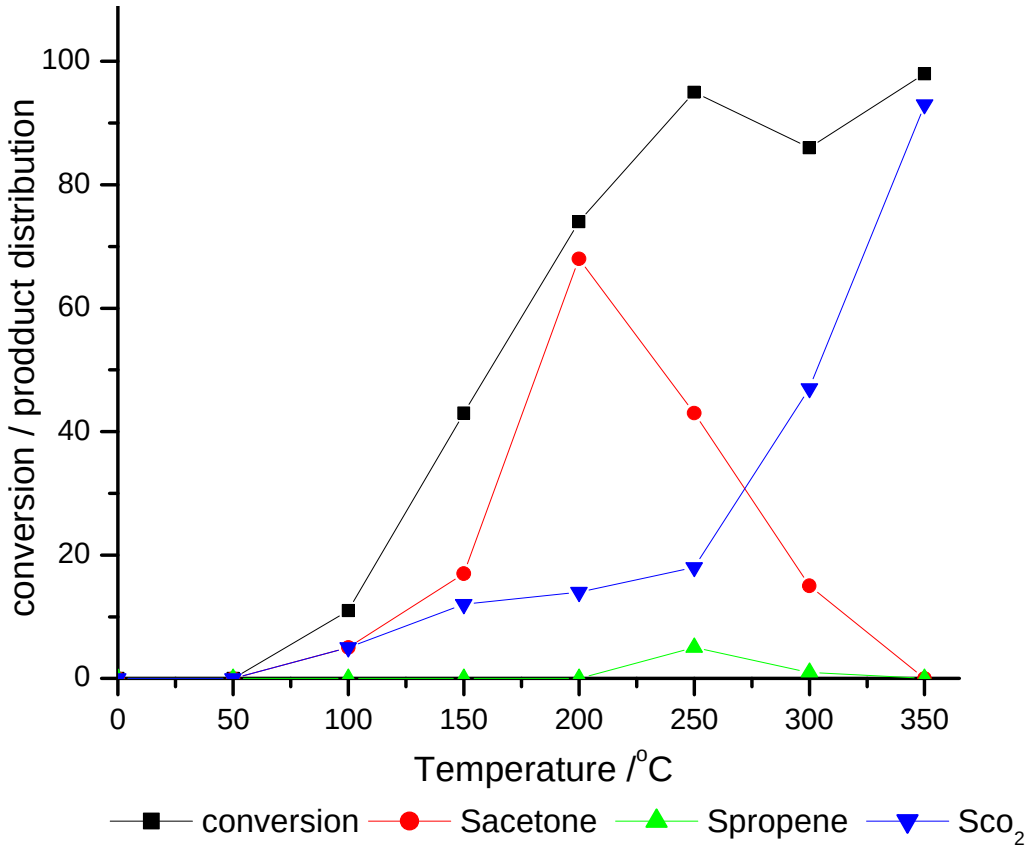


Figure 4.23: Conversion of 2-propanol to various products over Au/TiO_2

The activity of the Au/CeO_2 catalyst is shown in Figure 4.24. T_{50} was found at 171 ^oC, the highest temperature when compared with the other catalyst measured; but the Sco_2 was the highest at 35%. A noteworthy observation is that CO_2, water and acetone were the only products formed under the experimental conditions used. Acetone was formed at lower temperatures with near complete selectivity. At higher temperatures (>170 ^oC) there was a corresponding increase in selectivity towards CO_2. Complete oxidation was achieved at 200 ^oC, a temperature below what the other supports showed.

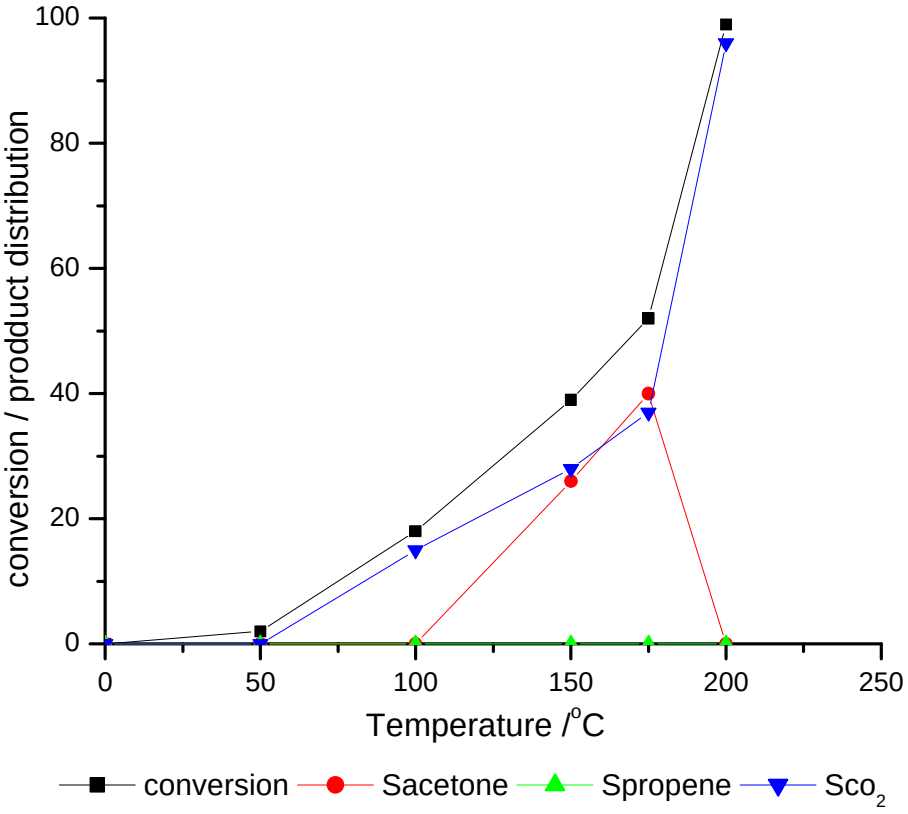


Figure 4.24: Conversion of 2-propanol to various products over Au/CeO_2 catalyst

The CeO_2 support is well known for its superior redox properties which allow lattice oxygen movement to the surface. This lattice oxygen could be used in the oxidation reaction [16]. CeO_2 supported catalysts were found to be highly active. Even though the Au/TiO_2 average gold particle sizes and distribution were the smallest, the catalyst failed to meet the same catalytic performance as the Au/CeO_2 catalyst.

4.3.1.2. 2-Propanol oxidation by Au on β-MnO_2 catalysts

Figure 4.25 shows at 200 °C and below the catalytic performance for β-MnO_2 was very low (< 5 %). An increase in temperature revealed an increase in conversion to 51 % but with a formation of acetone together with CO_2 as products. Significant amounts of propanol were

oxidised at a temperature above 250°C. At 300 °C the conversion was 92% with formation of acetone. Selectivity towards CO_2 was 59%.

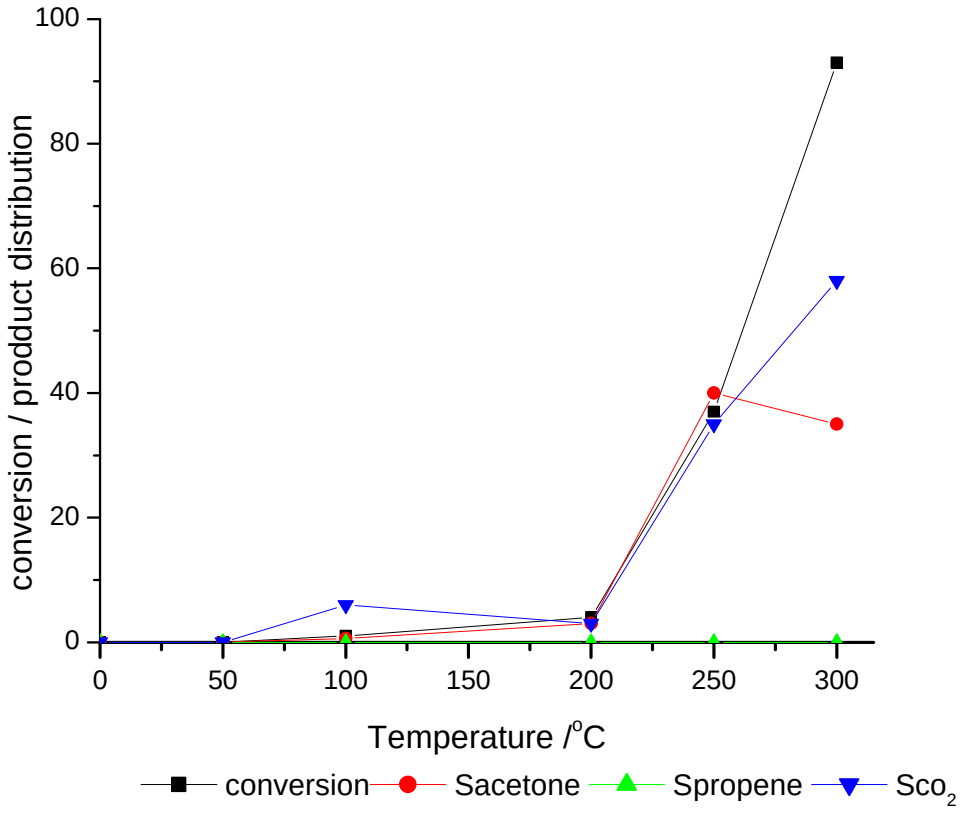


Figure 4.25: Conversion of 2-propanol to various products over support β-MnO_2

The oxidation activity of a 1% Au/β-MnO_2 loaded sample was studied. There were no structural differences between β-MnO_2 and Au/β-MnO_2 samples (see section 4.2.3.1). However, major changes in the 2-propanol oxidation reaction by Au/MnO_2 samples were observed when compared with β-MnO_2. At T_{50} for Au/MnO_2 300, Sco_2 is 43 % similar to the selectivity Sco_2 over β-MnO_2. However, there is a major difference in $S_{acetone}$. More acetone is produced over Au/β-MnO_2 300 than over MnO_2. Overall, the light off temperature of 2-propanol over the Au/β-MnO_2 300 (Figure 4.26) occurs at lower temperatures than over the β-MnO_2 support. The increased catalytic performance is associated with a higher acetone production. It is evident that β-MnO_2 is a poor 2-propanol combustion catalyst. However it is a total oxidation catalyst when gold was added to β-MnO_2.

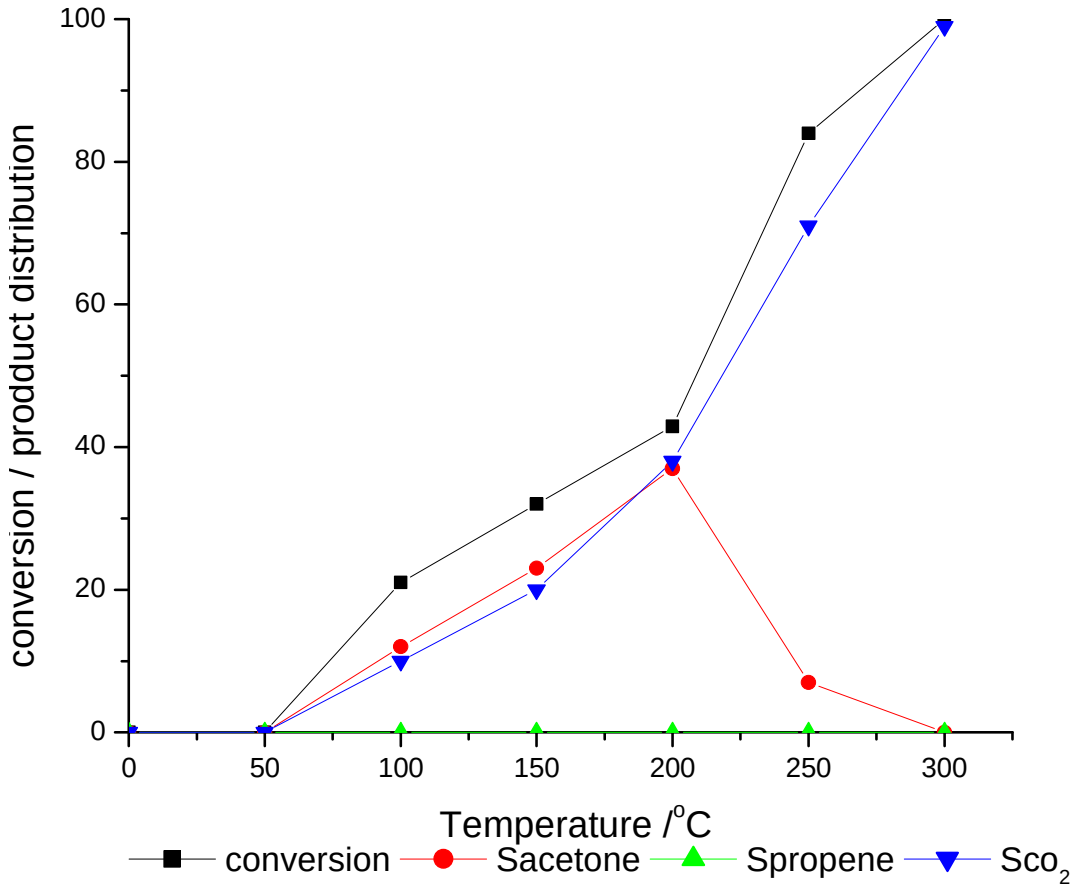


Figure 4.26: Conversion of 2-propanol to various products over Au/β-MnO_2 catalyst calcined at 300 °C

The Au/β-MnO_2 350 catalyst was also studied (Figure 4.27). The most notable changes in the catalyst due to the increased calcination temperature were the average gold particle size and distribution. Changes in the reducibility of the catalyst were also noted (see section 4.2.4.1).

The 2-propanol light off curve over Au/β-MnO_2 350 shifted to higher temperatures when compared with the 2-propanol light off curve over Au/β-MnO_2 300. At T_{90} there is a change in selectivity towards the production of CO_2; Sco_2 was 85% and 63% for Au/MnO_2 300 and Au/MnO_2 350 respectively.

It was well established that the oxidation reaction was influenced by the gold particle sizes, the crystallinity of the catalyst, the nature of the support and the surface structure of the catalyst [19-22]. Even well controlled gold particle sizes can lead to inactive catalysts unless the catalyst is treated to modify the Au-Mn interactions, for example by calcination [2].

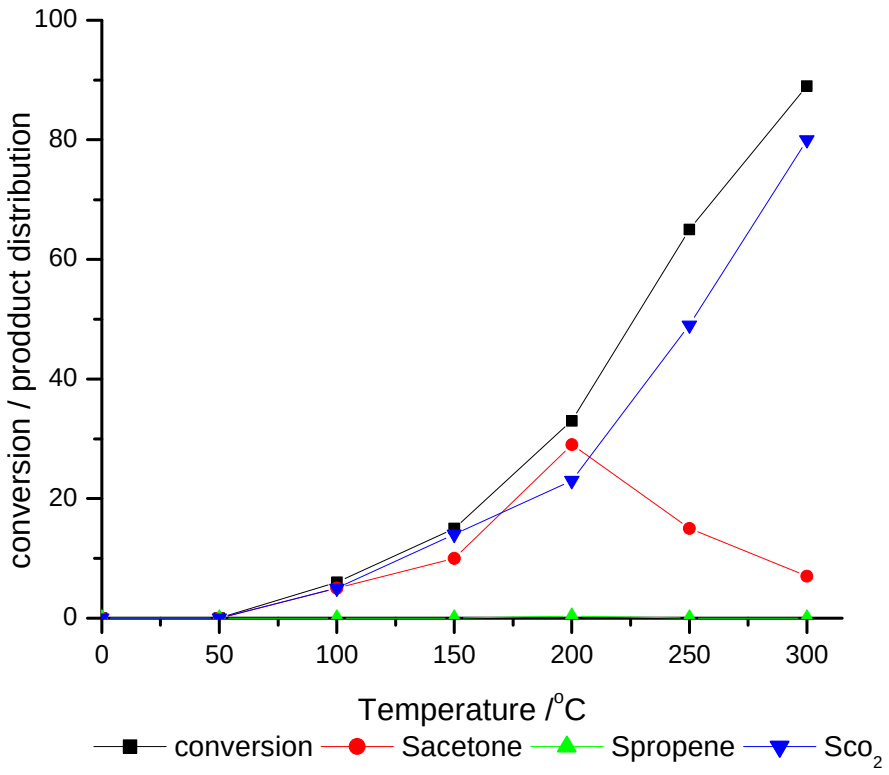


Figure 4.27: Conversion of 2-propanol to various products over Au/MnO_2 catalyst calcined at 350 °C

Prefabricated gold nanoparticles were deposited on β-MnO_2 catalyst to produce Au/β-MnO_2 GP. The sample Au/β-MnO_2 GP showed lower temperatures for 2-propanol oxidation (Figure 4.28). At 100 °C conversion is at 40% with trace amounts of acetone detected. Increasing temperature to 200 °C the conversion rises to 60%. An 84% conversion of 2-propanol the maximum for acetone selectivity was observed at 250°C. At T_{90}, Sco_2 was 79 % but $S_{acetone}$ was the highest amongst the Au/MnO_2 catalysts studied (at 37%). Complete oxidation with no trace acetone was observed at 300°C.

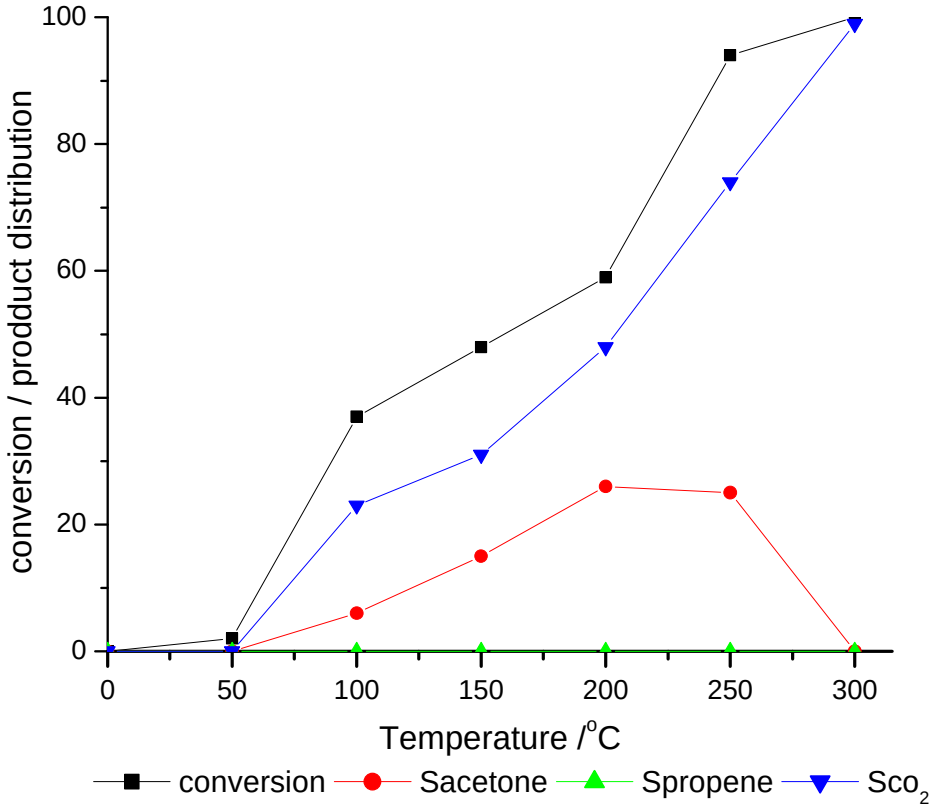


Figure 4.28: Conversion of 2-propanol to various product distribution over Au/MnO_2 GP catalyst prepared by colloid formation

The catalytic activity studies discussed above have shown that gold enhances the complete oxidation of 2-propanol by Mn oxides. The presence of gold was more efficient in improving the catalytic behaviour of the Mn oxide based catalysts when gold was added by deposition procedures.

There is a significant variation in the performance of the Au/TiO_2, Au/ZnO and Au/Al_2O_3, Au/CeO_2 and Au/MnO_2 catalysts, even though they were all prepared by the DP method. The Au/CeO_2 catalyst was more active while Au/MnO_2 was the least active at low temperature. At T_{50} and T_{90}, Au/MnO_2 required higher temperatures to achieve equivalent conversions than the Au/TiO_2, Au/ZnO and Au/Al_2O_3 catalysts. However at the same conversion levels, Au/MnO_2 had a better CO_2 selectivity. The Au/CeO_2 catalyst showed a high 2-propanol conversion, high CO_2 selectivity and lower acetone selectivity.

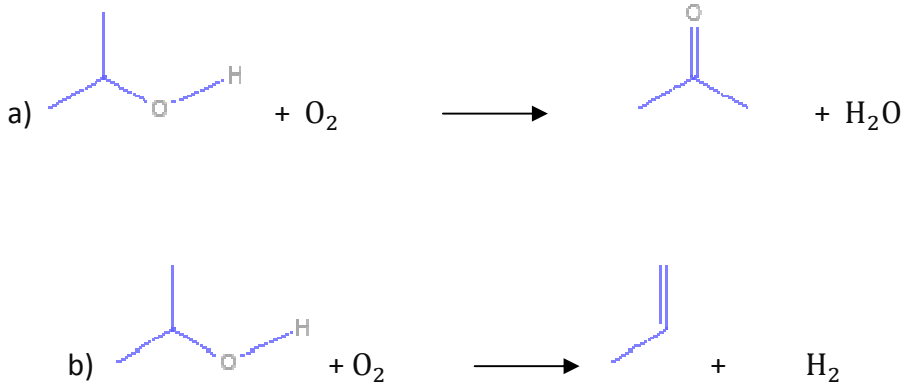
Au/Al_2O_3, Au/TiO_2 and Au/ZnO had high acetone selectivities at lower temperatures (< 200 ^oC). The Au/Al_2O_3 catalyst produced more propene at higher temperatures while the acetone selectivity decreased. These observations revealed that the activity differences are related to differences in the nature of the support. One characteristic that often is highlighted is the support's ability to provide effective lattice oxygen mobility. It has been shown that the surface structure determines the intensity of interaction and the catalytic activity. Literature reports show that the catalytic oxidation of Au catalysts depend on the interaction between gold and the support [21]. Generally CO oxidation on a gold catalyst, such as Au/TiO_2 and Au/Fe_2O_3, follows a Mars–van Krevelen mechanism. This involves the use of lattice oxygen as a reactant in the CO oxidation which is replaced with the oxygen from the feed mixture. The VOC combustion was assumed to occur through a Mars–van Krevelen mechanism [19, 23]. In this study it is seen that the highly reducible oxide, ceria, was the most active. Ceria contains a high oxygen coverage density over the surface which results in the easy breaking of metal-oxygen bonds.

The main products from the reactions were CO_2, acetone and water. Although water is one of the products formed, its presence was not quantified. During reaction, the products are formed by direct oxidation or through reaction of an intermediate. This intermediate is most likely acetone [21, 24]. There are reports of the formation of other organic compounds formed from 2-propanol oxidation. These include acetic acid and acetaldehyde [24]. However, in this study these products were not detected.

The partial oxidation of hydrocarbons over metal oxides has been widely reported [25, 26]. The partial oxidation of 2-propanol can occur via different pathways: dehydration to give propene, which is assumed to proceed at acidic sites, and dehydrogenation to give acetone that occurs at basic or redox sites (scheme 4.1).

The surface oxygen atom-hydrocarbon interactions are affected by the strength of the metal-oxygen bonds. These influence the selectivity in the oxidation reaction. Surface

species on the support change depending on whether dehydration or dehydrogenation occurs.



Scheme 4.1: Partial oxidation of 2-propanol by a) dehydrogenation and b) dehydration

The oxidation of 2-propanol to acetone does occur at low temperature and serves to indicate that basic sites are present on the catalyst surface. A similar behaviour has been described by Monicò and co-workers using Au/Fe_2O_3 for 2-propanol oxidation [19].

4.3.1.3 2-Propanol oxidation by MnO_x , Au/MnO_x, γ-MnO_2 and Au/γ-MnO_2 based catalysts

In addition to the use of the β-MnO_2 support which showed poor activity, MnO_x and γ-MnO_2 supports were also investigated. The MnO_x and γ-MnO_2 supports showed different characteristic properties from the β-MnO_2 support. This was particularly important for the gold loaded samples. The nature of support plays a role, affects the reducibility of oxides and hence influences the metal-support interactions which can override effects due to the Au particle sizes. It is widely accepted that the higher the degree of reducibility of the catalyst the higher the conversion towards desired products or selectivity. The MnO_x and γ-MnO_2 supports could be reduced at lower temperatures than the β-MnO_2 support (see Table 4.2).

Catalytic activity measurements for the 2-propanol oxidation MnO_x catalyst are given in Figure 4.29. The percentage of 2-propanol converted reached 90% at 250 ^oC on MnO_x. The highly amorphous MnO_x material had a T_{50} at 164 ^oC, 44% lower than T_{50} with the well ordered MnO_2 studied in section 4.3.1.2. MnO_x has a relatively higher surface area and better reducibility than pyrosulite. More often than not, high surface area catalysts produce higher conversion rates or activity, with better selectivity. The high surface area MnO_x was, as expected, more active for 2-propanol oxidation.

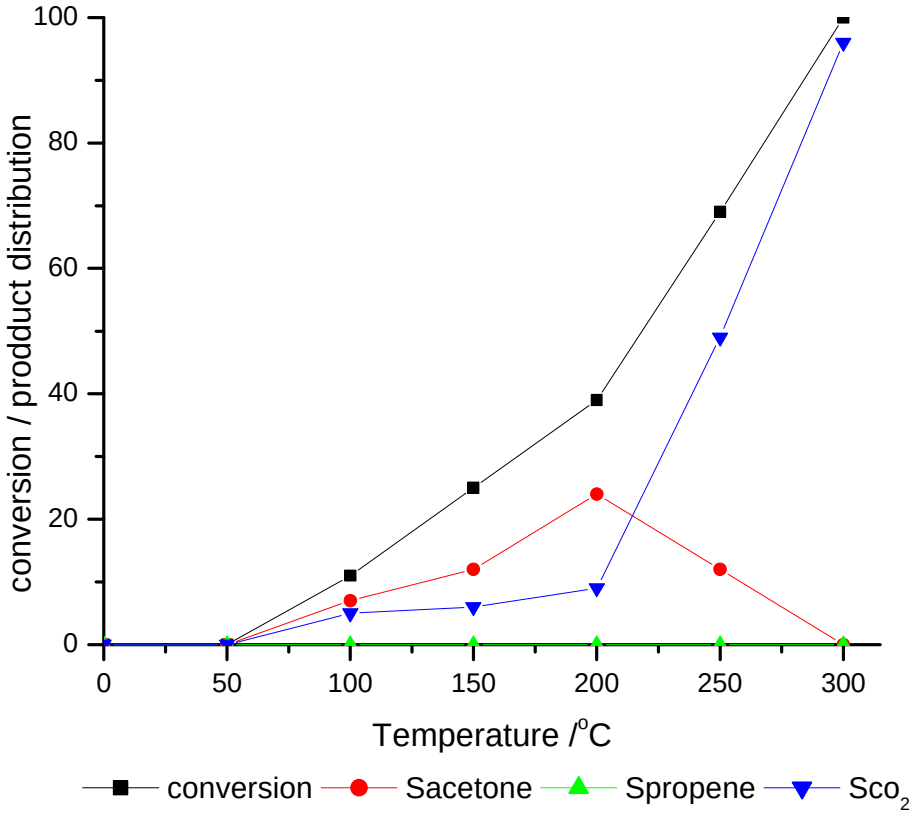


Figure 4.29: MnO_x prepared by co-precipitation and used for 2-propanol oxidation

The higher catalytic behaviour of the MnO_x sample could be attributed to the amorphous nature of the support that exposes a variety of crystal faces with diverse compositions and defects in unknown proportions. The presence of different oxygen activated species formed on the MnO_x as a result of the preparation procedure leads to different properties and activities of the catalyst.

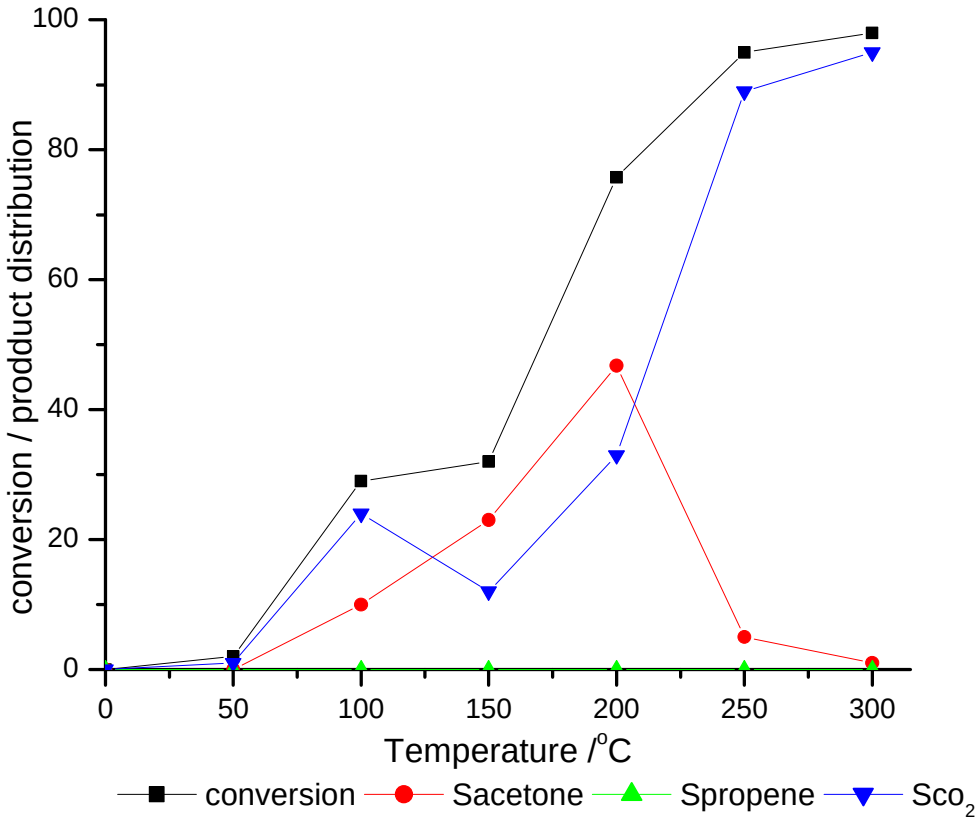


Figure 4.30: Au/MnO_x catalyst prepared by co-precipitation for the 2-propanol oxidation into various products

An Au/MnO_x catalyst was also studied for 2-propanol oxidation (Figure 4.30). At 100 ^{o}C and below the catalytic performance was very low (<30%) for the Au/MnO_x catalyst. Selectivity towards acetone was also low. At 150 ^{o}C Au/MnO_x converted about 30% of the propanol. Increasing the temperature to 200 ^{o}C, the performance of catalyst was strikingly improved (39 % to 78%). Sizeable quantities of acetone were produced.

A comparison of 2-propanol conversion over Au/MnO_x and Au/MnO_2 was made. There were noticeable differences in the catalyst activity for the complete oxidation of 2-propanol. The results in Figure 4.30 indicate that the Au/MnO_x catalyst was more active than the Au/MnO_2 catalysts (Figure 4.26 - 4.28) towards 2-propanol oxidation. Au/MnO_x was a good total oxidation catalyst. It has been shown that the structure and oxidation state of the Mn support influences the stabilisation of the active gold species and therefore impacts on the reaction pathway [27]. Samples prepared by co-precipitation produced mixed Mn species as

seen by XRD (Figure 4.12) and TPR (Figure 4.18) results. Figueroa et al demonstrated mixed Mn oxides in MnO_x identified as (Mn^{3+}) Mn_2O_3 and (Mn^{2+}) MnO_2 had an enhanced activity for ethanol oxidation compared with pure Mn_2O_3 and MnO_2 oxides [28]. The contribution of each Mn oxide and its phases is not known.

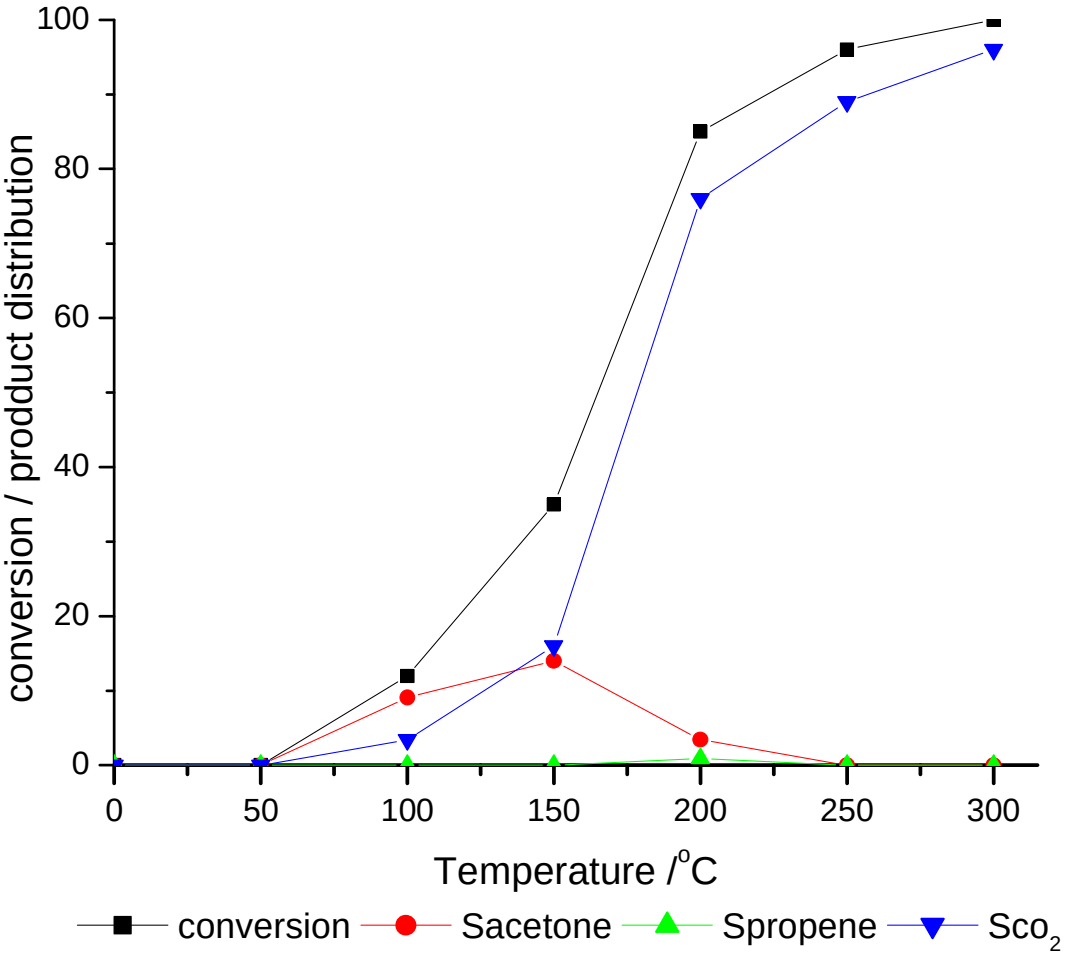


Figure 4.31: 2-Propanol oxidation over γ-MnO_2 catalyst

2-Propanol oxidation over γ-MnO_2 was studied (Figure 4.31). The selectivity was much higher than that over the β-MnO_2 at 200 °C. β-MnO_2 is made up of octahedral units (MnO_6), either corner or face sharing, that creates a crystal network tunnel to produce either the γ or the β phase. γ-MnO_2 is more porous because it is intertwined (1x1) and has (2x2) tunnels compared with (1x1) tunnels in β-MnO_2.

The percentage VOC conversion on Au/γ-MnO_2 reached 95 % at < 200 °C (Figure 4.32). The reaction T_{90} over Au/γ-MnO_2 catalyst was 28% lower than that of the Au/MnO_2 catalyst calcined at 300 or 350 °C. Though gold enhanced the catalytic activity on γ-MnO_2, the support itself was more active than the Au/β-MnO_2 300 and 350 catalysts. Lahousese and co-workers showed γ-MnO_2 was more active than a Pt/TiO_2 catalyst. The VOC oxidation reaction at steady state, i.e. VOC conversion, over γ-MnO_2 catalyst was found to be > 90% while over Pt/TiO_2 about 20% conversion was used at an operating temperature 150 °C [29].

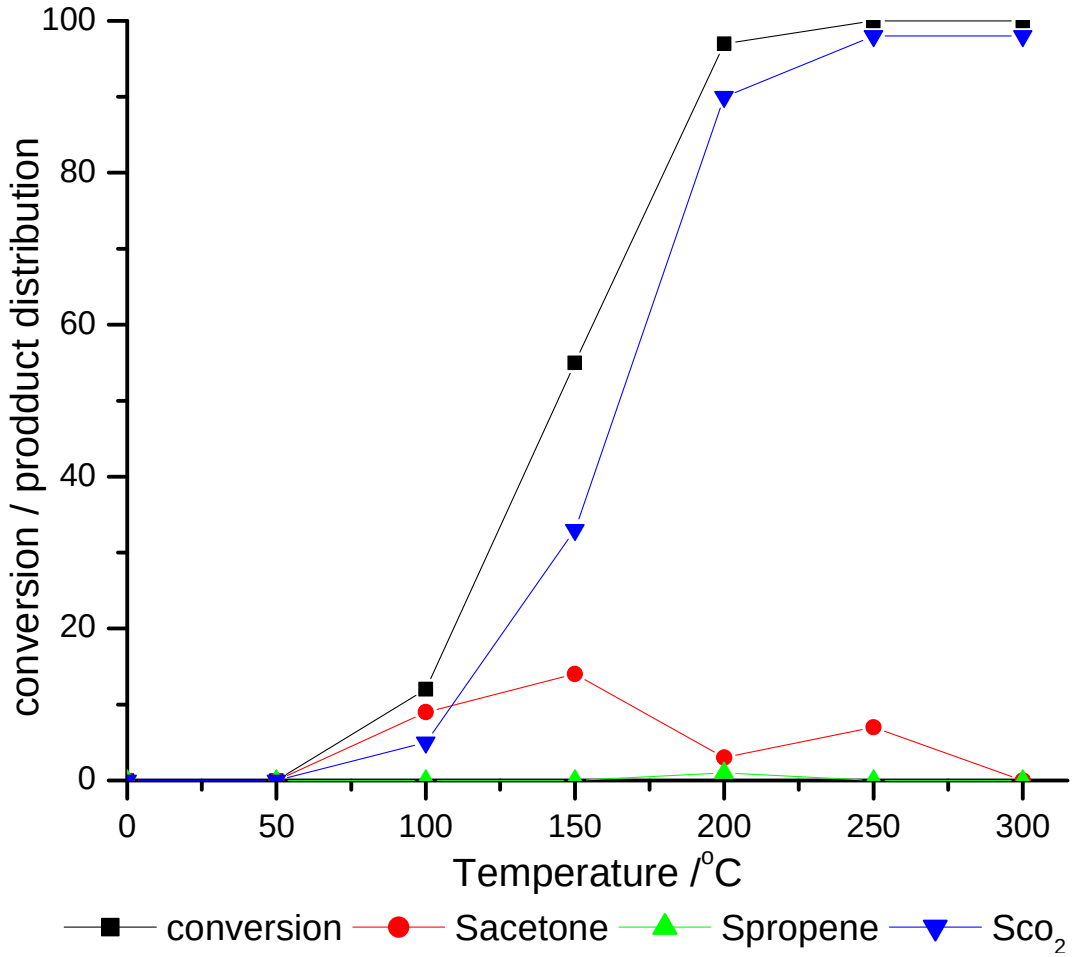


Figure 4.32: 2-Propanol oxidation over the Au/γ-MnO_2 catalyst

Furthermore, the activity of the Au/γ-MnO_2 sample was greater than over the Au/MnO_x and the CO_2 selectivity (S_{CO_2}) was also better. $S_{acetone}$ does not reach above 20 %. In fact, the activity increases sharply with temperature from 100 to 300 °C.

The Au/γ-MnO_2 catalyst was shown to be the most active catalyst of all the manganese based catalyst. The catalyst activity is in the order from most to least active was: Au/γ-MnO_2>Au/MnO_2 GP> Au/MnO_x>Au/MnO_2 300 >Au/MnO_2 350. According to Lamaita, et al and Peluso et al who investigated at γ-MnO_2 for the total oxidation of VOCs the γ-MnO_2 is more active, than β-MnO_2, because of internal water (OH groups) and the presence of oxygen vacancies in the nsutite structure [9, 30]. γ-MnO_2 has a higher internal porosity created by packing MnO_6 units and as a result has a higher surface area than β-MnO_2. The high surface area, γ-MnO_2, was more active in the 2-propanol oxidation reaction than low surface area, β-MnO_2 . At 150 ^oC, the Au/γ-MnO_2 catalyst has a conversion that is higher compared with the Au/CeO_2 catalyst. Also, the CO_2 selectivity over the Au/γ-MnO_2 catalyst is better when compared with CO_2 selectivity over the Au/CeO_2 catalyst.

4.3.1.4. 2-Propanol oxidation Ce-MnO_2 based catalyst prepared by wetness impregnation method

Amongst others, Kouraichi and co-workers studied Ce-Mn oxide systems in the hope they would be able to produce a more active catalyst than CeO_2 alone [31, 32]. In this study Ce/β-MnO_2 catalysts were prepared by incipient wetness impregnation and their activity studied. For the catalyst Ce/β-MnO_2, ceria was deposited on β-MnO_2. No ceria phase was detected (Figure 4.15). TEM images (Figure 4.10) showed ceria particles deposited on the β-MnO_2 rod surface. Very little interaction with the support caused only a small shift in the reduction temperature of the β-MnO_2. An increase of the cerium loading resulted in a decreased surface area in addition to decreased reduction temperature. This was an indication that the 1% Ce/β-MnO_2 and 10% Ce/β-MnO_2 samples were different. These catalysts were then used for 2-propanol oxidation to investigate their activity and to compare the activity with that of noble metals. The 2-propanol oxidation over 1% Ce/MnO_2 and 10% Ce/MnO_2 catalysts are shown in Figures 4.33 and 4.34 respectively.

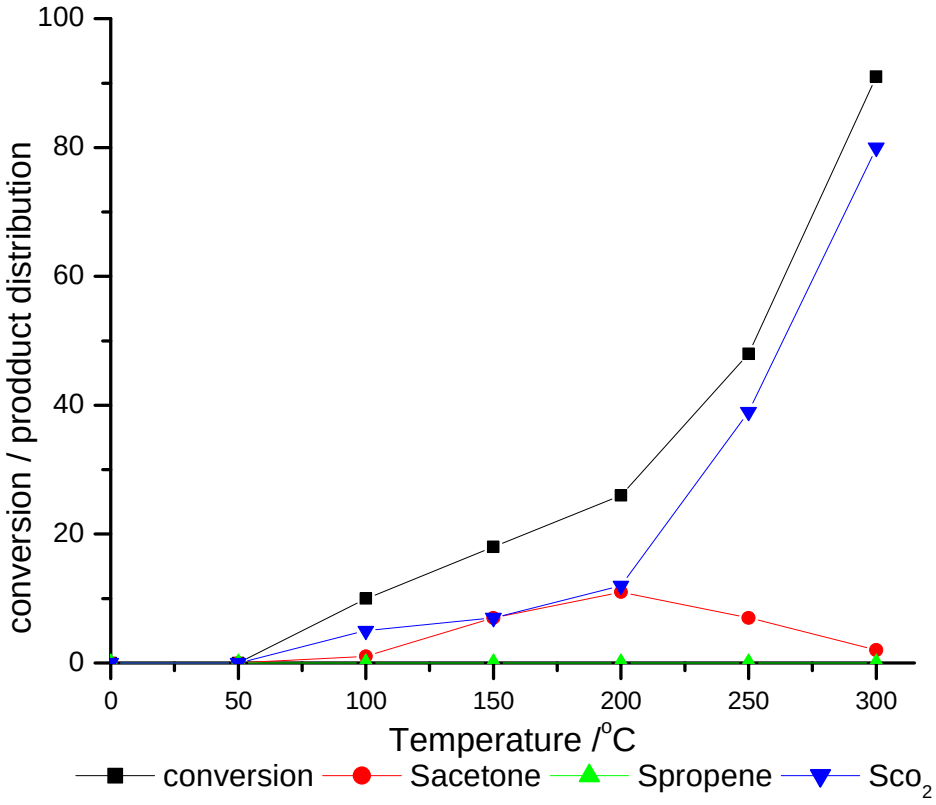


Figure 4.33: 2-Propanol oxidation over a 1% Ce/β-MnO_2 catalyst

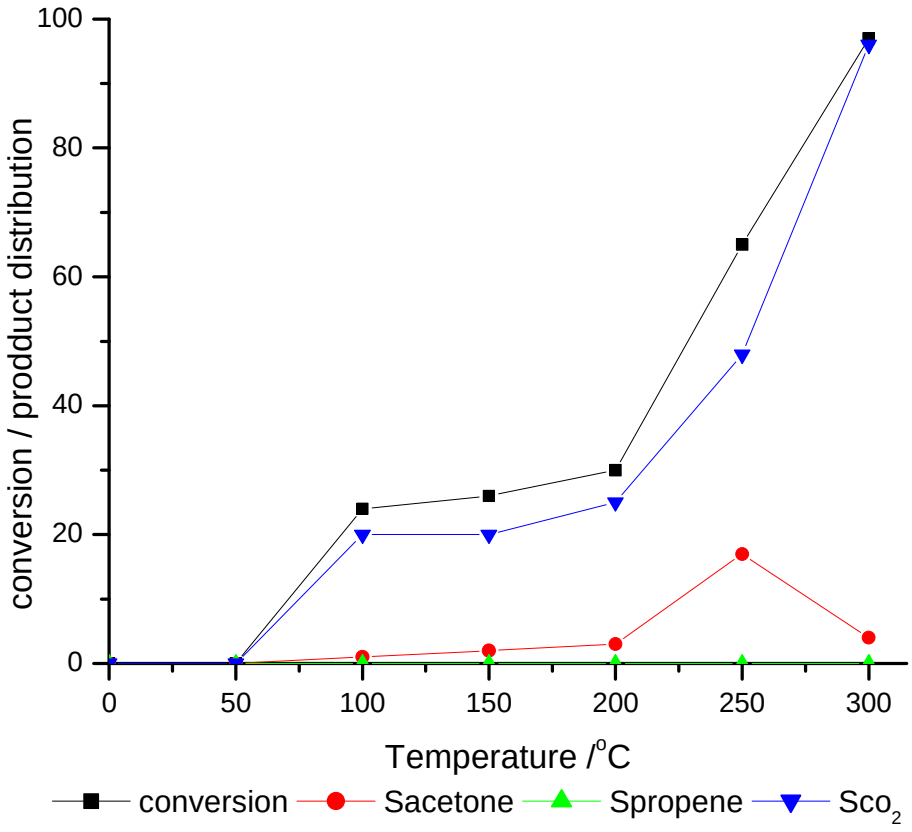


Figure 4.34: 2-Propanol oxidation over a 10% Ce/β-MnO_2 catalyst

Figure 4.33 show the 2-propanol oxidation over 1% Ce/β-MnO_2 catalyst. The activity of 1% Ce/β-MnO_2 is better than the activity of to β-MnO_2 sample (Figure 4.25). The conversion of 2-propanol as a function of reaction temperature, over a 10% Ce/β-MnO_2 catalyst is shown in Figure 4.34. The oxidation of 2-propanol had commenced at 100 ^{o}C reaching complete combustion at 300 ^{o}C. Under the experimental conditions CO_2, water and acetone were the only products formed. The selectivity to acetone ($S_{acetone}$) is initially near zero and increases with temperature but finally decreases while the selectivity to CO_2 (Sco_2) increased with temperature. The activity of 10% Ce/β-MnO_2 for 2-propanol oxidation was greater than the activity over 1% Ce/β-MnO_2 for 2-propanol oxidation. The activity of 2-propanol oxidation increased with increasing ceria loadings. Therefore, the ceria species was an active component in the Ce/β-MnO_2 catalysts.

The activity increased with cerium loading and thus indicated improvements to β-MnO_2 at temperatures above 200 °C: the 10% Ce/β-MnO_2 has greater activity than the 1% Ce/β-MnO_2. Although ceria and β-MnO_2 oxides are highly reducible oxides the Ce/β-MnO_2 catalysts were less active when compared with the gold loaded samples. Synergism between ceria and β-MnO_2 was developed in the catalyst. The mechanism by which VOCs are oxidised to CO_2 and water proceeds via the Mars van Krevelen mechanism associated with the release of the mobile oxygen. Ce-Mn oxide catalysts have been studied for VOC oxidation. The better catalytic oxidation of the Ce/β-MnO_2 catalyst relates the fact that ceria is an oxygen storage compound and provides mobile oxygen to the catalyst [16]. A ceria based catalyst has been shown to produce a high activity for toluene oxidation [33] also seen in this study.

4.3.2. 2-Butanol catalytic oxidation

There are a wide variety of compounds in the VOC category. In addition to 2-propanol, we also assessed the catalytic performance of Au/Al_2O_3, Au/TiO_2, Au/ZnO, Au/CeO_2 and Au/β-MnO_2 300 catalyst in the 2-butanol combustion reaction. Figure 4.35-4.39 shows the

percentage conversion of 2-butanol into its products over several catalysts as a function of temperature. Butanone and CO_2 were detected and no butane product was observed. The temperatures at which 50% and 90% of 2-butanol is oxidized is give in Table 4.4 as T_{50} and T_{90}, respectively.

Table 4.4: The temperatures at which 50% and 90% 2-butanol was converted over various catalysts

Catalyst code	$T_{50\%}$ /^oC	$T_{90\%}$/^oC
Au/Al_2O_3	90	267
Au/ZnO	90	192
Au/CeO_2	101	116
$Au/\beta\text{-}MnO_2$	166	278
Au/TiO_2	100	246

T_{50} and T_{90} are respectively temperatures at which 50% and 90% of 2-butanol reacted

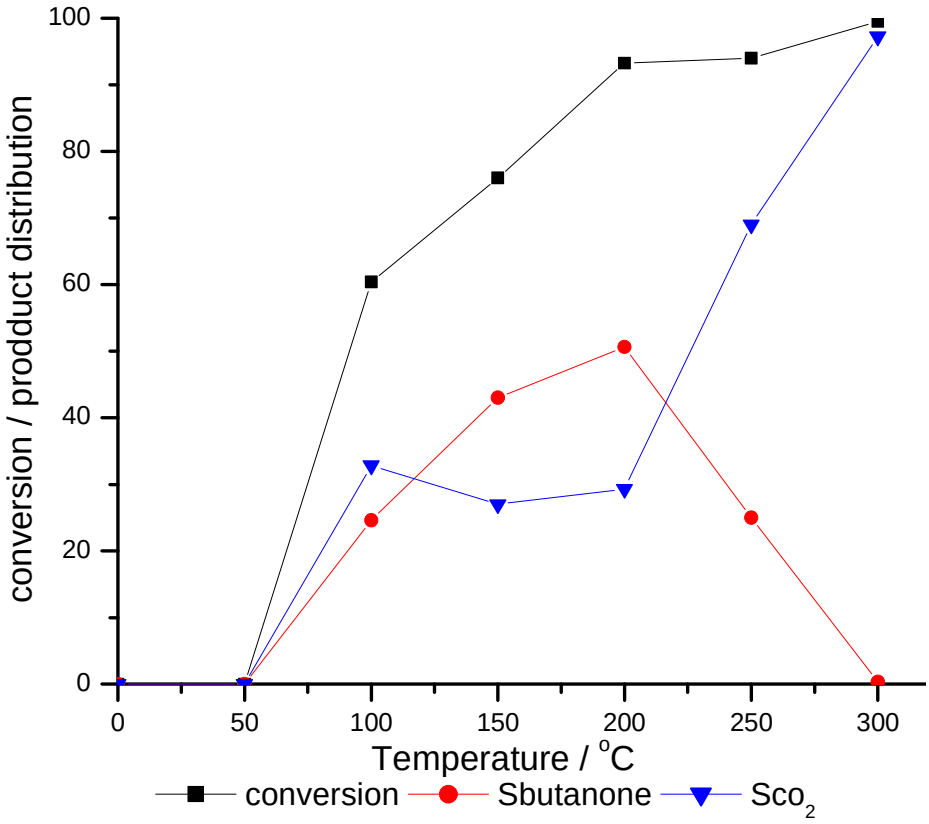


Figure 4.35: 2-Butanol oxidation over the Au/ZnO catalyst

Figure 4.35 shows the oxidation of 2-butanol over the Au/ZnO catalyst reaction. The catalyst shows high activity in the temperature range above 100 ^{o}C. The conversion of 2-butanol is detectable at 100 ^{o}C, giving rise to butanone and CO_2. The conversion grows progressively with substantial changes in product selectivity. Moreover at 192 ^{o}C the catalyst attains a 90% 2-butanol conversion but with high $S_{butanone}$ (54%) production.

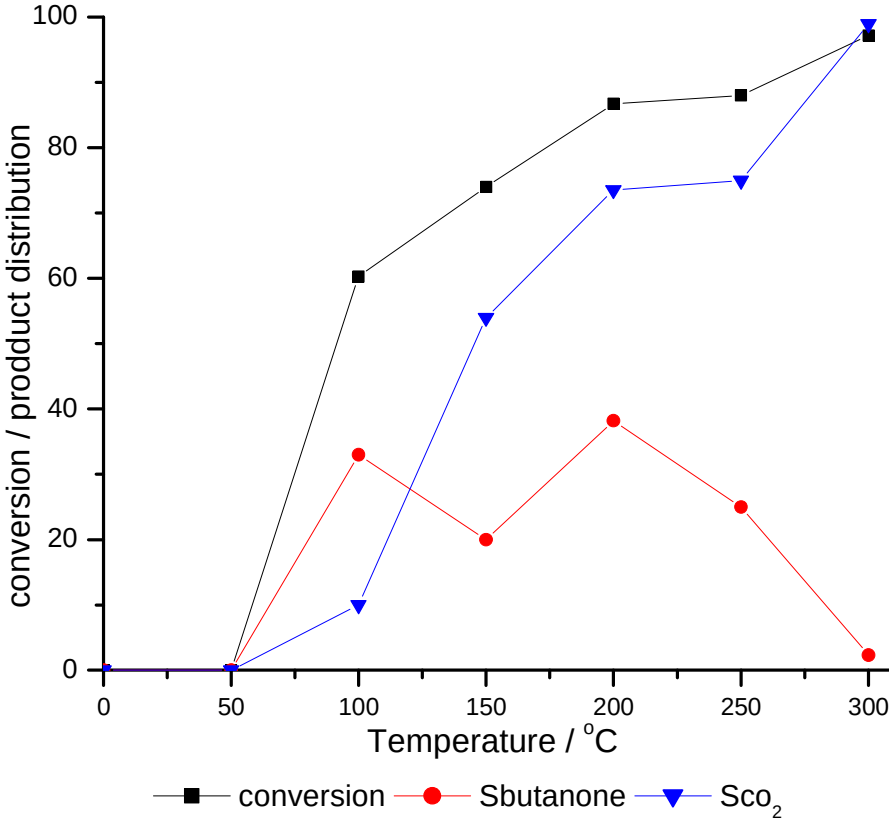


Figure 4.36: 2-Butanol oxidation over the Au/Al_2O_3 catalyst

The 2-butanol conversion measured for the Au/Al_2O_3 catalyst is indicated in Figure 4.36. The oxidation of 2-butanol had commenced at 100 °C with a conversion of 60%. T_{90} was reached at 267 °C with a high CO_2 selectivity at 83%. Butanone selectivity ($S_{butanone}$) was at 16%. At 300 °C complete combustion of 2-butanol was observed.

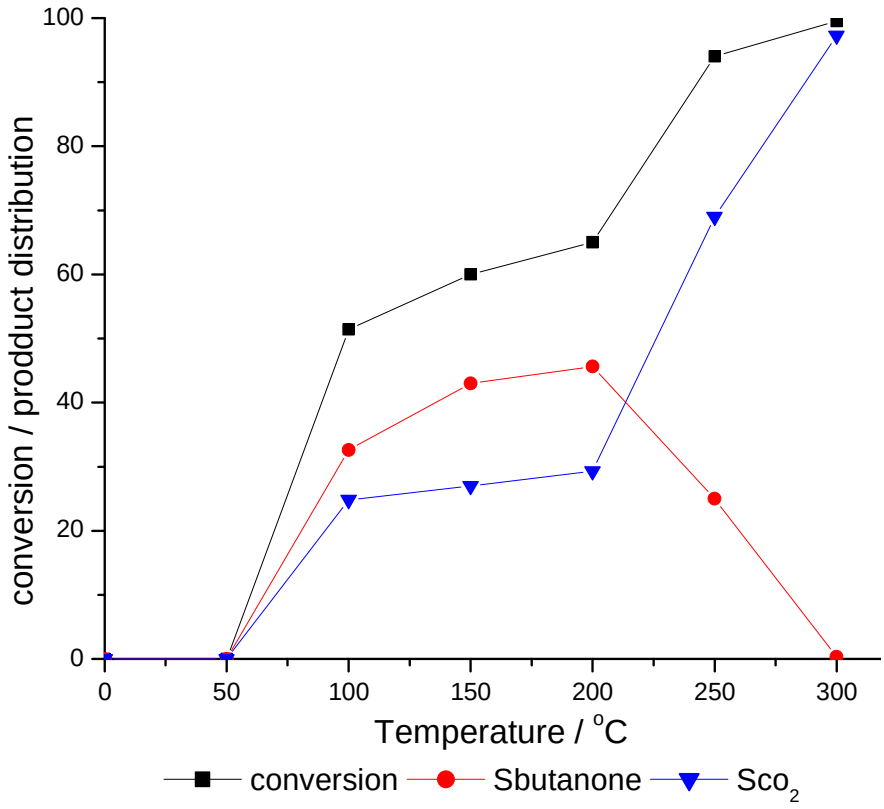


Figure 4.37: 2-Butanol oxidation over the Au/TiO_2 catalyst

In Figure 4.37 the oxidation of 2-butanol over Au/TiO_2 catalyst into various products is depicted. The Au/TiO_2 catalyst, in terms of 2-butanol conversion, was lower for this catalyst than the Au/ZnO and Au/Al_2O_3 catalysts. From Figure 4.37, it can be seen that with the Au/TiO_2 catalyst 2-butanol oxidation is already at 50 % at 100 ^oC with significant formation of butanone and CO_2 (32% and 24% selectivity respectively). The Au/TiO_2 catalyst showed its highest catalytic activity with 2-butanol oxidation conversion at 98% at 250 ^oC. At 200 ^oC, maximum butanone selectivity is reached. Further increase in temperature results in a decrease butanone selectivity as the total oxidation to CO_2 becomes more significant.

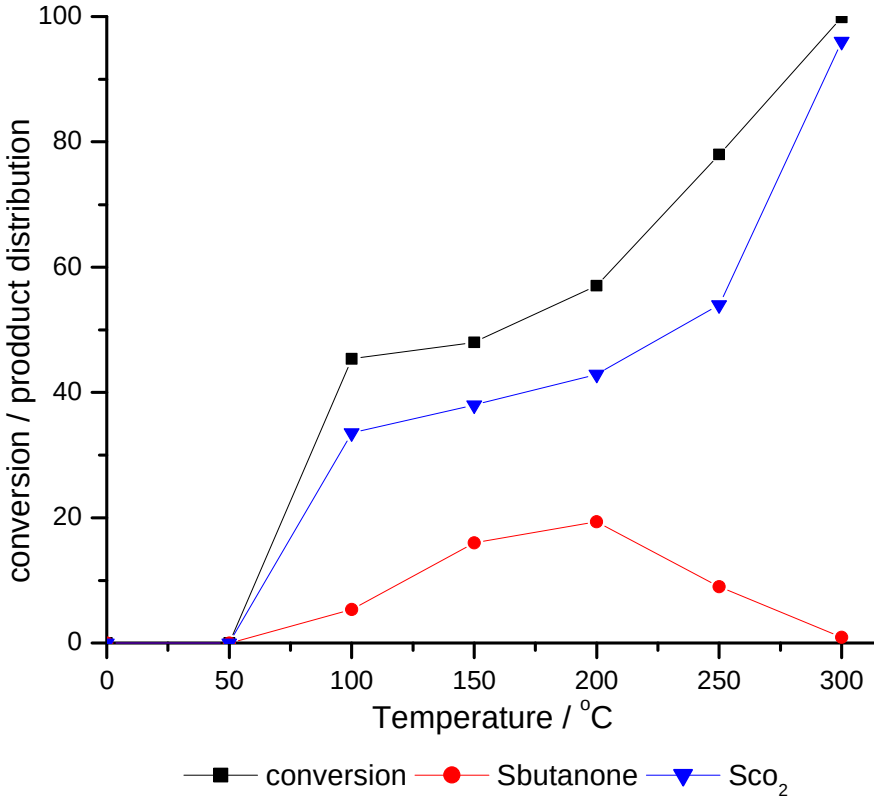


Figure 4.38: 2-Butanol oxidation over the Au/MnO_2 300 catalyst

The 2-butanol oxidation over Au/MnO_2 300 was studied and the results are shown in Figure 4.38. The T_{50} for 2-butanol oxidation over Au/MnO_2 300 was observed at 166 °C and the selectivity towards CO_2 and butanone were 39% and 17%, respectively. As the temperature was increased T_{90} was reached at 278 °C with high CO_2 selectivity (78%). The catalytic data in Figure 4.38 shows that complete oxidation was reached at 300 °C. The selectivity to butanone ($S_{butanone}$) was initially below 10% and increased with temperature, but finally decreased. Selectivity to CO_2 (Sco_2) increased at all temperatures. $S_{butanone}$ for the Au/β-MnO_2 catalyst did not reach above 20%.

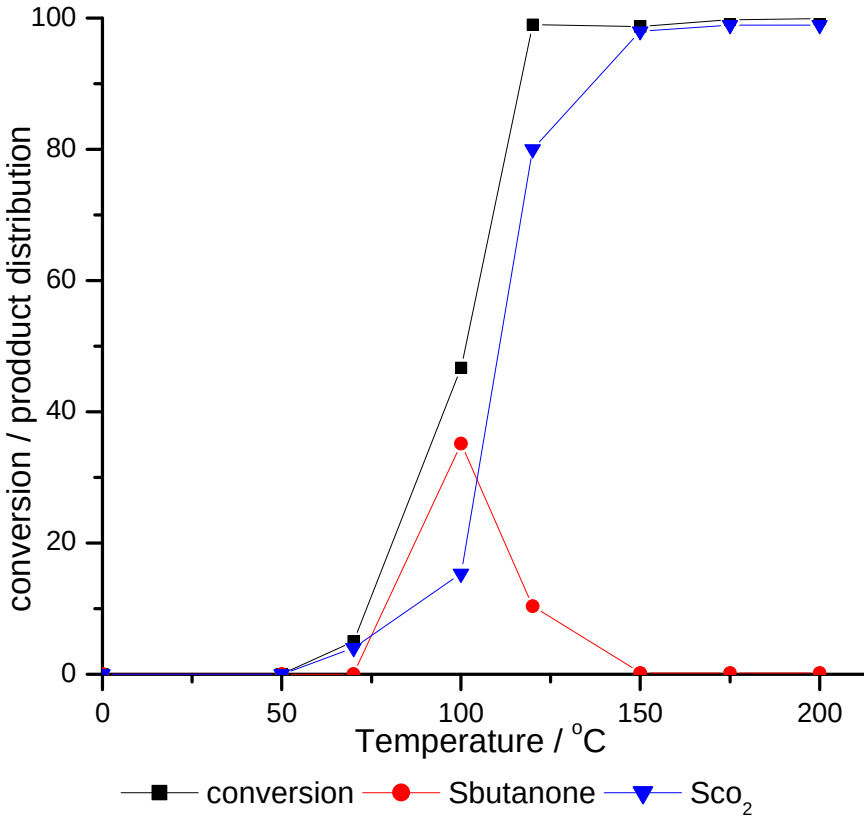


Figure 4.39: 2-Butanol oxidation over Au/CeO_2 catalyst

2-Butanol oxidation over the Au/CeO_2 catalyst is shown in Figure 4.39. Butanone is formed at 100 °C but decreases with temperature. At 150 °C 2-butanol is completely oxidised to CO_2 and no butanone is observed. The Au/CeO_2 catalyst showed the lowest T_{90} temperature recorded, that it was the most active catalyst. The Au/CeO_2 catalyst showed a higher activity than found for Au/Al_2O_3, Au/TiO_2, Au/ZnO, and $Au/\beta\text{-}MnO_2$ 300 for the 2-butanol oxidation reaction. The partial oxidation product butanone, was produced; this was more favoured than over the Au/ZnO and the Au/Al_2O_3 catalysts.

4.3.3. Toluene catalytic oxidation

Toluene, one of the BTEX compounds, is found in many air quality studies and has been shown to have a higher concentration than other VOCs emitted [34, 35]. The oxidation of the aromatic compound has been widely studied on various catalysts [22, 33]. We

investigated the use of gold catalysts in the oxidation of toluene to CO_2 and water. The catalysts used were Au/Al_2O_3, Au/TiO_2, Au/ZnO, Au/CeO_2 and Au/β-MnO_2 300. Figure 4.40 below shows the conversion of toluene as a function of temperature over the catalysts. In all cases, toluene oxidation increased with temperature. Carbon dioxide was the only reaction product and no organic compounds were detectable (Figure 4.41). The oxidation of toluene probably occurs in multiple steps that occurred concurrently [33].

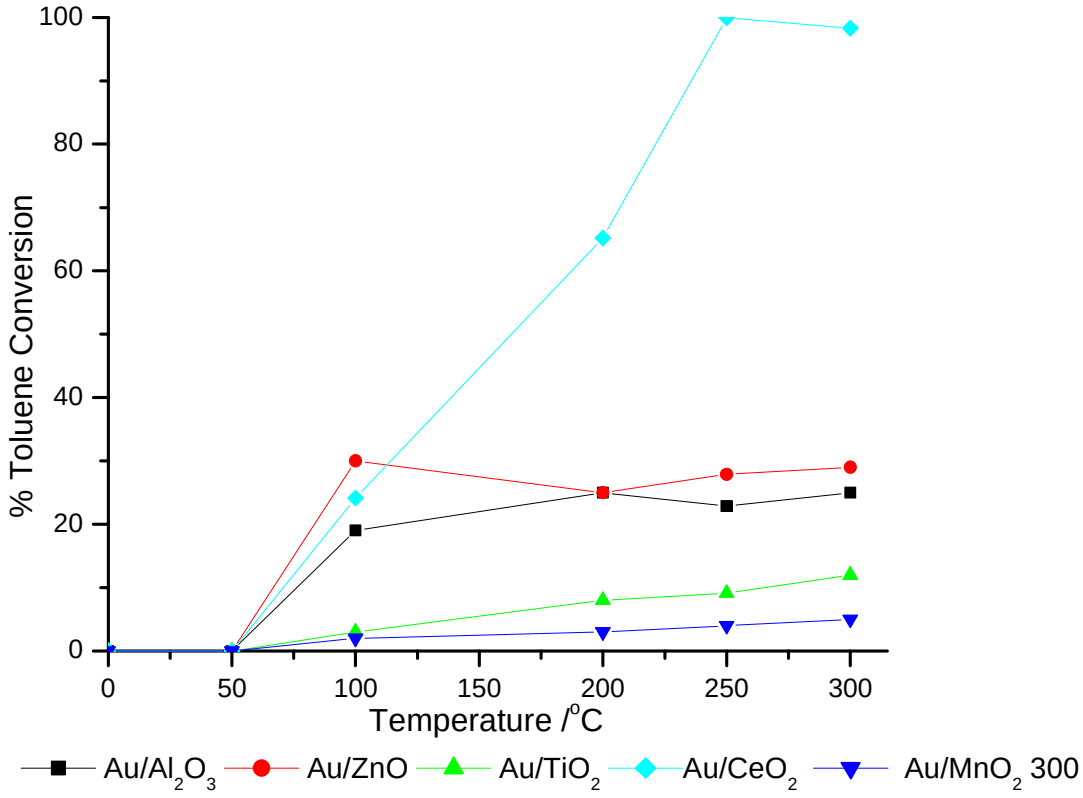


Figure 4.40: Toluene oxidation by gold catalyst

Under the conditions used toluene was initially oxidised at a temperature 100 °C over the Au/CeO_2 catalyst. The conversion increased from 24% at 100 °C to 99 % at 250 °C. The most promising catalyst for the complete oxidation of toluene was the catalyst Au/CeO_2. This is the only catalyst that completely oxidised toluene. Aromatics are difficult to oxidise when compared to alcohols [20]. It was observed that Au/TiO_2 and Au/β-MnO_2 300 catalysts were the least active catalysts; conversion did not reach 50% over the temperature range studied. Au/ZnO and Au/Al_2O_3 catalysts at 100 °C have activities at 30% and 18% respectively. No further increase in toluene conversion is observed with increasing temperature.

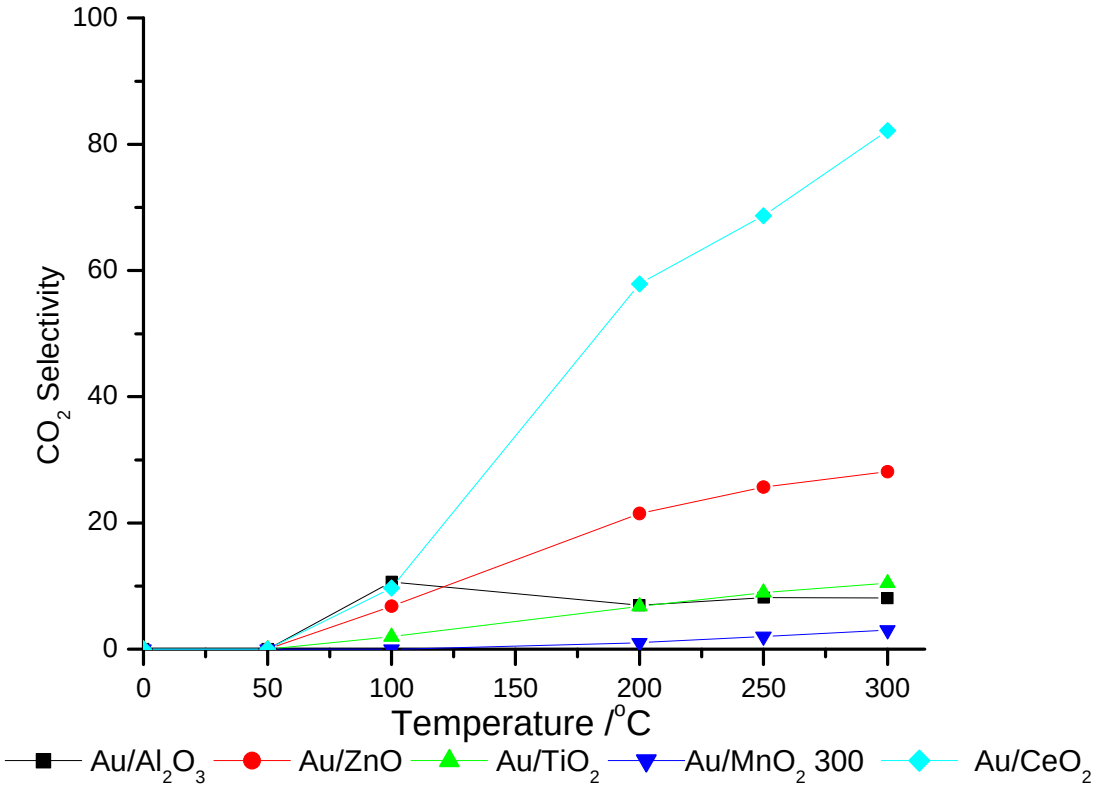


Figure 4.41: CO_2 selectivity for toluene oxidation over various gold-based catalysts

The catalyst found to be most effective in the complete oxidisation of toluene was Au/CeO_2. Also, it was found that the nature of the support is an important factor in the catalytic activity of a gold-based catalyst in the toluene oxidation reaction. The effect of the VOC studied is critical. The catalysts behaved differently when 2-butanol and 2-propanol were used instead of toluene.

4.4. References

[1] D. Philip, Spectrochim. Acta A 71 (2008) 80–85.

[2] J.D. Grunwaldt, C. Kiener, C. Wögerbauer and A. Baiker, J. Catal 181 (1999) 223-232.

[3] D.G. Duff, A. Baiker and P.P. Edwards, Langmuir 9 (1993) 2301-2309.

[4] L.C. Wang, L. He, Q. Liu, Y. Liu, M. Chen, Y. Cao, H. He and K. Fan, Appl . Catal. A-Gen. 344 (2008) 150-157.

[5] L.H. Chang, N. Sasirekha, Y.W. Chen and W.J. Wang, Ind. Eng. Chem. Res. 45 (2006) 4927-4935.

[6] E.R. Stobbe, B.A. de Boer and J.W. Geus, Catal. Today 47 (1999) 161-167.

[7] A.P. Malloy and S.W. Donne, J. Colloid Interface Sci. 320 (2008) 210-218.

[8] M. Yamashita, H. Ohashi, Y. Kobayashi, Y. Okaue, T. Kurisaki, H. Wakita and T. Yokoyama, J. Colloid Interface Sci. 319 (2008) 25-29.

[9] L.I. Hill, A. Verbaere and D. Guyomard, J. Power Sources 119-121 (2003) 226-231.

[10] S.S. Manoharan and R.K. Sahu, Chem. Commun. 8 (2002) 3068-3069.

[11] D. Delimaris and T. Ioannides, Appl. Catal. B: Environ. 84 (2008) 303-312.

[12] J. Carnö, M. Ferrandon, E. Björnbom and S. Järås, Appl . Catal. A-Gen. 155 (1997) 265-281.

[13] R. Xu, X. Wang, D. Wang, K. Zhou and Y. Li, J. Catal 237 (2006) 426-430.

[14] M. Comotti, W.C. Li, B. Spliethoff and F. Schuth, J. Am. Chem. Soc. 128 (2006) 917-924.

[15] P. Yadav, R.T. Olsson and M. Jonsson, Radiat. Phys. Chem. 78 (2009) 939-944.

[16] A. Trovarelli, G. Dolcetti, C. Deleitenburd, J. Kaspar, P. Finetti and A. Santoni, J. Chem. Soc. -Faraday T. 88 (1992) 1311-1319.

[17] L.H. Xiao, K.P. Sun, X.L. Xu and X.N. Li, Catal. Commun. 6 (2005) 796-801.

[18] M.I. Domínguez, M. Sánchez, M.A. Centeno, M. Montes and J.A. Odriozola, J. Mol. Catal. A: Chem. 277 (2007) 145-154.

[19] S. Minicò, S. Scirè, C. Crisafulli, R. Maggiore and S. Galvagno, Appl. Catal. B: Environ. 28 (2000) 245-251.

[20] F.N. Aguero, B.P. Barbero, O. Sanz, F.J.E. Lozano, M. Montes and L.E. Cadus, Ind. Eng. Chem. Res. 49 (2010) 1663-1668.

[21] S.Y. Liu and S.M. Yang, Appl . Catal. A-Gen. 334 (2008) 92-99.

[22] L.A. Palacio, J. Velásquez, A. Echavarría, A. Faro, F.R. Ribeiro and M.F. Ribeiro, J. Hazard. Mater. 177 (2010) 407-413.

[23] E.M. Cordi and J.L. Falconer, J. Catal 162 (1996) 104-117.

[24] M. Baldi, E. Finocchio, F. Milella and G. Busca, Appl. Catal. B: Environ. 16 (1998) 43-51.

[25] Y.A. Saleh-Alhamed, R.R. Hudgins and P.L. Silveston, J. Catal 161 (1996) 430-440.

[26] J. Gong, D.W. Flaherty, T. Yan and C.B. Mullins, Chemphyschem 9 (2008) 2461-2466.

[27] L.C. Wang, Q. Liu, X.S. Huang, Y. Liu, Y. Cao and K.N. Fan, Appl. Catal. B: Environ. 88 (2009) 204-212.

[28] S.J.A. Figueroa, F.G. Requejo, E.J. Lede, L. Lamaita, M.A. Peluso and J.E. Sambeth, Catal. Today 107-108 (2005) 849-855.

[29] C. Lahousse, A. Bernier, P. Grange, B. Delmon, P. Papaefthimiou, T. Ioannides and X. Verykios, J. Catal 178 (1998) 214-225.

[30] L. Lamaita, M.A. Peluso, J.E. Sambeth and H.J. Thomas, Appl. Catal. B: Environ. 61 (2005) 114-119.

[31] G. Qi, R.T. Yang and R. Chang, Appl. Catal. B: Environ. 51 (2004) 93–106.

[32] R. Kouraichi, J.J. Delgado, J.D. López-Castro, M. Stitou, J.M. Rodríguez-Izquierdo and M.A. Cauqui, Catal. Today 154 (2010) 195-201.

[33] C.H. Wang and S.S. Lin, Appl . Catal. A-Gen. 268 (2004) 227-233.

[34] A. Borbon, P. Coddeville, N. Locoge and J.C. Galloo, Chemosphere 57 (2004) 931-942.

[35] A.B. Hansen and F. Palmgren, Sci. Total Environ. 189-190 (1996) 451-457.

CHAPTER 5

5. CONCLUSIONS

The objective of this study was to investigate the feasibility of using gold based catalysts to oxidise volatile organic compounds. Gold supported on various supports were used for the oxidation of 2-propanol, 2-butanol and toluene. Overall, it was determined that a synergistic effect between gold nanoparticles and a suitable metal oxide was required to produce high catalytic activity.

Au/β-MnO_2 catalysts were synthesised by a deposition-precipitation method, and calcined at 300 and 350 ^{o}C. The two catalysts showed different activities at different temperatures. Low temperature calcination promoted a better catalytic performance. Pre-prepared gold nanoparticles were deposited on the β-MnO_2 support material. The amorphous manganese oxides, prepared by co-precipitation showed excellent activity due to the mixed oxidation states present. The surface structure of the support played a role in the oxidation reaction. Au/γ-MnO_2 was found to be a more superior catalyst than the Au/β-MnO_2 catalyst. Each of the supports had crystal planes showing different active sites that affected the reducibility and surface area of the catalysts. The structural differences in the different manganese dioxides resulted in an altered activity and reducibility of the catalysts. Gold based catalysts proved to be superior to Ce/MnO_2 catalysts. Ce was less active for the oxidation of 2-propanol than the Au based catalysts.

Overall, it was determined that the catalytic activity of gold based catalysts depends on the nature of the support. The nature of the volatile organic compound also played a role in influencing catalytic activity. The order of reactivity observed was: 2-butanol> 2-propanol> toluene over the same catalyst. The oxidation of VOCs occurred at temperatures below 300 ^{o}C. The Au/CeO_2 catalyst was found to exhibit superior catalytic activity towards aromatic VOC oxidation.

Au/MnO_x catalysts showed better CO_2 selectivity than Au/Al_2O_3 and Au/ZnO catalysts. Au/Al_2O_3 and Au/ZnO supported gold catalysts were poor combustion catalysts. They showed a high selectivity towards acetone, even at 100 ^oC. The amorphous manganese oxides, MnO_x, showed excellent activity due to the mixed oxidation states present.

FUTURE STUDIES

The work covered in this study served as a base for evaluating the feasibility of gold based catalysts for VOC oxidation. The catalysts were synthesised by simple wet preparation; deposition-precipitation and co-precipitation methods. Further work that can be done, with the aim of improving catalyst activity, should include further optimisation of the preparation methods. The pre-treatment of the catalysts and a more detailed study on the effect of gold loading and promoters is required. A novel catalyst treatment process that could be investigated would be to use microwave radiation. Also, treatment of the supports under different atmospheric conditions such as N_2, Ar, O_2 and air could be investigated in more detail.

The various manganese oxide (γ-MnO_2 and MnO_x) supports prepared were used for 2-propanol oxidation and the data compared to the β-MnO_2 support. In future, the study should include a comparison of the supports in the oxidation of other VOCs.

Additional characterisation of the catalysts by Fourier transform infrared (FTIR) spectroscopy and X-ray photoemission spectroscopy (XPS) would be invaluable in aiding the understanding of catalyst surface properties and the nature of active sites in the catalysts.

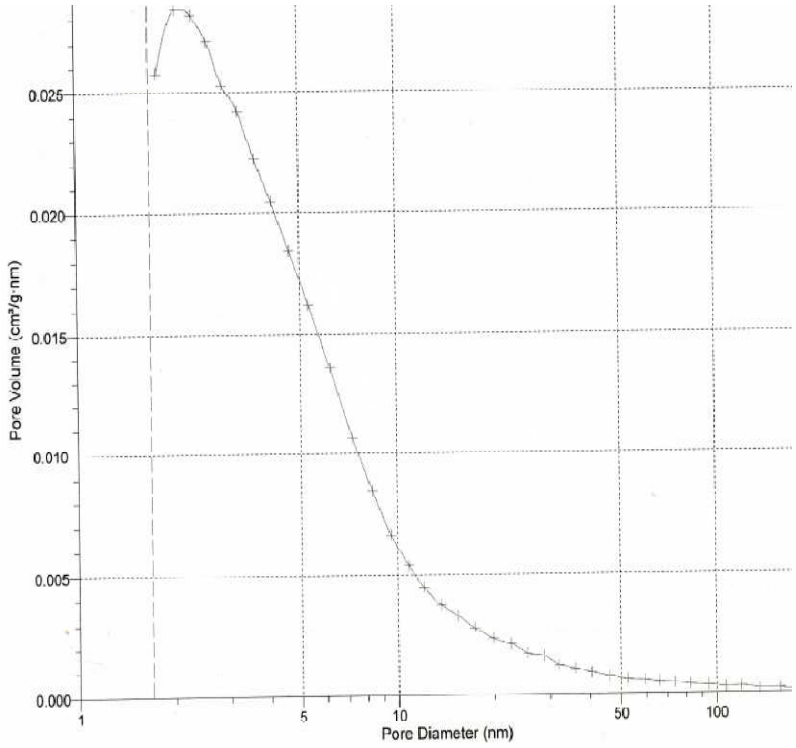
The catalysts prepared were found to show efficient behaviour under the conditions used. Future research work is needed to include catalyst activity when the reaction gas mixture is composed of multiple organic compounds.

Deactivation studies need to be considered to examine the stability and robustness of the catalyst and establish their viability under real working conditions.

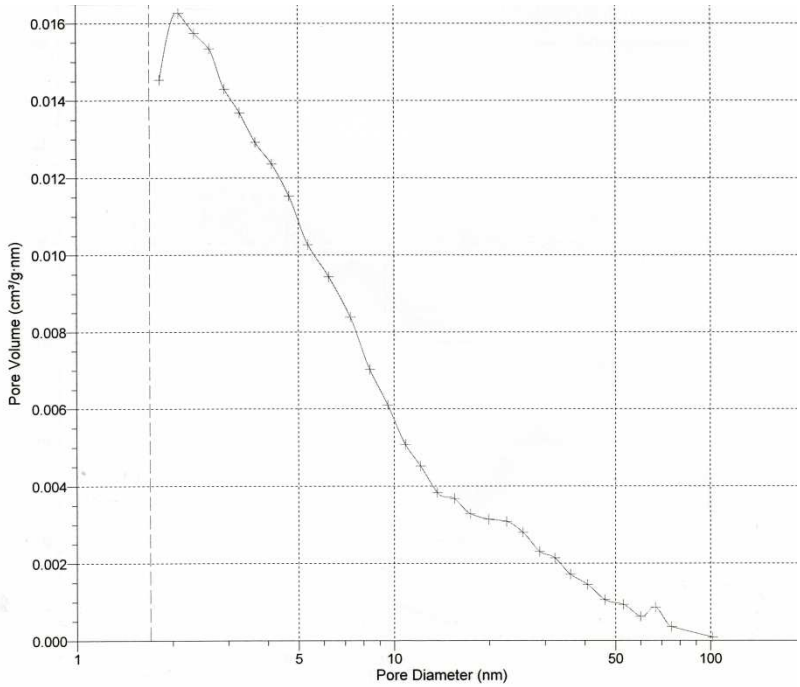
BIBLIOGRAPHY

1. G.C. Bond, C. Louis and D.T. Thompson, Catalysis by gold, Imperial College Press; distributed by World Scientific, London; Singapore, 2006.

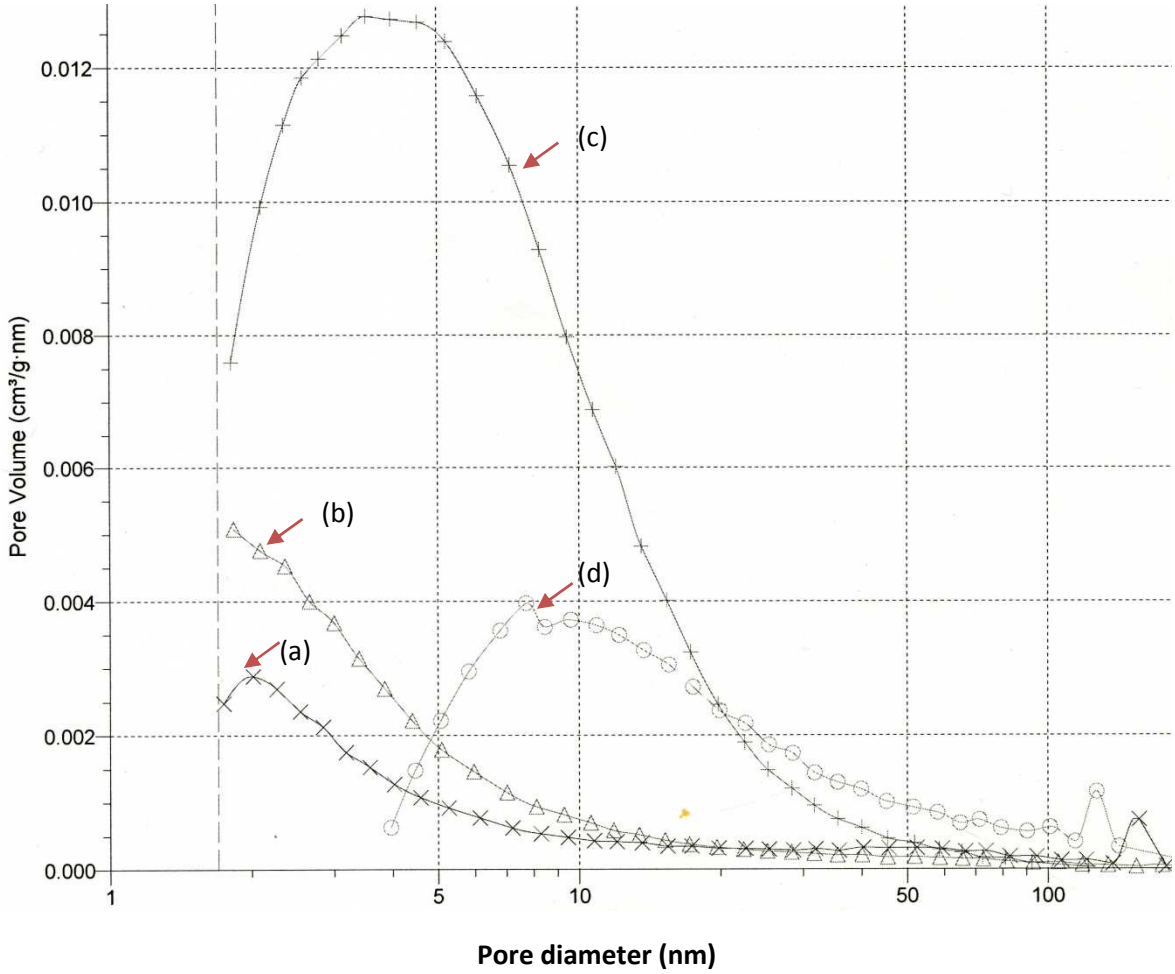
APPENDIX A



Appendix A1: A plot of BHJ adsorption pore volume (dV) over pore diameter (dD) for Au/MnO_2 300 sample

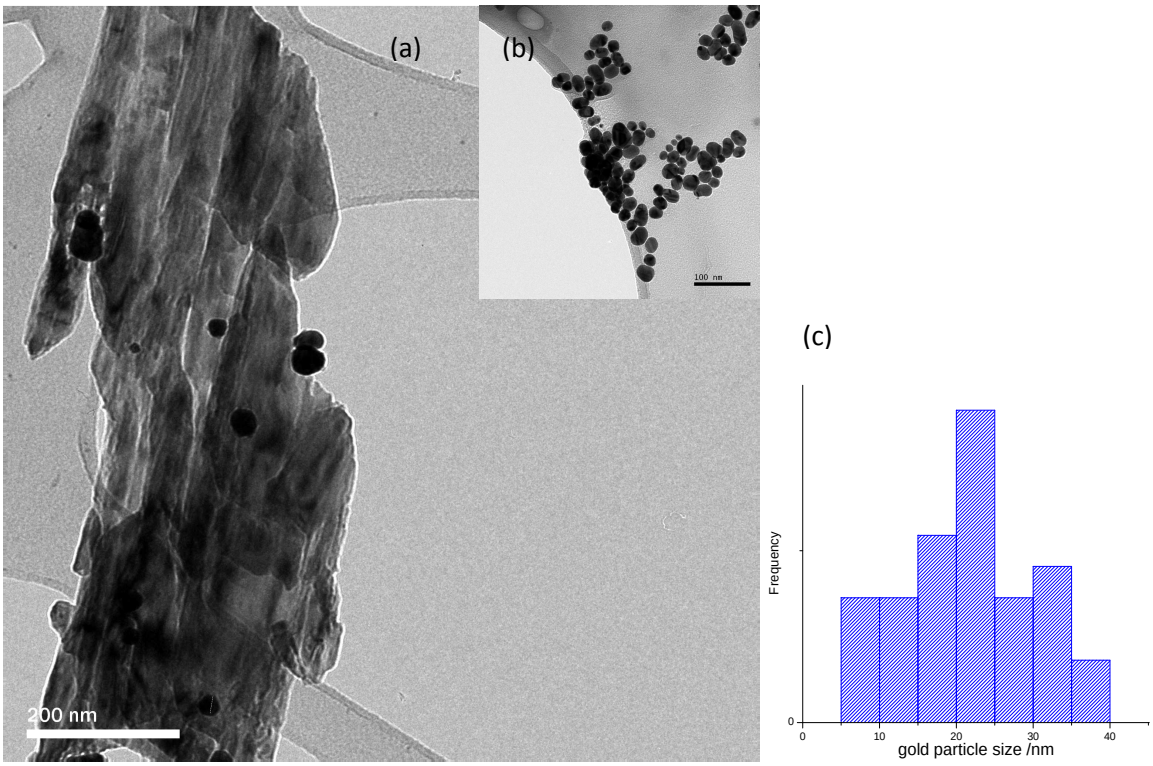


Appendix A2: A BHJ adsorption (dV) /(dD) pore volume graph for Au/MnO_x



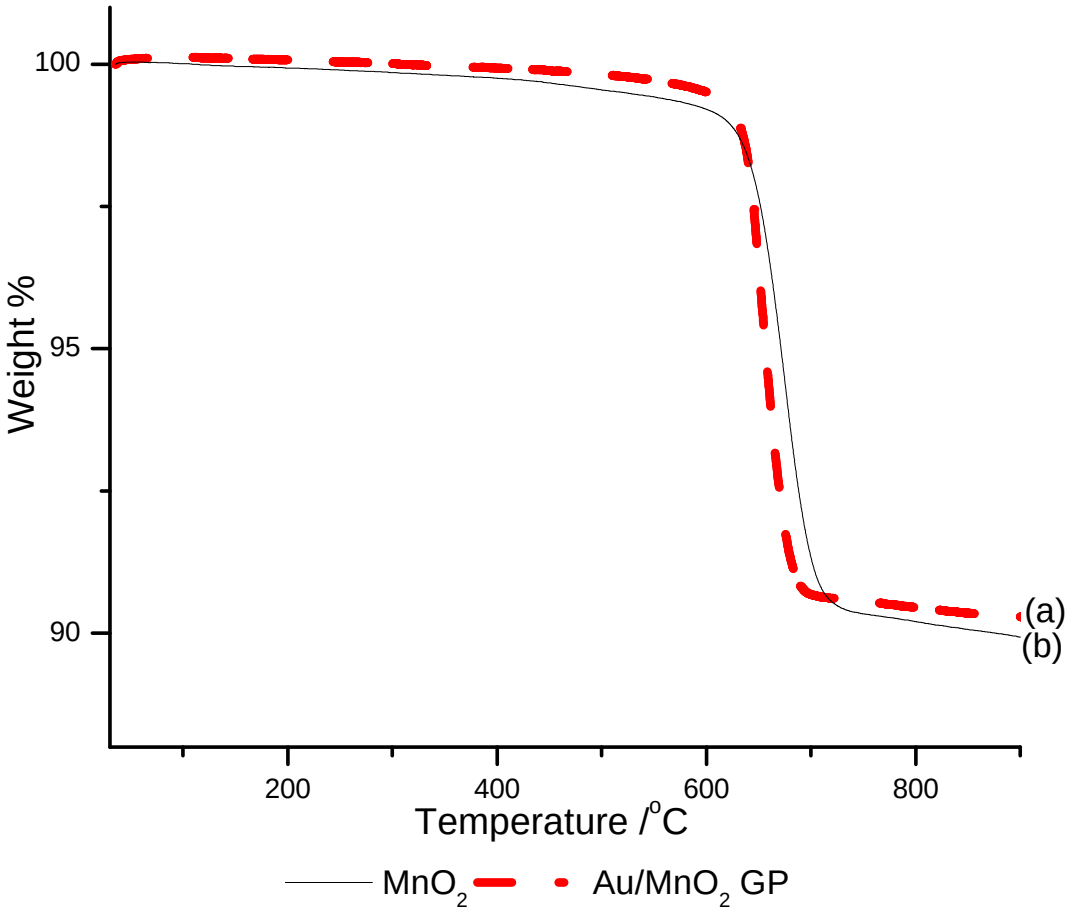
Appendix A3: pore volume BJH Adsorption dV/dD Pore Volume with Faas Correction

APPENDIX B



Appendix B: TEM images of a) Au/MnO_2 GP catalyst prepared by colloid formation b)gold nanoparticles prepared by colloid solution without using $NaBH_4$ and c) bar graph showing gold particle size distribution

APPENDIX C



Appendix C: the TGA profile of β-MnO_2 (-) and Au/β-MnO_2 GP (- -) samples

APPENDIX D

a) Au loading as wt.% in the sample was measured by $= \frac{m_{Au}}{m_{Au} + m_{support}} \text{ x}100.$

This is the amount of Au per gram of the support were m_{Au} is the mass of gold in the gold precursor and $m_{support}$ is the mass of the support used.

b) At least 300 particles were counted and the particles size was measured as the arithmetic mean $d_{Au} = \frac{\sum x_i d_i}{\sum x_i}$ Where x_i is the number of particles of diameter d_i.